NOVEL MAGNETIC EXTRACTANTS FOR REMOVAL OF POLLUTANTS FROM WATER

By

TAREK MOHSEN TRAD

Bachelor of Science

Beirut Arab University

Beirut, Lebanon

1999

Submitted to the Faculty of the
Graduate College of the
Oklahoma State University
In partial fulfillment of
The requirements for
The Degree of
DOCTOR OF PHILOSOPHY
December, 2006

NOVEL MAGNETIC EXTRACTANTS FOR

REMOVAL OF POLLUTANTS

FROM WATER

Thesis Approved:

_____Dr. Allen W. Apblett_____

Thesis Adviser

_____Dr. Ziad El Rassi_____

_____Dr. Nicholas F. Materer_____

_____Dr. Gary L. Foutch_____

_____Dr. A. Gordon Emslie_____

Dean of the Graduate College

DEDICATION

Dedicated to my beloved mother

ACKNOWLEDGMENTS

First and foremost, this work has been possible due to the patience and exceptional guidance of my thesis adviser, Dr. Allen W. Apblett. His encouragement, motivation, generous support, and wise counsel have shaped my attitude toward my research and helped progress my learning experiences. I feel privileged to have an adviser, who is always open to discussion, and whose assistance cannot be overestimated. Dr. Apblett's magnanimous attitude, constructive criticism, tremendous scientific knowledge, and great personality will always inspire me to be a better scientist as well as a better person. I truly believe that his dedication to research and teaching has contributed immensely to building a sound foundation for my future career in Inorganic Chemistry.

I am grateful to the valuable advice and friendly support of my committee members, Dr. Ziad El Rassi, Dr. Nicholas Materer, and Dr. Gary Foutch. Their knowledge helped me broaden my views in science and technology. I deeply appreciate their willingness to help throughout this study.

My sincere thanks are extended to my friends and colleagues, all present and former members of Dr. Apblett's research group, for their honesty, kindness, and professionalism. Their friendly cooperation and valuable discussions were indispensable.

Thank you for your encouragement and comradeship, and for providing a lively and pleasant working environment for the past few years.

Special thanks to Phoebe Doss, Terry Colberg, and Dr. Susheng Tan for their technical support on electron microscopy techniques.

I would also like to thank Professor Neil Purdie, the faculty and staff of the Department of Chemistry at Oklahoma State University for their kindness and gracious assistance.

I am particularly grateful to my brothers Jawad and Ghaleb for their endless support, affection, and trust. Thanks are also due to my mother and my sister Lama for selflessly encouraging my endeavor to pursue my PhD abroad, and placing an unshaken faith in my ability to accomplish my challenging task. I love you all dearly.

Finally, in memory of my father, I thank him for believing that one day I will be wearing the chemist's "white coat".

TABLE OF CONTENTS

CHAPTER **PAGE**

LIST OF FIGURES

FIGURE **PAGE**

LIST OF TABLES

TABLE **PAGE**

CHAPTER 1

GENERAL INTRODUCTION

BACKGROUND

Water contamination

Advancement in science and technology is continuously serving a growing population in a landscape controlled and affected by human activity. The presence, therefore, of a large number of chemical and biological pollutants should be expected in drinking water. This pollution of water resources caused by an increasing population, occur via the use and disposal of chemical, agricultural, and animal products as well as industrial waste. Natural water contamination sources can be classified into three categories [1]:

1. Natural pollution
2. Waste disposal practices
3. Nonpoint sources due to human activities

The major percentage of inorganic substances found in groundwater comes from natural origins. However, significant amounts are also contributed from human activities. Natural leaching of minerals can lead to ground water contamination by chlorides, sulfates, nitrates, fluorides, and iron that sometimes can exceed the United States

Environmental Protection Agency's (EPA) limits. The type and degree of natural contamination largely depend on the geological location.

Waste disposal practices causing water contamination are primarily the disposal of solid wastes, municipal wastewater, private sewage, and brine associated with the petroleum industry, as well as industrial wastewater impoundments and land spreading of sludge. Other waste discharges injected in deep wells and originating from mines, animal feedlots, and radioactive substances can also have a severe impact on drinking water quality.

Nonpoint sources of water pollution are dispersed throughout both rural and urban areas. The main nonpoint sources of potential water contamination are listed below [2].

- Accidental leaks and spills of chemicals and petroleum products from broken pipelines, underground storage tanks, tanker trucks, and other accidents that occur during material storage and transport processes.
- Pesticide and herbicide pollution from agricultural activities.
- Mining of coal and metal sulfide ores causing trace metal and acid contamination of surface and groundwater.
- Atmospheric contaminants and acid rain.
- Metallurgical processing of base metals such as zinc, copper, lead, and cadmium.
- Chemical pollutants from waste disposal facilities and chemical industries.

The constant and long-term release of toxic contaminants provided by these sources into the environment will always be a major human concern. Environmental agencies and governments all over the world are continuously supporting the development of novel water treatment techniques and pollution control methods.

Today's water treatment plants tend to follow a basic approach which consists of the following steps: pretreatment, prefiltration, filtration, chemical treatment, and disinfection. However, this process lacks the ability to remove trace metal and organic compounds from raw water. Therefore, advanced treatment methods are implemented in order for a basic water treatment facility to deliver high quality drinkable water. Available advanced technologies employed in water treatment plants worldwide include membrane separation (reverse osmosis), granular activated carbon (GAC), ozonation and hydrogen peroxide, ultraviolet light, and organic polymers [2]. These technologies are able to remove bacteria, viruses, naturally occurring metals and synthetic organic chemicals, as well as radioactive elements, thus, leading to effective health protection.

The cost of applying common water treatment technologies in rural areas is a critical problem. This study focuses on using magnetic separation as a cost effective technology for the removal of water pollutants. The following section introduces the technology and its mechanism of operation.

Magnetic Separation

Magnetic separation is a modern solution for many industrial and environmental problems. It has been developed as a pollution-control technique for the treatment of steel mills' effluents [3] waste water [4] radioactive water [5], separation of mining ores [6], clay processing [7], desulfurization of coal [8], filtration of cooling water in nuclear reactors [9], and decontamination of drinking water [10]. Magnetic separation is a well established method but the development of high gradient magnetic separators has

significantly improved the separation process and paved the way for new areas of application. High gradients are of paramount importance in these magnetic systems and they can be achieved by inducing high curvature magnetic elements introduced within the separation matrix [11]. This idea encouraged researchers to apply high gradient magnetic separation (HGMS) to more complicated separations through the use of modified magnetic particles that are selective for the removal of proteins, cells, or environmental pollutants such as dyes, heavy metal ions, radionuclides, and soluble organic contaminants [12-17].

A typical HGMS system is comprised of an electromagnet and a column packed with magnetically susceptible wires or steel wool. Applying a magnetic field across the packed column allows the wires to dehomogenize the field creating high field gradients around them which retain the magnetic particles by attracting them magnetically to the wire surface [18]. An illustration of an HGMS is presented in Figure 1-1 showing both stages of operation with the magnetic field turned on in the first stage and off in the second (A and B respectively) [19].

The retention of magnetic particles is strongly influenced by the particle size, their magnetic properties, and most importantly the magnetic field gradients. In an applied magnetic field, the following equation represents the magnetic force on a particle [18] :

$$F_m = \mu V_p M_p . \nabla H \qquad (1)$$

Where F_m is the magnetic force, μ is the permeability of free space, V_m is the particle's volume, M_p is the magnetization of the particle, and H is the magnetic field where the particle is located. For favorable attraction or entrapment of particles, the magnetic force

driving the particles toward the wires must be greater than the forces of gravity, inertia, and diffusion acting on the particle. It should also dominate the fluid drag during flow [20].

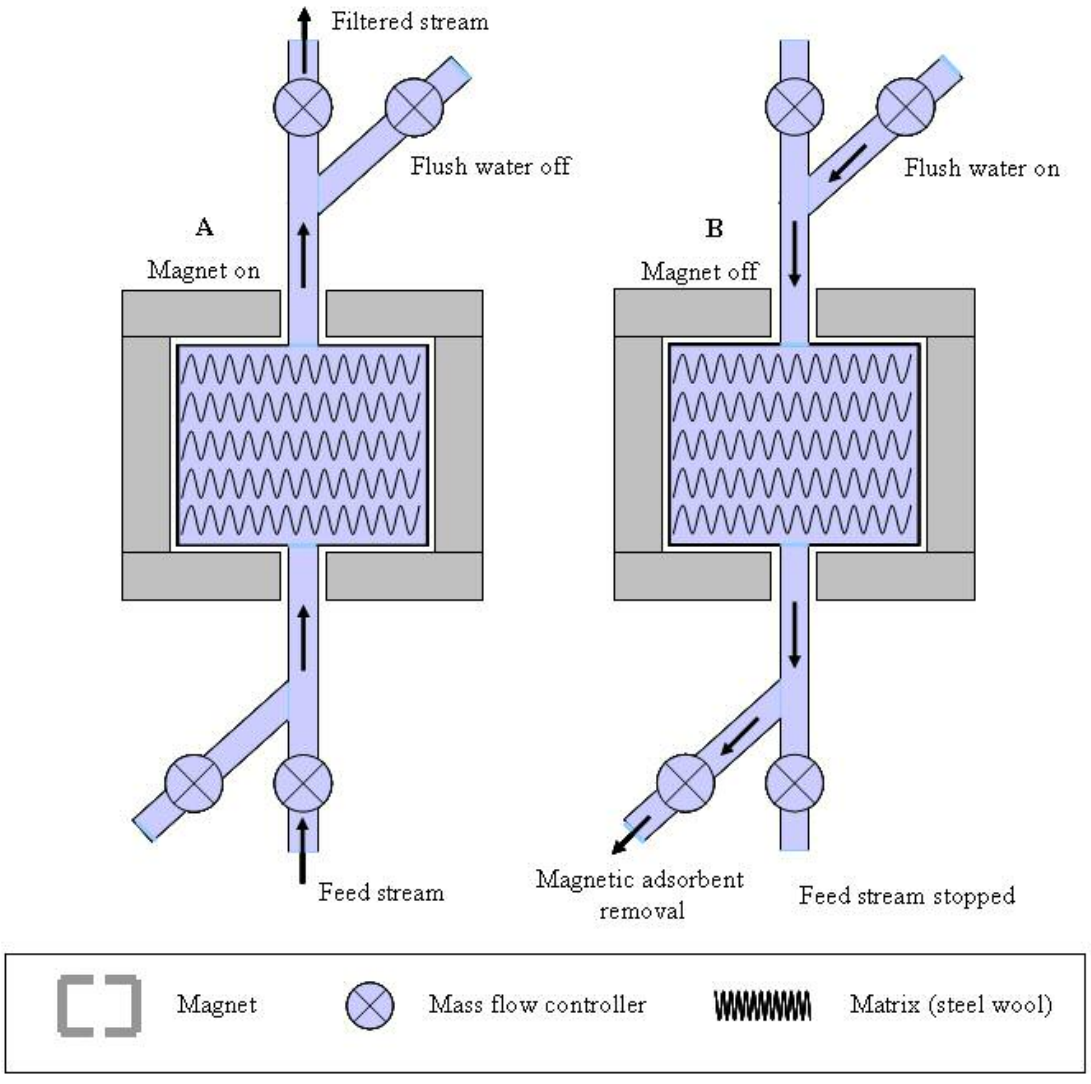

Figure 1-1: A typical HGMS system showing fluid flow during the filtration (A), and during the washing and removal cycle of the magnetic adsorbent (B) [19]

The application of efficient magnetic filtration to organic, heavy metal, and petroleum-related decontamination and waste treatment is attractive because of the

numerous advantages it has over existing particle separation methods such as centrifugation and ultrafiltration. Some of these advantages are the rapid removal of contaminants from aqueous waste streams, simplicity of equipment, and ease of operation. Moreover, the ability to electronically control the electromagnet allows for safer mechanical handling of the technique by minimizing the exposure of workers to toxic contaminants. The main challenge faced by researchers in the area of magnetic filtration is the development of efficient filtering aids that bind the contaminants and allow their magnetic removal, since most contaminants of concern are not magnetic in nature. The following sections explain different aspects of nanoparticles and magnetic particle technology and provide background information on some important magnetic materials. These materials has been exploited and modified in this research to produce a new generation of magnetic adsorbents useful in environmental, industrial, and biomedical applications. The efficiency of the developed magnetic adsorbents for the removal of decane, 2,4,6-dinitro-o-cresol (DNOC) pesticide, Congo red dye, and arsenate are presented and discussed in later chapters.

MAGNETIC ACTIVATED CARBON

Activated carbon is considered one of the most important adsorbents used in water treatment. The majority of the world's activated carbon production is used in liquid-phase applications. The general process by which pollutants are removed from the aqueous phase by activated carbon is adsorption, where the binding of molecules to the surface is governed by van der Waals' dispersion forces and electrostatic interactions.

Consequently, these factors will lead to increased concentration of the adsorbate at the solid-liquid interface as opposed to the bulk aqueous phase.

Usually, activated carbon is prepared from raw materials with high carbon content and low inorganic content. These materials can be activated physically by a two-step process at high temperatures (700 – 800 °C). Normally, the steps involve carbonization in an inert atmosphere followed by activation in steam or carbon dioxide. On the other hand, chemical activation is a single step process involving the carbonization of the precursor impregnated with a chemical agent such as phosphoric acid or potassium hydroxide at temperatures between 500 – 800 °C. The porosity and surface area of the resultant activated carbon vary depending on the starting material used, activation process, and reaction conditions.

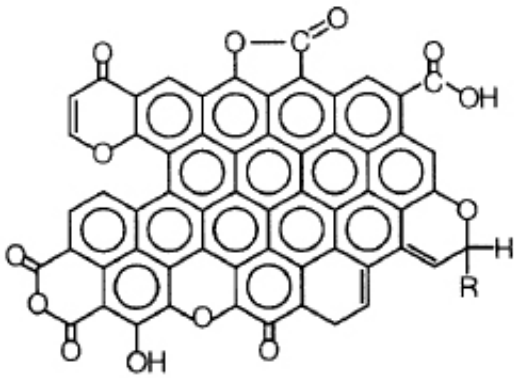

Figure 1-2: possible oxygen-containing functional groups on the edges of a graphene layer [21]

Raw materials used for the production of activated carbon are the primary source of heteroatoms such as nitrogen, sulfur, and oxygen in the carbonaceous matrix. Inorganic matter which leads to undesired ash content causing a decrease in mechanical strength and low adsorption capacity can also exist in low percentages. Activated

carbon's interesting surface chemistry emanates from the presence of a variety of surface functionalities due to the bonding of highly oxidized oxygen at the edge of the graphene layers and the structural defects. Figure 1-2 shows possible oxygen-containing functional groups on the edges of a graphene layer [21].

The development of activated carbon particles with useful magnetic properties is not thoroughly investigated. However, a few routes for the synthesis of this material including high energy ball milling and metal precipitation were reported [22-24]. Numerous drawbacks such as low porosity, high remnant magnetization, and formation of large aggregates of magnetic and nonmagnetic iron oxides within the activated carbon's structure were experienced by the aforementioned routes.

In the next chapter, a simple process for the preparation of magnetic activated carbon samples is described. The material obtained was characterized using a number of analytical techniques and its efficiency in the magnetic removal of many water pollutants was studied.

MAGNETIC NANOPARTICLES

Structures on length scales from 1 to 100 nm are described as "nanostructured" materials. Their remarkable structural, mechanical, electrical, optical, chemical, and magnetic properties that are different from their bulk counterparts make them technologically useful and potentially applicable in the areas of color imaging, information storage, biomedicine, and magnetic separation [25-28]. The intensity of magnetic nanoparticle and nanostructure research studies have led to the development of a variety of magnetic nanoparticles from metals to ceramics using a broad range of

synthetic techniques from chemistry, physics, and materials science disciplines [29]. These investigations improved the understanding of nanoparticle formation mechanisms and provided valuable information about the structural and magnetic properties of the products [29].

Synthetic routes

Chemical synthesis of magnetic nanoparicles has been reviewed by Drofenic and coworkers [30]. The described preparation techniques are: Co-precipitation, sol-gel, high-energy milling, hydrothermal synthesis, microemulsion, spray pyrolysis, and sonochemical syntheses.

Coprecipitation is a classical method used for the synthesis of simple oxides from solution. The simultaneous precipitation of various cations using suitable agents leads to the formation of a mixed precursor which is subsequently calcined yielding the final product. This method is effective for the preparation of ferrites. For example, the calcination temperature typically used for the preparation of barium-hexaferrites was significantly reduced using the coprecipitation method [31].

The sol-gel route is basically used for making ceramics and glass materials from metal alkoxides. Hydrolysis and polycondensation of the starting material forms a colloidal suspension or a “sol”. Uniform particles are subsequently formed by precipitating the sol. The versatility of the sol-gel technique and the flexibility of this system for making different forms of ceramic or glass materials make it an important process in materials science.

Ferrite nanoparticles can also be synthesized using high-energy ball milling. Formation of nanoparticles in this case can occur by dry milling of solid materials at prolonged periods of time followed by heat treatment. Solid-state displacement reactions are induced by the mechanochemical treatment leading to loss in symmetry of the crystal or ligand field resulting in micro-plastic deformation. The produced nanoparticles dispersed in a matrix of soluble byproduct are separated by a simple washing process.

Normally, crystalline, anhydrous ceramic particles are prepared using the hydrothermal method where temperatures used are in the range between the boiling point of water and its critical temperature (~ 374°C) and pressures of up to 15 MPa. In this method, calcination steps required by the sol-gel and co-precipitation techniques are avoided and particles of increased crystallinity are produced.

The microemulsion-assisted technique involves the incorporation of a soluble metal salt in the aqueous phase of a water-in-oil microemulsion where it resides within the aqueous droplets surrounded by the oil. In order to form product C from reactants A and B, two different microemulsions with one reactant dissolved in the core of each has to be prepared. Mixing the microemulsions will lead to the formation of particles entirely enclosed within the aqueous droplets of the final microemulsion. Inter-droplet exchange and nuclei aggregation are probable factors involved in the growth of these particles.

Spray pyrolysis is a continuous, rapid, and simple technique used for the synthesis of well-defined nanoparticles at continuous high production rates. Under thoroughly controlled experimental conditions, a solution of aerosol droplets is sprayed and evaporated in a reactor forming a precipitate, which then undergo thermolysis at higher temperatures yielding unisized nanoparticles. However, spray pyrolysis most often leads

to dense macroporous solids after heat treatment. Thus, the main problem associated with this method is agglomeration, which tends to occur during the synthesis procedure.

Nanoparticles of metals, alloys, and metal oxides have also been prepared using sonochemical methods. Acoustic cavitation is the source of chemical activity of ultrasound. This non-inertial cavitation is a process where bubbles formed in a fluid as a result of a high energy input such as an acoustic field rapidly implode leading to its collapse. Unlike inertial cavitation that produces a shock wave upon bubble collapse, acoustic cavitation generates a transient localized hot-spot with high effective temperatures reaching 5000 °C and very short lifetime (nanosecond). Due to this phenomenon, nanometric clusters produced during the sonochemical process are stabilized by the rapid cavitational cooling rate (> 10^9 K/s) exceeding rates obtained by conventional methods.

The properties of magnetic nanoparticles

Magnetic nanoparticles exhibit very interesting intrinsic properties. Generally, these properties along with size effects and nanoparticle interactions govern their magnetic behavior [30]. Magnetization is determined by size effects when the magnetic system is composed of noninteracting particles. On the other hand, particle interactions control the magnetic properties of fine-grained nanostructures [29].

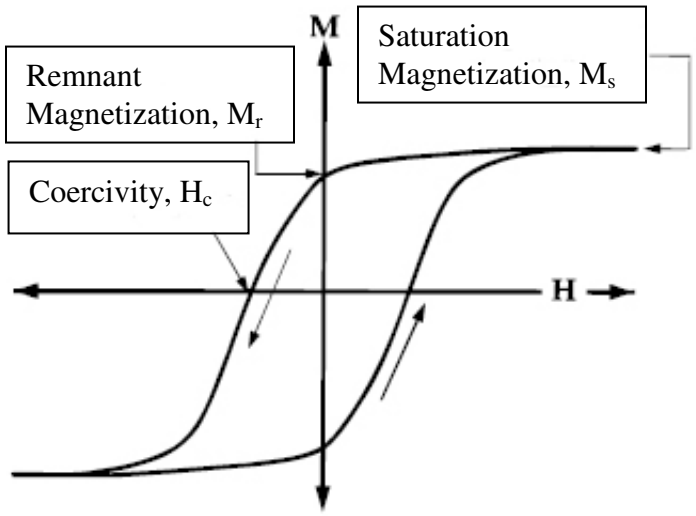

Figure 1-3: Magnetization versus field hysteresis loop showing the saturation magnetization M_s, remnant magnetization M_r, and coercivity H_c [29]

Magnetic parameters can be determined by plotting magnetization versus field as shown in Figure 1-3. Saturation magnetization, M_s, is the maximum value of magnetization realized when a large magnetic field is applied causing an alignment of spins with the field. Remnant magnetization, M_r, is the value of magnetization at zero field and the remnant ratio is the ratio of remnant magnetization to saturation magnetization and it ranges from 0 to 1. Coercivity, H_c, also called the coercive field is the intensity of the magnetic field required to bring the magnetization of a material back to zero after saturation magnetization has been reached. Dependence of coercivity on particle size was experimentally studied [32]. A plot showing the behavior of coercivity as size changes is illustrated in Figure 1-4 [29]. Based on these studies, the formation of domain walls was found to be energetically favorable in particles with diameters larger than the critical diameter, D_c. Magnetization changes thus occur through these domain walls. The decrease in particle size approaching critical particle diameter renders the formation of domain walls energetically unfavorable and the particles, as shown in Figure

1-4, are called single domain. Therefore, magnetization changes no longer exist through the motion of domain walls. An interesting magnetic behavior is observed as particle size continues to decrease below the single domain limit where thermal fluctuations can significantly affect the spins, preventing the existence of stable magnetization [33]. For these small sized particles, atomic moments are firmly aligned as a single large magnetic moment. Theoretically, in this case, H_c approaches zero and the system is called superparamagnetic [34]. The existence of single domain particles was theoretically predicted by Frenkel and Dorfman, with critical diameter estimates made by Kittel [29,35]. For magnetite and maghemite, single-domain particles with critical diameters of 128 nm and 166 nm, respectively, were estimated.

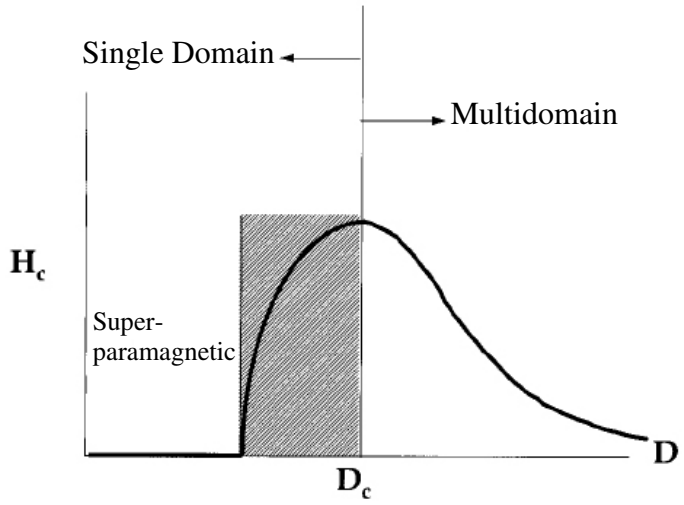

Figure 1-4: Dependence of coercivity on particle size in ultrafine particle systems

Additionally, anisotropy associated with size, shape, stress, and crystal structure can have an effect on magnetization behavior [36]. In nanomaterials, shape and crystalline anisotropies are predominant. Anisotropy can be represented as:

$$E = KVSin^2\theta \qquad (2)$$

Where K is the effective uniaxial anisotropy energy per unit volume, V is the particle volume, and θ is the angle between the easy axis and the moment.

Depending on the application intended, specific properties are needed. For example, magnetic separation of water pollutants using magnetic nanoparticles requires the adsorbents to exhibit no remnant magnetization, and superparamagnetic properties. Furthermore, the magnetic adsorbents should be non-toxic, and chemically stable in the neutral pH of water.

In cases where magnetic nanoparticles have been used as adsorbents in HGMS, their aggregation resulted in faster and easier attraction [37]. Adsorptive separations were also performed quicker than standard porous materials because limiting factors such as pore diffusion are insignificant at the nanoscale [38]. In magnetic particle technology, iron oxides such as magnetite (Fe_3O_4), its oxidized form maghemite (γ-Fe_2O_3), and metal ferrites are the most used materials.

MAGNETITE AND MAGHEMITE

Magnetite and maghemite are ferromagnetic iron oxides of the inverse-spinel type structure that has the general formula of $A(B)_2O_4$, where A and B represent different metal ions occupying specific sites in the crystal structure. γ-Fe_2O_3 differs only by the fact that all iron is in the trivalent state and by the presence of vacancies in octahedral positions to compensate for the increased positive charge from the oxidation of Fe(II) [39].

Jules Lefort was one of the pioneers in the chemical synthesis of iron oxide dispersions back in 1852 [40]. He introduced the synthesis procedure involving the

precipitation of ferrous and ferric salts mixtures using potassium hydroxide. In the late 1930's, Elmore reported the development of a simpler method for making ferromagnetic colloids of magnetic powder [41]. Thirty years later, the first stable dispersion of magnetite particles in kerosene was prepared by Papell [40]. Many other procedures were followed such as Khalafalla and Reimers' involving the preparation of magnetite particles from ground nonmagnetic wustite [40]. Recently, nanoparticles of magnetite were produced as a result of reacting aqueous mixtures of $FeCl_3$ and $FeCl_2$ with ammonia [42]. High temperature reaction of iron (III) acetylacetone also proved effective in making monodisperse magnetite nanoparticles [43].

Maghemite can be formed using common routes of synthesis such as controlled oxidation of magnetite and thermal dehydration of lepidocrocite, γ-FeO(OH) [44-46]. Thermal transformation of iron(III) oxalate can lead to superparamagnetic nanoparticles of maghemite [39]. Furthermore, thermal treatment of iron-carboxylate complexes has been used to produce nanoparticles of variable size [47]. Normally, maghemite is transformed into hematite (α-Fe_2O_3) at high temperatures (approximately 400 °C) where the mechanism of such transformation is dependant on reaction conditions.

NICKEL FERRITE

Spinel ferrites are magnetic materials of high technological importance, widely used in a variety of applications. They have the general formula of MFe_2O_4, (M = Ni, Zn, Mn, Co, Mg) where the unit cell contains 32 oxygen atoms in cubic closest packing with eight tetrahedral and 16 octahedral occupied sites [48]. Ferrospinels, the inverse type in particular, are very useful due to their unique magnetic structure, high saturation

magnetization, and high magnetocrystalline anisotropy [48]. Nickel ferrite ($NiFe_2O_4$) powders have been studied for possible employment in microwave devices, catalysis, and magnetic recording fluids [49]. Ferrimagnetic behavior of nickel ferrite originates from magnetic moment of anti-parallel spins between Ni^{2+} ions at octahedral sites and Fe^{3+} ions at tetrahedral sites [50]. Conventionally, nickel ferrite nanoparticles are prepared by traditional solid state, coprecipitation, mechanical milling, and sol-gel techniques [51-54]. The preparation methodology can alter the particles' composition and microstructure which have a direct effect on the properties. A better control over these factors can be achieved by adopting wet chemical synthesis routes such as coprecipitation, radio-frequency thermal method, hydrothermal method, and microemulsion [49,55-57].

In water treatment, many investigations were performed on the magnetic separation of heavy metals, particulate matter, dissolved organic compounds, and biological contaminants using metal ferrite nanoparticles [58-60]. However, not enough research has been done on surface functionalization of such nanoparticles for purpose of selective adsorption in the area of magnetic separation.

OBJECTIVE AND SCOPE OF THE RESEARCH

This research aims at developing magnetic extractants that can be utilized in conjunction with magnetic filtration devices to efficiently and economically remove a number of pollutants from aqueous solutions and mixtures. In Chapters 2 and 4, two types of magnetic materials were synthesized, characterized, and used in a variety of environmental applications. The first type of magnetic materials was based on activated carbon, where raw materials used for the development of high surface area activated

carbon were modified to produce novel magnetically-active activated carbons (MAC's). The unique properties and adsorption capacity of these materials allowed their application in the extraction of hydrocarbons from water and in breaking oil in water emulsions as represented in Chapter 3. In the second phase of the project, nano-composites of organic-capped magnetite and nickel ferrite were successfully obtained by non-hydrolytic thermal treatment of organometallic precursors. The nanoparticles were characterized using a variety of techniques including transmission electron microscopy, infrared spectroscopy, X-ray diffraction, and thermogravimetric analysis. Chapter 5 describes an investigation on the ability of the nanoparticulate extractants for the removal of 4,6-dinitro-o-cresol pesticide from aqueous solutions. Finally, MAC and capped nanoparticles samples were used in extracting arsenate from water using magnetic filtration. Langmuir isotherms were fitted with the adsorption data and adsorption capacities were determined.

REFERENCES

[1] Patrick, R.; Ford, E.; Quarles, J.; Pye, V. I. *Groundwater contamination in the United States*; 2nd ed.; University of Pennsylvania Press: Philadelphia, 1987.

[2] Sullivan, P. J.; Agardy, F. J.; Clark, J. J. J. *The environmental science of drinking water*; 1st ed.; Elsevier Butterworth-Heinemann: Burlington, MA, 2005.

[3] Svoboda, J. *Magnetic methods for the treatment of minerals*; Elsevier: Amsterdam ; New York, 1987.

[4] Bolto, B. A. *Waste Management (Amsterdam, Netherlands)* **1990**, *10*, 11-21.

[5] Dubourg, M. *Radioprotection* **1998**, *33*, 35-46.

[6] Svoboda, J.; Lazer, M.; Te Riele, W. A. M. *IEEE Transactions on Magnetics* **1987**, *MAG-23*, 283-93.

[7] Lawver, J. E.; Hopstock, D. M. *Minerals Science and Engineering* **1974**, *6*, 154-172.

[8] Petrakis, L.; Ahner, P. F.; Kiviat, F. E. *Separation Science and Technology* **1981**, *16*, 745-772.

[9] De Latour, C. *IEEE Transactions on Magnetics* **1973**, *9*, 314-316.

[10] Liu, Y. A.; IEEE Magnetics Society.; Auburn University. Engineering Foundation. *Industrial applications of magnetic separation : proceedings of an International Conference at Franklin Pierce College, Rindge, New Hampshire, July 30-August 4, 1978*; Institute of Electrical and Electronic Engineers: New York, 1979.

[11] Ebner, A. D.; Ritter, J. A.; Ploehn, H. J. *Separation and Purification Technology* **1997**, *11*, 199-210.

[12] Bucak, S.; Jones, D. A.; Laibinis, P. E.; Hatton, T. A. *Biotechnology Progress* **2003**, *19*, 477-484.

[13] Safarik, I.; Safarikova, M. *Journal of chromatography. B, Biomedical sciences and applications* **1999**, *722*, 33-53.

[14] Safarik, I. *Water Research* **1995**, *29*, 101-105.

[15] Kaminski, M. D.; Nunez, L. *Journal of Magnetism and Magnetic Materials* **1999**, *194*, 31-36.

[16] Buchholz, B. A.; Nunez, L.; Vandegrift, G. F. *Separation Science and Technology* **1996**, *31*, 1933-1952.

[17] Moeser, G. D.; Roach, K. A.; Green, W. H.; Laibinis, P. E.; Hatton, T. A. *Industrial & Engineering Chemistry Research* **2002**, *41*, 4739-4749.

[18] Gerber, R.; Birss, R. R. *High gradient magnetic separation*; Research Studies Press: Chichester ; New York, 1983.

[19] Parker, M. R. *Physics in Technology* **1981**, *12*, 263-268.

[20] Moeser, G. D.; Roach, K. A.; Green, W. H.; Hatton, T. A.; Laibinis, P. E. *AIChE Journal* **2004**, *50*, 2835-2848.

[21] Moreno-Castilla, C.; Rivera-Ultrilla, J. *MRS Bulletin* **2001**, *26*, 890-894.

[22] Rudge, S. R.; Kurtz, T. L.; Vessely, C. R.; Catterall, L. G.; Williamson, D. L. *Biomaterials* **2000**, *21*, 1411-1420.

[23] Oliveira, L. C. A.; Rios, R. V. R. A.; Fabris, J. D.; Garg, V.; Sapag, K.; Lago, R. M. *Carbon* **2002**, *40*, 2177-2183.

[24] Lu, A.-H.; Schmidt, W.; Matoussevitch, N.; Boennemann, H.; Spliethoff, B.; Tesche, B.; Bill, E.; Kiefer, W.; Schueth, F. *Angewandte Chemie, International Edition* **2004**, *43*, 4303-4306.

[25] Selim, S.; (Colorado School of Mines, USA). Application: US
US, 1997, p 17 pp.

[26] Gass, J.; Poddar, P.; Almand, J.; Srinath, S.; Srikanth, H. *Advanced Functional Materials* **2006**, *16*, 71-75.

[27] Jordan, A.; Scholz, R.; Wust, P.; Fahling, H.; Felix, R. *Journal of Magnetism and Magnetic Materials* **1999**, *201*, 413-419.

[28] Karapinar, N. *International Journal of Mineral Processing* **2003**, *71*, 45-54.

[29] Leslie-Pelecky, D. L.; Rieke, R. D. *Chemistry of Materials* **1996**, *8*, 1770-1783.

[30] Drofenik, M.; Lisjak, D.; Makovec, D. *Materials Science Forum* **2005**, *494*, 129-136.

[31] Lisjak, D.; Drofenik, M. *Journal of the European Ceramic Society* **2004**, *24*, 1841-1845.

[32] Stoner, E. C.; Wohlfarth, E. P. *Trans. Roy. Soc. (London)* **1948**, *A240*, 599-644.

[33] de Julian Fernandez, C. *Physical Review B: Condensed Matter and Materials Physics* **2005**, *72*, 054438/1-054438/10.

[34] Mukadam, M. D.; Yusuf, S. M.; Sharma, P.; Kulshreshtha, S. K. *Journal of Magnetism and Magnetic Materials* **2004**, *272-276*, 1401-1403.

[35] Kittel, C. *Physical Review* **1946**, *70*, 965-971.

[36] Cullity, B. D. *Introduction to magnetic materials*; Addison-Wesley Pub. Co.: Reading, Mass.,, 1972.

[37] Hubbuch, J. J.; Thomas, O. R. T. *Biotechnology and Bioengineering* **2002**, *79*, 301-313.

[38] Ditsch, A.; Lindenmann, S.; Laibinis, P. E.; Wang, D. I. C.; Hatton, T. A. *Industrial & Engineering Chemistry Research* **2005**, *44*, 6824-6836.

[39] Zboril, R.; Mashlan, M.; Petridis, D. *Chemistry of Materials* **2002**, *14*, 969-982.

[40] Arshady, R. *Microspheres, Microcapsules & Liposomes* **2001**, *3*, 1-37.

[41] Elmore, W. C. *Physical Review* **1938**, *54*, 309-310.

[42] Fried, T.; Shemer, G.; Markovich, G. *Advanced Materials (Weinheim, Germany)* **2001**, *13*, 1158-1161.

[43] Sun, S.; Zeng, H. *Journal of the American Chemical Society* **2002**, *124*, 8204-8205.

[44] Gallagher, K. J.; Feitknecht, W.; Mannweiler, U. *Nature (London, United Kingdom)* **1968**, *217*, 1118-1121.

[45] Schwertmann, U.; Cornell, R. M. *Iron oxides in the laboratory : preparation and characterization*; 2nd completely rev. and extended ed.; Wiley-VCH: Weinheim ; New York, 2000.

[46] Gillot, B.; Nouaim, H.; Mathieu, F.; Rousset, A. *Materials Chemistry and Physics* **1991**, *28*, 389-397.

[47] Lanjewar, R. B.; Garg, A. N. *Indian Journal of Chemistry, Section A: Inorganic, Bio-inorganic, Physical, Theoretical & Analytical Chemistry* **1991**, *30A*, 350-356.

[48] Cheng, Y.; Zheng, Y.; Wang, Y.; Bao, F.; Qin, Y. *Journal of Solid State Chemistry* **2005**, *178*, 2394-2397.

[49] Zhou, J.; Ma, J.; Sun, C.; Xie, L.; Zhao, Z.; Tian, H.; Wang, Y.; Tao, J.; Zhu, X. *Journal of the American Ceramic Society* **2005**, *88*, 3535-3537.

[50] Kinemuchi, Y.; Ishizaka, K.; Suematsu, H.; Jiang, W.; Yatsui, K. *Thin Solid Films* **2002**, *407*, 109-113.

[51] Peng, C.-H.; Hwang, C.-C.; Hong, C.-K.; Chen, S.-Y. *Materials Science & Engineering, B: Solid-State Materials for Advanced Technology* **2004**, *B107*, 295-300.

[52] Yang, J. M.; Tsuo, W. J.; Yen, F. S. *Journal of Solid State Chemistry* **1999**, *145*, 50-57.

[53] Nathani, H.; Gubbala, S.; Misra, R. D. K. *Materials Science & Engineering, B: Solid-State Materials for Advanced Technology* **2004**, *B111*, 95-100.

[54] Giannakopoulou, T.; Kompotiatis, L.; Kontogeorgakos, A.; Kordas, G. *Journal of Magnetism and Magnetic Materials* **2002**, *246*, 360-365.

[55] Shi, Y.; Ding, J.; Liu, X.; Wang, J. *Journal of Magnetism and Magnetic Materials* **1999**, *205*, 249-254.

[56] Son, S.; Taheri, M.; Carpenter, E.; Harris, V. G.; McHenry, M. E. *Journal of Applied Physics* **2002**, *91*, 7589-7591.

[57] Nakamura, S.; Sakamoto, W.; Yogo, T. *Journal of Materials Research* **2005**, *20*, 1590-1596.

[58] Van Velsen, A. F. M.; Van der Vos, G.; Boersma, R.; De Reuver, J. L. *Water Science and Technology* **1991**, *24*, 195-203.

[59] Chun, C.-L.; Park, J.-W. *Journal of Environmental Engineering (Reston, Virginia)* **2001**, *127*, 443-449.

[60] Peng, Z. G.; Hidajat, K.; Uddin, M. S. *Journal of Colloid and Interface Science* **2004**, *271*, 277-283.

CHAPTER 2

SYNTHESIS AND CHARACTERIZATION OF MAGNETIC ACTIVATED CARBONS (MACs)

INTRODUCTION

Magnetic particle technology and its application in solving environmental problems has been an active field of study in recent years. Magnetic particles can be easily separated from aqueous or gaseous effluents by a simple magnetic process after their use as adsorbents for a wide range of contaminants. Examples of this technology are the use of magnetite particles for the clarification of sewage, magnetic poly(oxy-2,6-dimethyl-1,4-phenylene) for the adsorption of water soluble organic dyes, and polymer-coated steel pellets for oil spill remediation [1-3]. The potential of nanomagnet containing materials for use in advanced technologies arises from their exceptional properties [4-7]. For magnetic separation applications, it is important that the particles used must exhibit superparamagnetic behavior at room temperature and show no remnant magnetization [8,9]. Organophosphorus-extractant coated superparamagnetic carriers are examples of efficient nanomagnets used in magnetically separating actinides from nuclear waste solutions [10]. However, important limitations for these materials, such as low adsorption capacity and low surface areas can limit their applications considerably. Therefore, magnetic materials with new functionalities are needed, and can be realized

through the development of novel synthetic strategies. In particular, composites with high surface areas and accessible porosity would reinforce the magnetic separation technique by extending its applicability to different fields such as waste treatment, catalysis, and drug delivery [11]. There are three basic factors governing the successful production of such composites. First, the matrix should be derived from inexpensive and widely available starting material. Second, the use of iron oxides as the magnetic phase is preferred due to their non-toxicity, stability, and low-cost. Third, in order to optimize the capacity for separation, composites with tunable magnetic properties should be attained. Activated carbons (AC) have been used extensively in environmental chemistry as adsorbents for organic and inorganic contaminants, and in catalysis as supports for noble metal catalysts. Their low cost, remarkable effectiveness, and wide availability, make them good candidates for synthesizing magnetic extractants [12]. In many of their liquid phase applications, activated carbon separation posed a significant problem due to the necessity of expensive and complex procedures such as centrifugation or filtration [11]. Combining tunable magnetic properties with activated carbons' high surface area and porosity through the fabrication of magnetic porous carbons would greatly improve the separation process, rendering it more economically viable.

There are few methods describing the synthesis of magnetic activated carbons and these do not comply with all the aforementioned fundamental factors [13,14]. High-energy milling techniques were reported to produce only low-porosity activated carbon, and iron oxide precipitation strategies yielded materials with large aggregates (>100 nm) of magnetic and nonmagnetic iron oxides. Other procedures involving the deposition of metallic cobalt nanoparticles over commercial highly porous ordered carbon (CMK-3 and

CMK-5) are of a complex nature and have no industrial advantages. Specifically, this synthetic route also suffers from serious environment limitations due to the toxicity of cobalt [15]. Recently, a new method describing the preparation of magnetically active mesoporous carbon was reported [16,17]. This involved the polymerization of pyrrole monomer inside a silica template followed by dispersion of the composite in $FeCl_3$ solution. The Poly(pyrrole)-silica composite was then carbonized under nitrogen to produce the magnetically separable activated carbon. However, the major drawback of this method was the lack of control over the size of the magnetic nanoparticles, thereby yielding magnetic composite exhibiting remnant magnetization.

In this chapter, a simple strategy for the synthesis of magnetically separable activated carbons is presented. The method involves the formation of highly dispersed magnetite and nickel ferrite nanoparticles throughout the porous structure of activated carbon. These materials were prepared by including metal salts in the conventional recipe for activated carbon manufacture. Decomposition of these salts during the pyrolysis step yields the desired magnetic composites. After the characterization of the magnetic powder samples, environmental testing was performed including the adsorption of many organic water contaminants. The application of these materials is carefully reported in Chapters 3 and 6.

EXPERIMENTAL

Chemicals and characterization methods

All chemicals were purchased and used without any further purification. Following are the chemicals involved in this project listed with their supplier. Iron(II) sulfate heptahydrate [$FeSO_4.7H_2O$, Aldrich]; Nickel(II) sulfate hexahydrate [$NiSO_4.6H_2O$, Aldrich]; Nickel hydroxide [$Ni(OH)_2$, Alfa Aesar]; microcrystalline cellulose [$(C_6H_{10}O_5)_n$, EM Science] ; Iron(II) gluconate [$Fe[HOCH_2(CHOH)_4CO_2]_2.2H_2O$, Alfa-Aesar], and nickel gluconate (prepared according to the procedure described later in this chapter). Paper towels were purchased from Acclaim, and sawdust was provided by the Physical Sciences' woodshop at Oklahoma State University.

The magnetic composites were characterized by several techniques. Powder X-ray diffraction (XRD) patterns were recorded on a Bruker AXS D8 Advance diffractometer using Cu Kα radiation with a current flux of 30 mA and an acceleration voltage of 40 kV. For infrared spectroscopic measurements, roughly 10 mg of the material was mixed with approximately 100 mg FTIR-grade potassium bromide and the blend was finely ground. Spectra in the 4000-400 cm^{-1} region were collected by diffuse reflectance of the ground powder with a Nicolet Magna-IR 750 spectrometer. Surface area analysis was performed via the Brunauer Emmett Teller (BET) multilayer nitrogen adsorption method using a Quantachrome Nova 1200 instrument. Scanning Electron Microscopy (SEM) photographs were recorded using a JEOL Scanning Electron Microscope. All pyrolyses for preparation of the modified and unmodified activated carbon were performed in a Thermolyne 21100 tube furnace.

Preparation of nickel gluconate hydrate

The preparation of this precursor was performed according to a procedure described by A. Vecoven [18]. 0.020 moles of nickel hydroxide (1.855 g) and 0.04 moles (15.692 g) of a 45-50 % solution of D-gluconic acid were added to 300 ml of distilled water. The mixture was heated under reflux and stirred constantly for 48 hours. The resulting green solution was concentrated by evaporating about two thirds of the solvent under a reduced pressure atmosphere in a rotary evaporator. The water bath was set at a temperature range between 50 and 60 °C. Isolation of nickel gluconate was accomplished by precipitating it from the dark green solution with 700 ml of methanol. The resulting light green solid was recovered by filtration using a medium porosity glass filter and was then washed several times with 200 ml of methanol. Drying under vacuum overnight, yielded 5.91 g of product.

Synthesis of magnetic activated carbons MAC-1 and MAC-2 using paper towels as a starting material

MAC-1: Saturated iron(II) gluconate solution was prepared by dissolving 4.820 g of iron(II) gluconate in approximately 50 ml of distilled water. The solution was left to settle for 6 hours at room temperature. Using a pipette, the solution was added drop wise to 10.10 g of paper towels to incipient wetness. The wet towels were left to dry under air for 24 hours. After drying, the towels were shredded and placed in an open pyrex tube, then thermally treated under a nitrogen atmosphere at 500 °C in a tube furnace. Twelve hours later, the sample was left to cool under air at room temperature for a few hours. During the cooling step, the resulting powder was exposed to air at which point it became

quite hot due to rapid oxidation of iron(II) oxide to magnetite. This phenomena was observed for all iron oxide containing activated carbons. Fine grinding of the product and thorough washing with methylene chloride yielded a black powder that weighed 3.100 g and was magnetic in nature.

MAC-2: 15.00 g of commercial paper towels were treated with an iron(II) and nickel(II) gluconate solution. The solution was made by dissolving 4.821 g of iron(II) gluconate in 50 ml of water followed by mixing with 2.245 g of nickel (II) gluconate dissolved in 25 ml of water. Paper towels treated with the gluconate solution via the incipient wetness impregnation method were dried in air for 24 hours then pyrolized under nitrogen at 500 °C for 12 hours. The product from this reaction weighed 5.620 grams and was crushed and finely ground to give a magnetic black powder. Finally the powder was washed several times with hexane and methylene chloride then dried under vacuum overnight.

Synthesis of MAC from treated sawdust

MAC-3: 100.00 g of coarse fir sawdust was sieved and treated with 50 ml of 10 % sulfuric acid solution. An iron(II) sulfate solution made by dissolving 5.00 g of $FeSO_4.7H_2O$ in 100 ml of water was added to the sawdust and the mixture was stirred over a hot plate for 30 minutes. After evaporating about 50 ml of the solvent, 20.32 g of the treated sawdust was packed in an open pyrex tube and fired at 500 °C under nitrogen for 4 hours. This resulted in a yield of 6.41 g of black magnetic charcoal.

MAC-4: For the preparation of this sample, the same amounts of ferrous sulfate and sulfuric acid were used to impregnate the sawdust as was used for MAC-3. In this case,

however, the treated sawdust was dried under air overnight. 15.70 g of it was initially pyrolized at 500 °C for 4 hours under nitrogen. The temperature was decreased to 200 °C and the sample was maintained at this temperature for 5 hours under air. Further cooling to room temperature allowed for the sample to be collected, ground, and weighed. The overall yield of this reaction was 4.74 g.

MAC-5: Preparation of this magnetic charcoal was accomplished according to the procedure mentioned above (MAC-4). However, a solution of 1:2 mole ratio Ni(II) gluconate to Fe(II) gluconate was used for treatment instead of the ferrous sulfate. Incipient wetness impregnation of the sawdust with the gluconate solution followed by its thermal treatment yielded the desired magnetic product. The initial weight of the treated sawdust prior to pyrolysis was 20.67 g. The final weight of the product was 5.85 g.

Similarly, *MAC-6* was prepared using nickelous sulfate and ferrous sulfate solution as a source for magnetic character.

Synthesis of activated carbon from sawdust without the addition of any iron or nickel salts was performed for comparative reasons. The reaction conditions were similar to those used in the preparation of magnetic charcoals derived from sawdust. This sample of activated carbon was designated as *SBAC*.

Synthesis of cellulose-based magnetic activated carbons

The matrix of this family of magnetic carbons was derived from microcrystalline cellulose. The following section describes the preparation of two magnetic powders, MAC-7 and MAC-8, along with an unmodified activated charcoal CBAC.

MAC-7: By incipient wetness impregnation, 30 ml of a concentrated iron(II) gluconate solution were added to 15.01 g of cellulose. 8 ml of 10 % H_2SO_4 solution were introduced to the wet cellulose by drop wise addition. A 21.58 g portion of the dried, treated cellulose were pyrolyzed and cooled according to the method for MAC-4 preparation. The reaction yielded 5.51 g of fine black magnetic powder.

MAC-8: In this case, a concentrated solution of $FeSO_4.7H_2O$ made by dissolving 7.50 g of the iron salt in 16 ml of water was used as an iron source instead of iron(II) gluconate. The amount of modified cellulose used for heat treatment was 23.96 g, and the yield of the reaction was 6.02 g.

CBAC is a cellulose based activated charcoal synthesized using the technique mentioned in this section. The cellulose used for this activated carbon was only treated with a 10 % sulfuric acid solution, and dried before pyrolysis.

RESULTS AND DISCUSSION

Magnetic character

A facile method for making magnetically-active activated carbons was developed. These composites were simply prepared by impregnating different starting materials (paper towels, sawdust or cellulose) with iron or iron/nickel sulfate or gluconate aqueous mixtures and then subjecting them to a procedure for preparation of activated carbon [19]. X-ray powder diffraction revealed the presence of nanocrystalline iron or nickel salts in the resulting materials along with traces of calcium sulfate derived from calcium ions naturally present in wood. In the iron-containing activated carbon, the iron oxide phase was identified by XRD to be magnetite (Fe_3O_4). The XRD pattern of the

sawdust/nickel + iron sulfate derived activated carbon displayed broad reflections for γ-Fe_2O_3 (maghemite) and $FeNi_2S_4$ (violarite) as shown in Figure 2-1 [20]. On the other hand, when nickel and iron gluconates were used, $NiFe_2O_4$ (trevorite) was detected in the sample and the intensity of violarite was significantly decreased (Figure 2-2). This accompanied approximately a 100 m^2/g increase in surface area. The broadness of the X-ray diffraction reflections of these phases clearly indicated that the bulk of the metal oxides are dispersed as nanoparticles. The advantage of this is the prevention of the particles from becoming permanently magnetized.

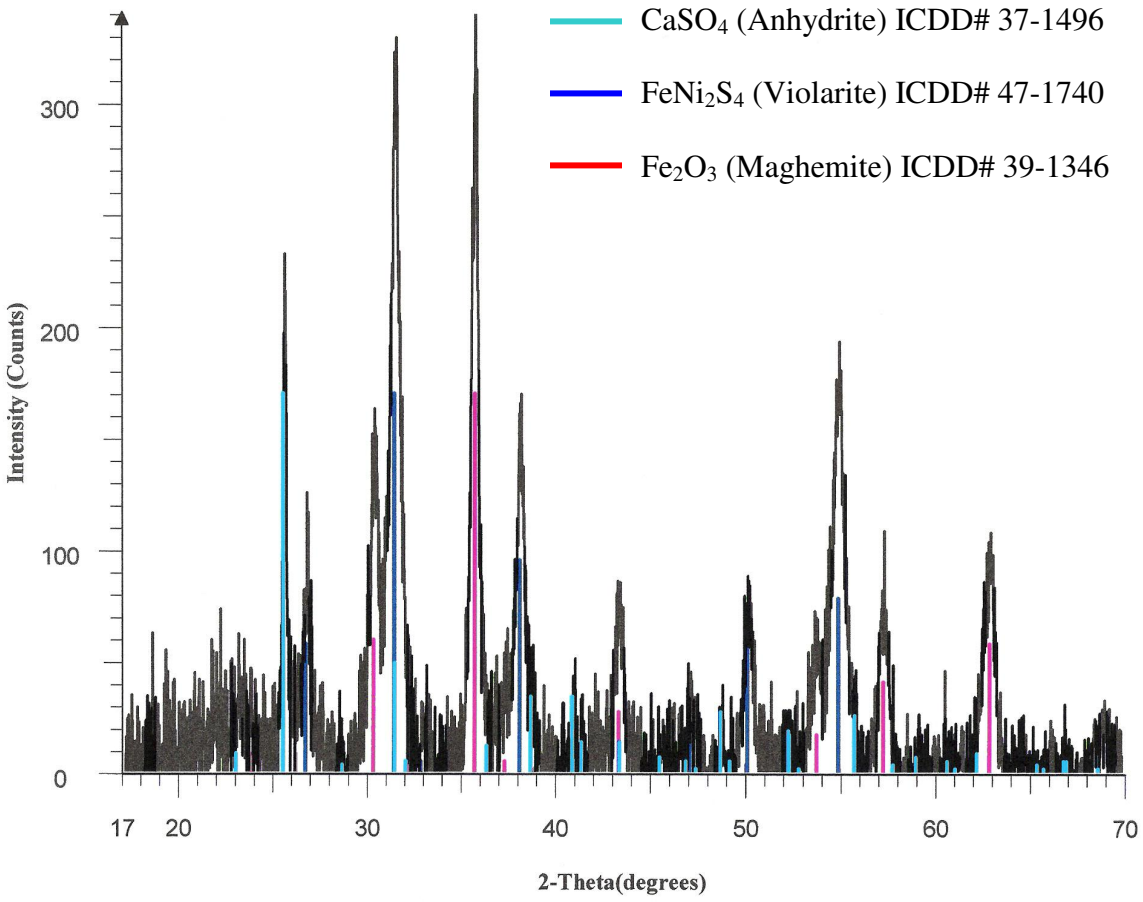

Figure 2-1: The XRD pattern of MAC-6, magnetic activated charcoal prepared from sawdust treated with nickel and iron sulfates

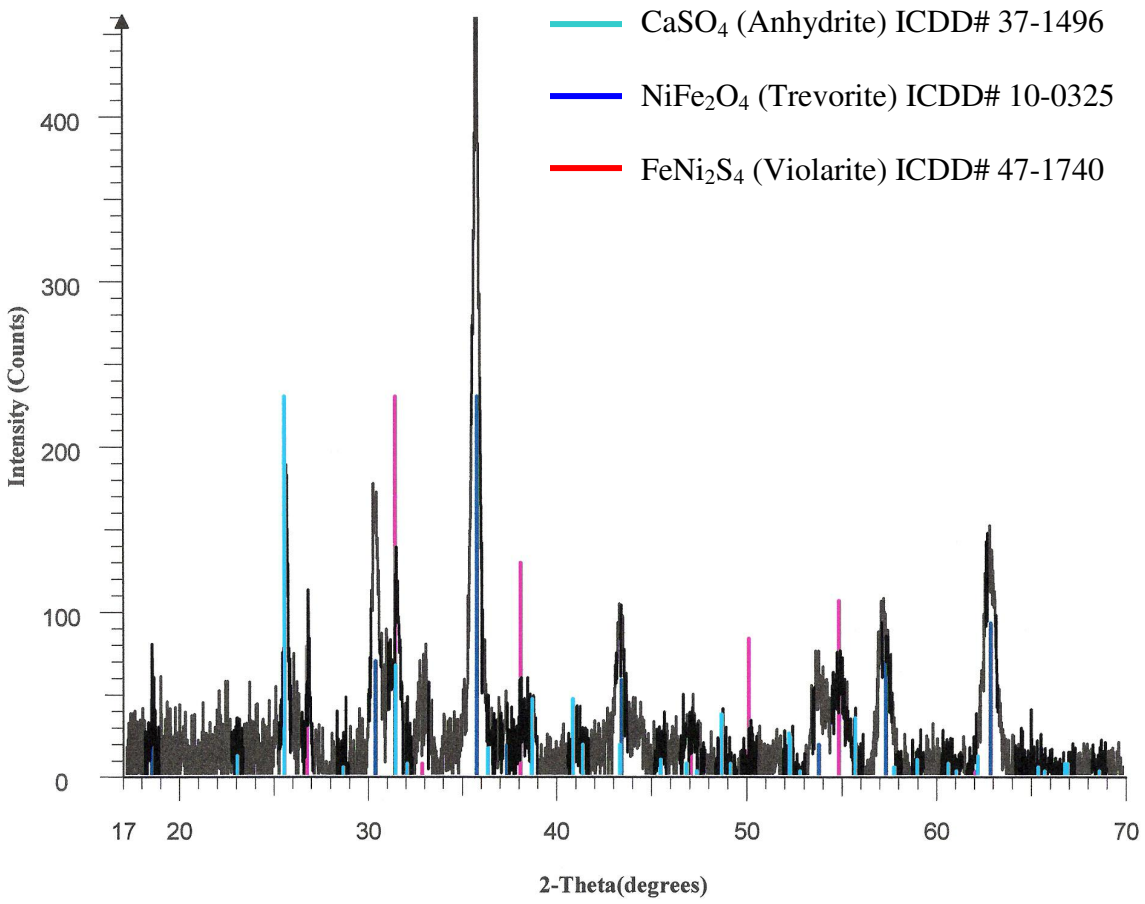

Figure 2-2: The XRD pattern of MAC-5, magnetic activated charcoal prepared from sawdust treated with nickel and iron gluconates

No remnant magnetization was observed for the magnetic powders when the power to the magnet was switched off. This prevented the powder from clumping together or sticking to non magnetized steel. This property is beneficial and essential to magnetic particles used for environmental applications. The XRD pattern of MAC-6 is presented in Figure 2-1 and reveals evidence for the formation of iron oxide nanoparticles with a defect spinel structure (maghemite, γ-Fe_2O_3). When iron and nickel gluconates were used during the sawdust treatment step, nickel ferrite was observed in the XRD pattern of MAC-5 (Figure 2-2). Notably, the reduction of the amount of sulfate led to a decrease in the amount of the violarite phase. The XRD pattern of a magnetic carbon obtained from a

source with high organic content (cellulose) is reported in Figure 2-3. This diffractogram suggests that the main magnetic phase present is maghemite and it shows no observable traces of anhydrite or violarite. Thus, an enhancement in the magnetization of this sample can be produced by reducing maghemite to magnetite through hydrogen gas treatment at elevated temperatures (600 °C) [21]. This enhancement, however, would be minimal since magnetite and maghemite exhibit a difference in magnetic moments of only about 15 % in bulk, which creates an equivalency between these two phases when either is used in environmental applications such as separation [11].

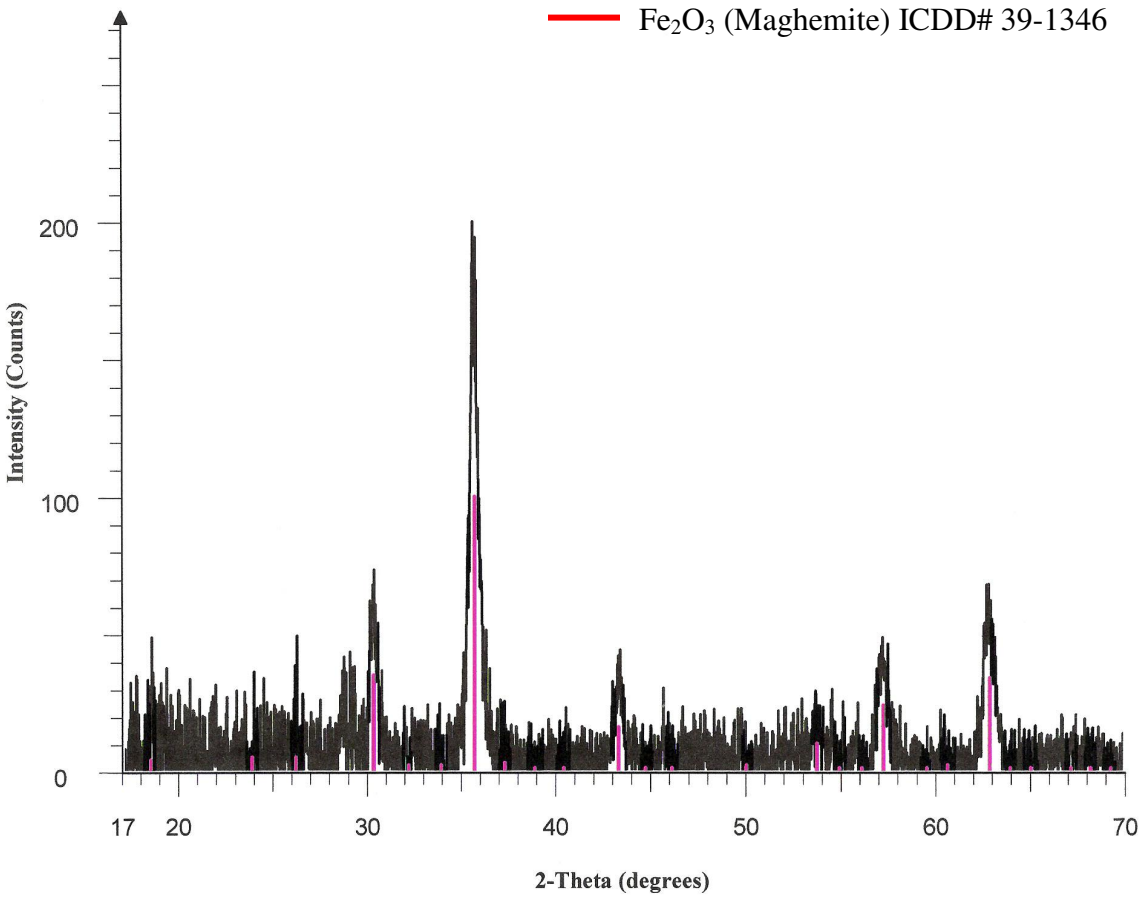

Figure 2-3: The XRD pattern of MAC-7, magnetic activated charcoal prepared from cellulose treated with nickel and iron gluconates

Experimentally, all of the magnetic activated carbon particles are visibly attracted by a magnet. Moreover, these particles show the same clear attraction when they are contained as aqueous dispersions in glass vials.

BET surface area

A comparison of the surface areas for the different magnetic and non-magnetic activated carbons is shown in Table 2-1. It is evident that the use of gluconates in the treatment step, yielded composites with higher surface areas. Conversion of the gluconate to carbon, increasing the carbon content of the product is suggested to have a direct involvement with this increase. On the other hand, the surface area of the non-magnetic raw activated carbon is somewhat lower than that of their magnetic counterparts. This enhancement in the overall surface area of the magnetic composite can be attributed to the formation of high surface area iron oxide and nickel ferrite nanoparticles in the carbon matrix. An observation that disagrees with previously reported results on the synthesis of iron/carbon composite particles from commercially available activated carbon [13]. In this mentioned investigation, high energy ball milling of high surface area (1440 m^2/g) commercial activated carbon and iron mixtures, produced a lower surface area (226 m^2/g) magnetic composite. The significant loss in surface area was suggested to be due to crushing or occlusion of pores. Hence, the method developed in this study holds structural, environmental, and economical advantages on existing techniques such as high energy ball milling.

Table 2-1: BET surface areas of the magnetic and non-magnetic activated charcoals

Sample Name	Starting Material	Ni / Fe Source	BET Surface Area S_a (m^2/g)
MAC-1	Paper towels	Fe(II) gluconate	42
MAC-2	Paper towels	Fe(II) + Ni(II) gluconates	78
MAC-3	Sawdust	Fe(II) sulfate	273
MAC-4	Sawdust	Fe(II) sulfate	316
MAC-5	Sawdust	Fe(II) + Ni(II) gluconates	365
MAC-6	Sawdust	Fe(II) + Ni(II) sulfates	265
MAC-7	Cellulose	Fe(II) gluconate	288
MAC-8	Cellulose	Fe(II) sulfate	279
SBAC	Sawdust	Acid treatment only	183
CBAC	Cellulose	Acid treatment only	237

Chemistry of the carbon surfaces

The two main factors governing the adsorptive characteristics of activated carbon are its porous structure and the chemical nature of the surface [22]. In general, the

infrared spectra for all of the prepared samples are very similar, and there are only minute differences observed in the region 1200 – 1700 cm^{-1}. Activated carbons usually exhibit a broad band in this region, an observation reported by many researches but still to be interpreted definitely [23]. FT-IR spectra of four of the activated carbon samples are displayed in Figures 2-4 and 2-5. The various bands and shoulders exhibited by the SBAC spectrum were attributed to different vibration modes in atomic groups and structures, are presented in Table 2-2. Basal planes comprise more than 90% of the activated carbon surface [24]. Normally, the olefinic C=C stretching band appears at 1650 cm^{1} and the shift towards lower wavenumbers in the absorption maximum may occur when the C=C bond is conjugated with another C=C bond, a C=O bond, or an aromatic nucleus [24]. Therefore, an association of the C=C stretching band of the graphene groups and the bands observed near 1589 cm^{-1} in Figures 2-4 and 2-5 can be valid. Increased aromatization upon heat treatment is clearly indicated by the intense aromatic C=C and aromatic C-H bending vibrations of the activated charcoals pyrolyzed at temperature of 500 °C [25]. This specific temperature was chosen for pyrolysis to avoid the formation of an intermediate melt in the char resulting from the decomposition and softening of some raw material fractions at temperatures above 500 °C, which will clog and seal off part of the activated carbon pores [26]. A definite outcome of this increase will include a significant decline in both micropore volume and BET surface area of the MAC [26]. Moreover, it is well known that as the carbonization temperature increases, structural modifications occur, mainly showing a decrease in the CO, C-O, CH_2 and CH_3, and OH containing structures, which might have a negative effect on the magnetic activated carbons' adsorption efficiency [27].

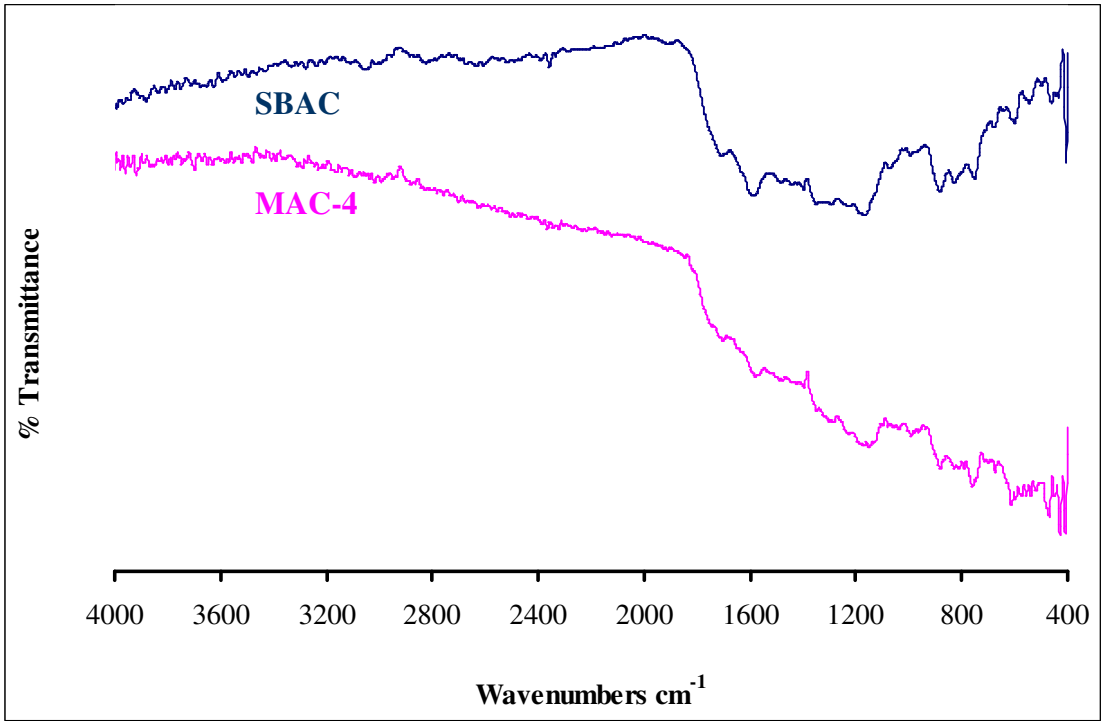

Figure 2-4: FT-IR spectra of unmodified sawdust-derived activated carbon (SBAC) and the sawdust-derived activated carbon/iron oxide composite (MAC-4)

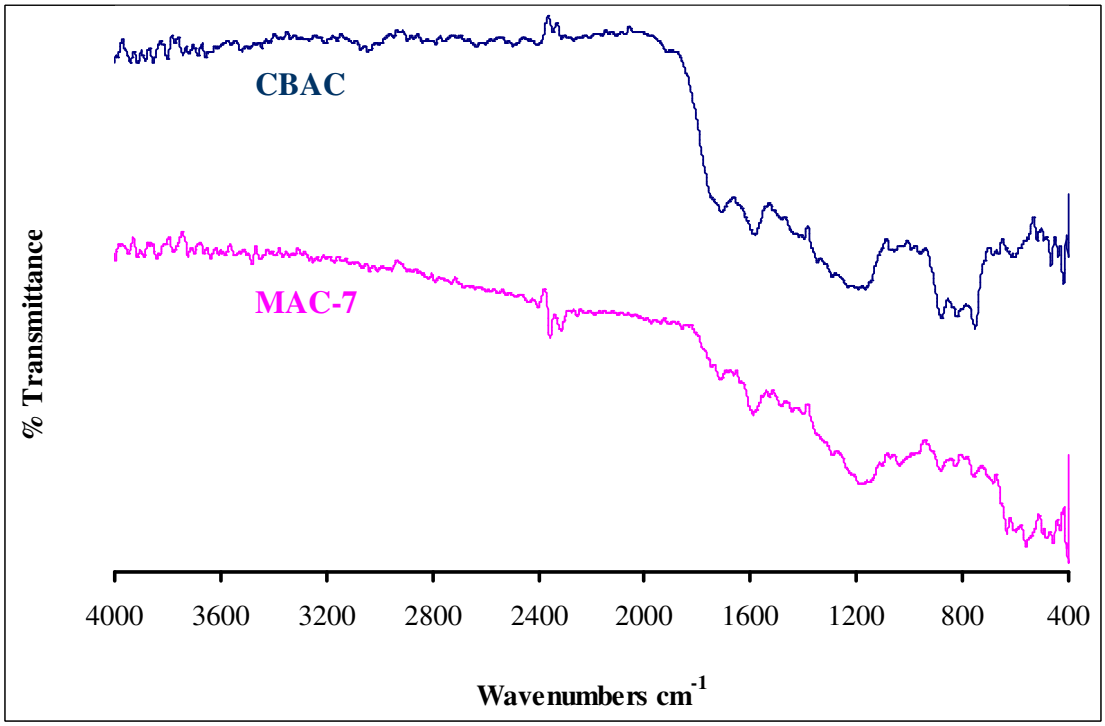

Figure 2-5: FT-IR spectra of unmodified cellulose-derived activated carbon (CBAC) and cellulose-derived activated carbon/iron oxide composite (MAC-7)

Table 2-2: FT-IR assignments for SBAC spectrum

Band Position in Wavenumbers (cm^{-1})	**Abbreviation**	**Assignment**
1680	υ(C=O)	C=O stretching vibrations in carbonyl groups
1589	υ(C=C)	C=C stretching vibrations in aromatic rings (skeletal)
1450	υ(C=C)	C=C stretching vibrations in aromatic rings
1397	υ(C-O)	C-O stretching vibrations in carboxylate groups
1162	υ(C-O)	C-O stretching vibrations in alcohols, phenols, ester or ether groups
880	γ(C-H)	C-H out of plane bending in benzene derivatives
828	γ(C-H)	C-H out of plane bending in benzene derivatives
750	γ(C-H)	C-H out of plane bending in benzene derivatives

It can be seen that the FT-IR spectra of the unmodified activated carbons and the corresponding magnetic composites are analogous, indicating a similarity in surface functional groups and chemical nature.

Morphology and microstructure

The morphology of the magnetic activated carbons was studied by scanning electron microscopy. Figure (2-6-a and d) shows clusters of MAC-3 and MAC-5 particles in their as-prepared size range where an irregularity in their shape is observed. These clusters can be easily broken by shear or sonnication. Iron and nickel elemental mapping at higher magnification for random regions of both samples were generated and presented in Figure 2-6 (c and f). Here, the presence of iron (the red dots) within the entire particle is revealed for MAC-3. When a combination of iron and nickel salts is used, the presence of both metals, hence the formation of nickel ferrite particles within the MAC structure was clearly unraveled by the elemental mapping technique. In Figure 2-6 (f), iron and nickel signals (red and green dots) are clearly observable in unison along the magnified V-shaped area chosen. This proves the experimental observation of the attraction of all magnetic carbon particles when subjected to an external magnetic field. Similarly, SEM images and iron elemental mapping scan of cellulose based maghemite/activated carbon composites are shown in Figure 2-7.

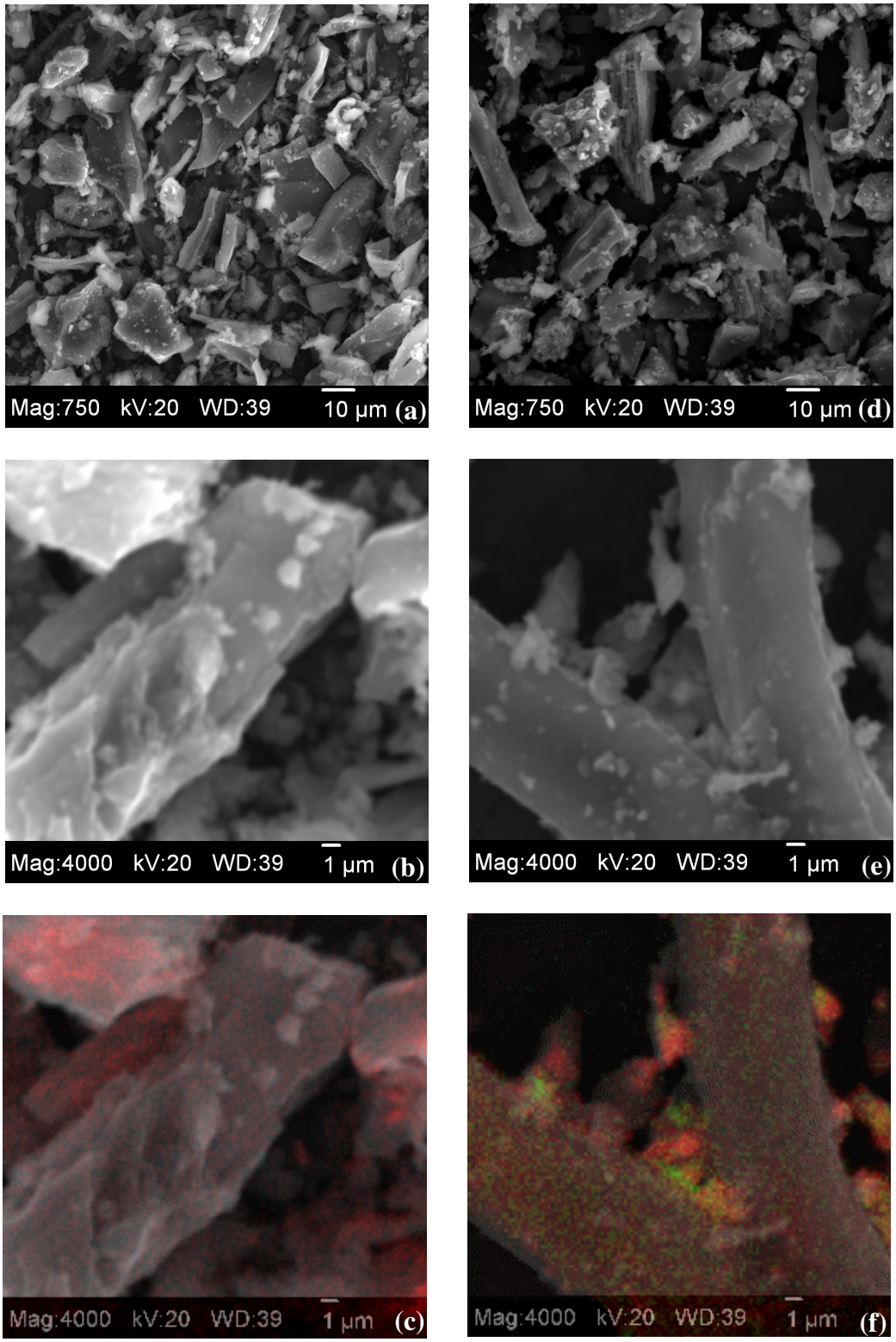

Figure 2-6: SEM images and elemental mapping scans of the sawdust-derived activated carbon/iron oxide composite, MAC-3 (a, b, and c) and the sawdust-derived activated carbon/nickel ferrite composite, MAC-5 (d, e, and f)

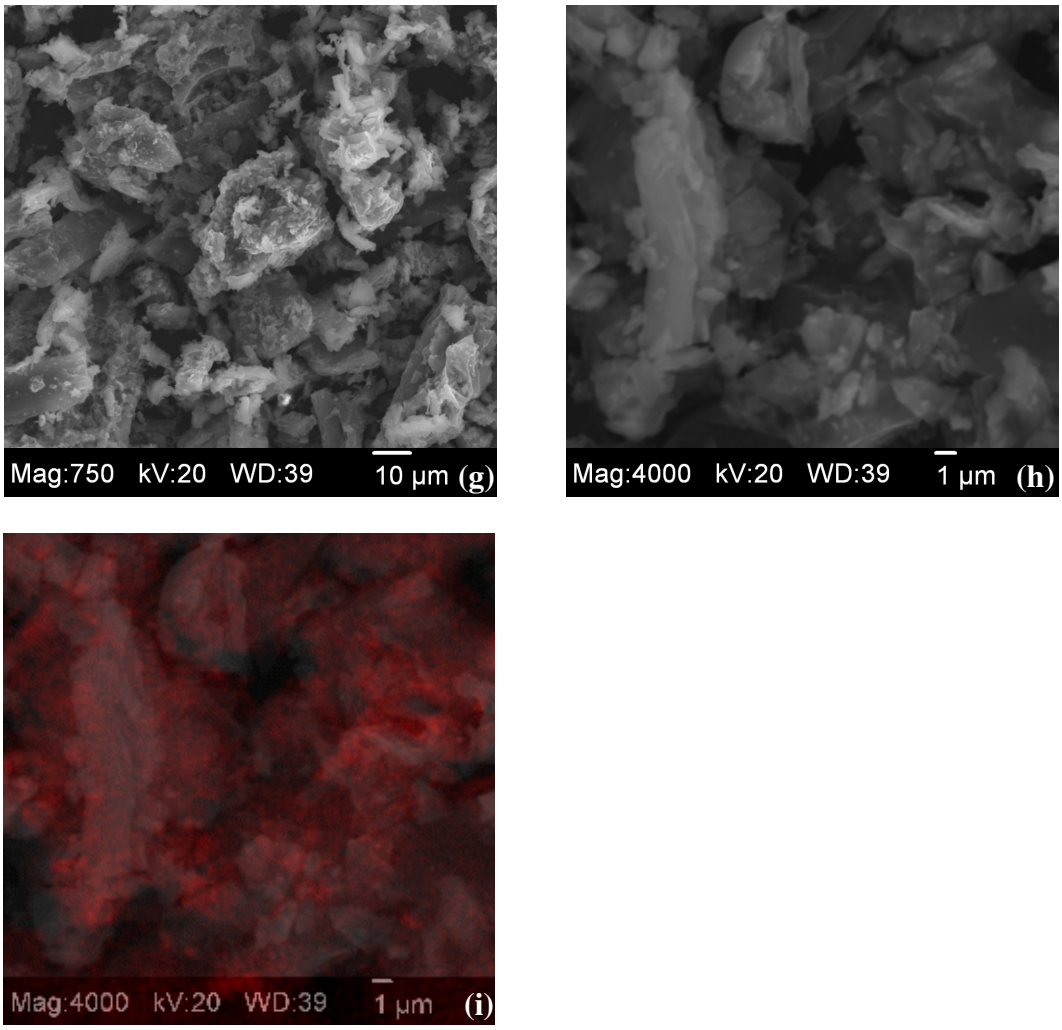

Figure 2-7: SEM images and elemental mapping scan of cellulose-derived activated carbon/iron oxide composite, MAC-7 (g, h, and i)

CONCLUSIONS

In summary, the development of simple and versatile route for the preparation of magnetically separable composites from industrial and household byproducts was attained. The magnetic activity of the charcoals is provided by iron oxide and nickel ferrite nanoparticles formed within the porous network via thermal treatment at 500 °C of the treated starting material under nitrogen, and activation at 200 °C under air. The obtained MAC's, exhibited relatively large surface areas and no remnant magnetization. These two important properties along with the ability of the composites to be easily manipulated by a low external magnetic field allow for their use as magnetic extractants. In the next chapter, selected samples were tested and employed in the magnetic removal of decane, 4, 6-dinitro-o-cresol, and Congo red dye from aqueous solutions.

REFERENCES

[1] Booker, N. A.; Keir, D.; Priestley, A. J.; Ritchie, C. B.; Sudarmana, D. L.; Woods, M. A. *Water Science and Technology* **1991**, *23*, 1703-1712.

[2] Safarik, I.; Safarikova, M.; Buricova, V. *Collection of Czechoslovak Chemical Communications* **1995**, *60*, 1448-1456.

[3] Orbell, J. D.; Godhino, L.; Bigger, S. W.; Nguyen, T. M.; Ngeh, L. N. *Journal of Chemical Education* **1997**, *74*, 1446-1448.

[4] Skumryev, V.; Stoyanov, S.; Zhang, Y.; Hadjipanayis, G.; Givord, D.; Nogues, J. *Nature (London, United Kingdom)* **2003**, *423*, 850-853.

[5] Redl, F. X.; Cho, K. S.; Murray, C. B.; O'Brien, S. *Nature (London, United Kingdom)* **2003**, *423*, 968-971.

[6] Tartaj, P.; Serna, C. J. *Journal of the American Chemical Society* **2003**, *125*, 15754-15755.

[7] Berry, C. C. *Journal of Materials Chemistry* **2005**, *15*, 543-547.

[8] Nam, J.-M.; Thaxton, C. S.; Mirkin, C. A. *Science (Washington, DC, United States)* **2003**, *301*, 1884-1886.

[9] Pankhurst, Q. A.; Connolly, J.; Jones, S. K.; Dobson, J. *Journal of Physics D: Applied Physics* **2003**, *36*, R167-R181.

[10] Nunez, L.; Kaminski, M. D. *Journal of Magnetism and Magnetic Materials* **1999**, *194*, 102-107.

[11] Fuertes, A. B.; Tartaj, P. *Chemistry of Materials* **2006**, *18*, 1675-1679.

[12] RC Bansal, J. D., Stoeckli F. *Active Carbon*; Marcel Dekker: NY, 1985.

[13] Rudge, S. R.; Kurtz, T. L.; Vessely, C. R.; Catterall, L. G.; Williamson, D. L. *Biomaterials* **2000**, *21*, 1411-1420.

[14] Oliveira, L. C. A.; Rios, R. V. R. A.; Fabris, J. D.; Lago, R. M.; Sapag, K. *Journal of Chemical Education* **2004**, *81*, 248-250.

[15] Lu, A.-H.; Schmidt, W.; Matoussevitch, N.; Boennemann, H.; Spliethoff, B.; Tesche, B.; Bill, E.; Kiefer, W.; Schueth, F. *Angewandte Chemie, International Edition* **2004**, *43*, 4303-4306.

[16] Lee, J.; Lee, D.; Oh, E.; Kim, J.; Kim, Y.-P.; Jin, S.; Kim, H.-S.; Hwang, Y.; Kwak, J. H.; Park, J.-G.; Shin, C.-H.; Kim, J.; Hyeon, T. *Angewandte Chemie, International Edition* **2005**, *44*, 7427-7432.

[17] Lee, J.; Jin, S.; Hwang, Y.; Park, J.-G.; Park, H. M.; Hyeon, T. *Carbon* **2005**, *43*, 2536-2543.

[18] Vecoven, A. C., *Innovative processes for metal oxide ceramic synthesis,* Oklahoma State University, 2001.

[19] Yehaskel, A. *Activated carbon : manufacture and regeneration*; Noyes Data Corp.: Park Ridge, N.J., 1978.

[20] Apblett, A.; Al-Fadul, S. M.; Trad, T. M. *Ceramic Transactions* **2003**, *143*, 15-22.

[21] Oliveira, L. C. A.; Rios, R. V. R. A.; Fabris, J. D.; Garg, V.; Sapag, K.; Lago, R. M. *Carbon* **2002**, *40*, 2177-2183.

[22] Coughlin, R. W.; Ezra, F. S. *Environmental Science and Technology* **1968**, *2*, 291-297.

[23] Akhter, M. S.; Keifer, J. R.; Chughtai, A. R.; Smith, D. M. *Carbon* **1985**, *23*, 589-591.

[24] Sabio, E.; Gonzalez, E.; Gonzalez, J. F.; Gonzalez-Garcia, C. M.; Ramiro, A.; Ganan, J. *Carbon* **2004**, *42*, 2285-2293.

[25] Jagtoyen, M.; Thwaites, M.; Stencel, J.; McEnaney, B.; Derbyshire, F. *Carbon* **1992**, *30*, 1089-1096.

[26] Lua, A. C.; Yang, T. *Journal of Colloid and Interface Science* **2004**, *276*, 364-372.

[27] Olivares-Marin, M.; Fernandez-Gonzalez, C.; Macias-Garcia, A.; Gomez-Serrano, V. *Applied Surface Science* **2006**, *252*, 5980-5983.

CHAPTER 3

REMOVAL OF 4, 6-DINITRO-O-CRESOL, CONGO RED DYE, AND DECANE FROM WATER USING MAGNETIC ACTIVATED CARBONS

INTRODUCTION

The widespread contamination of surface and ground waters by organic compounds can profoundly impact wildlife and drinking water quality. Nitroaromatic and phenolic compounds are among the most common water contaminants because they are widely used as pesticides, herbicides, chemical cleaning agents, and solvents. Due to their poor biodegradability, toxicity, and accumulation potential in animal and plant tissues, they represent an increasing environmental problem [1,2]. As a result, these materials have been classified as hazardous pollutants because of their harmful effect on human health via the many possible routes of entry into the food chain [3]. Dyes and pigments, another major group of organic water pollutants, are generally found in the discharged effluents of textile, dyeing, leather, pulp and paper, and printing industries [4]. Their annual worldwide production comprise 70,000 tons and 10,000 types, of which about 20-30% are released into the environment through wastewaters and industrial effluents [5]. Many dyestuffs and pigments are structurally stable and difficult to biodegrade and many are considered to be carcinogenic and highly toxic to living beings [6]. Medical reports have shown that some dyes can cause dermatitis, skin irritation, allergy, and cancer in

humans [7]. Thus, early removal of organic pollutants from industrial effluents before they get introduced into unpolluted natural waters is of significant interest to environmental agencies and researchers all over the world.

Basic water treatment methods including screening, aeration, sedimentation, flocculation, filtration (using sand beds), chlorination (disinfection), and hardness reduction are not particularly engineered to remove organic compounds and trace metals [8]. Moreover, using these processes that are important for the improvement of drinking water quality can create additional pollution problems through the incorporation of potentially toxic manufactured chemicals such as organic flocculents (acrylamide and epichlorohydrin) and disinfectants (chlorine, chloramine, or bromine). Therefore, the attainment of high quality drinking water is usually accomplished when advanced water treatment technologies are used. The most common of these technologies are the following [8]:

- Granular activated carbon (GAC), used since the 1900s for the removal of dissolved organic compounds from water.
- Ion exchange resins, used for decades mainly to remove inorganic ions.
- Ultraviolet light, recently being evaluated for the treatment of aquatic viruses and bacteria, and oxidation of organics using photochemically generated hydroxyl radicals.
- Ozonation, used on a large scale in Europe to oxidize some organic compounds and as an alternative water disinfecting process (instead of bromine and chlorine).
- Membrane separation (reverse osmosis), a method developed in the early eighties for the removal of organic and inorganic contaminants from water.

- Organic polymers, a number of advanced polymers are introduced in the flocculation step in order to provide enhanced coagulation.

Magnetic filtration has emerged in the last few decades as a modern water treatment technology that can provide rapid, efficient removal of pollutants from aqueous waste streams. The electronic control over magnetic filters eliminates the need for mechanical contact, thus making the technology safer for water treatment plant workers by minimizing their exposure to harmful agents [9]. However, since most common pollutants are generally non-magnetic, materials that can bind to environmental contaminants and be magnetically separated from aqueous solutions must be developed [9].

Activated carbon is considered as one of the best technologies implemented in water purification systems and is the most used [10]. This material can be produced from a variety of carbonaceous solid precursors. Activated carbon's large surface areas, variable surface chemistry, and highly developed porosity account for their versatility in adsorbing pollutants [11]. These unique properties in combination with appropriate magnetic activity can provide the basis for developing highly effective magnetic adsorbents. In Chapter 2, the successful demonstration of the feasibility of synthesizing such adsorbents from low-cost carbonaceous materials was described. In this chapter, the removal of a number of water pollutants using magnetic activated carbons as single component magnetic extractants for magnetic filtration is discussed.

EXPERIMENTAL

Materials and methods

All ACS grade reagents used in this study were purchased either from Strem Chemicals or Aldrich Chemical Company. Along with HPLC grade hexane and other solvents, all of these chemicals were used as received without any further purification. Reverse osmosis and deionization methods were used to purify water.

Magnetic and non-magnetic activated carbons prepared and characterized in Chapter 2 were used as adsorbents for 4, 6-dinitro-*o*-cresol (DNOC). The samples chosen for this application were sawdust based magnetic activated carbon MAC-3, cellulose based activated carbon CBAC, and cellulose based magnetic activated carbons MAC-7 and MAC-8. Commercial activated carbon Darco G-60 (with a specific surface area of 651 m^2/g) purchased from Fisher Scientific was also used as received. Adsorption experiments were performed by reacting a fixed amount of the adsorbent (0.1 g) with a series of DNOC concentrations. Each mixture was left to react on a rotor mill for approximately 5 hours. After calculating the equilibrium concentrations, adsorption capacities were determined using the Langmuir isotherm.

A magnetic activated carbon (MAC-9) made from sawdust according to the procedure described in Chapter 2 (MAC-9, SSA= 258 m^2/g), was physically activated and tested for the adsorption of Congo red (Figure 3-1) from an aqueous solution. An accurately weighed quantity of the dye was dissolved in the purified distilled water for the preparation of a stock solution (133.14 mg l^{-1}). Calibration curves between absorbance and concentration were constructed using a UV/Vis spectrophotometer. The

concentrations of Congo red were determined using the absorbance at its characteristic wavelength of maximum absorption at 497 nm.

Low-cost magnetic extractants MAC-1 and MAC-2 prepared as described in Chapter 2 were tested for the removal of decane from water. The adsorbents were directly mixed with a decane solution with known concentration, left to react for a few hours then magnetically filtered. The decane in the filtrate was extracted by liquid-liquid extraction using hexane and the final decane concentration was determined by GC/MS as described below.

Magnetic filter

The lab scale magnetic filtration device was designed using a 24 V extended-reach-electromagnet with a 170 pound pull and dimensions 3”x1”x1.4” and filtration columns. The electromagnet was powered by a 30 watt direct current power supply. A filtration column constructed by packing glass pipettes loosely with fine grade steel wool was attached to the latter. An illustration of this device is shown in Figure 3-2.

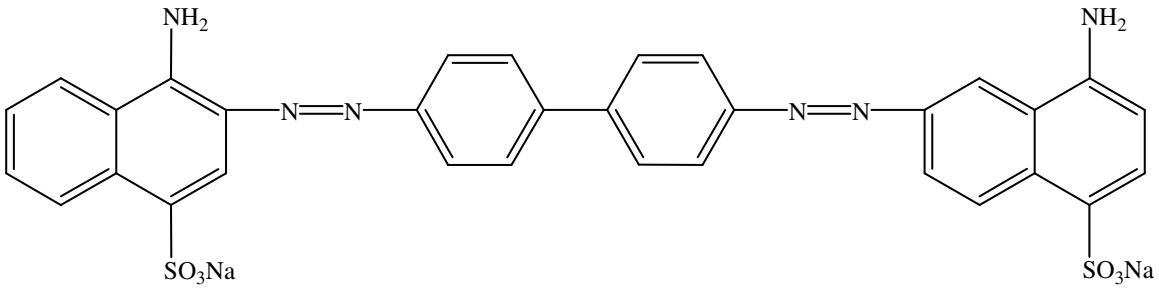

Figure 3-1: The molecular structure of congo red

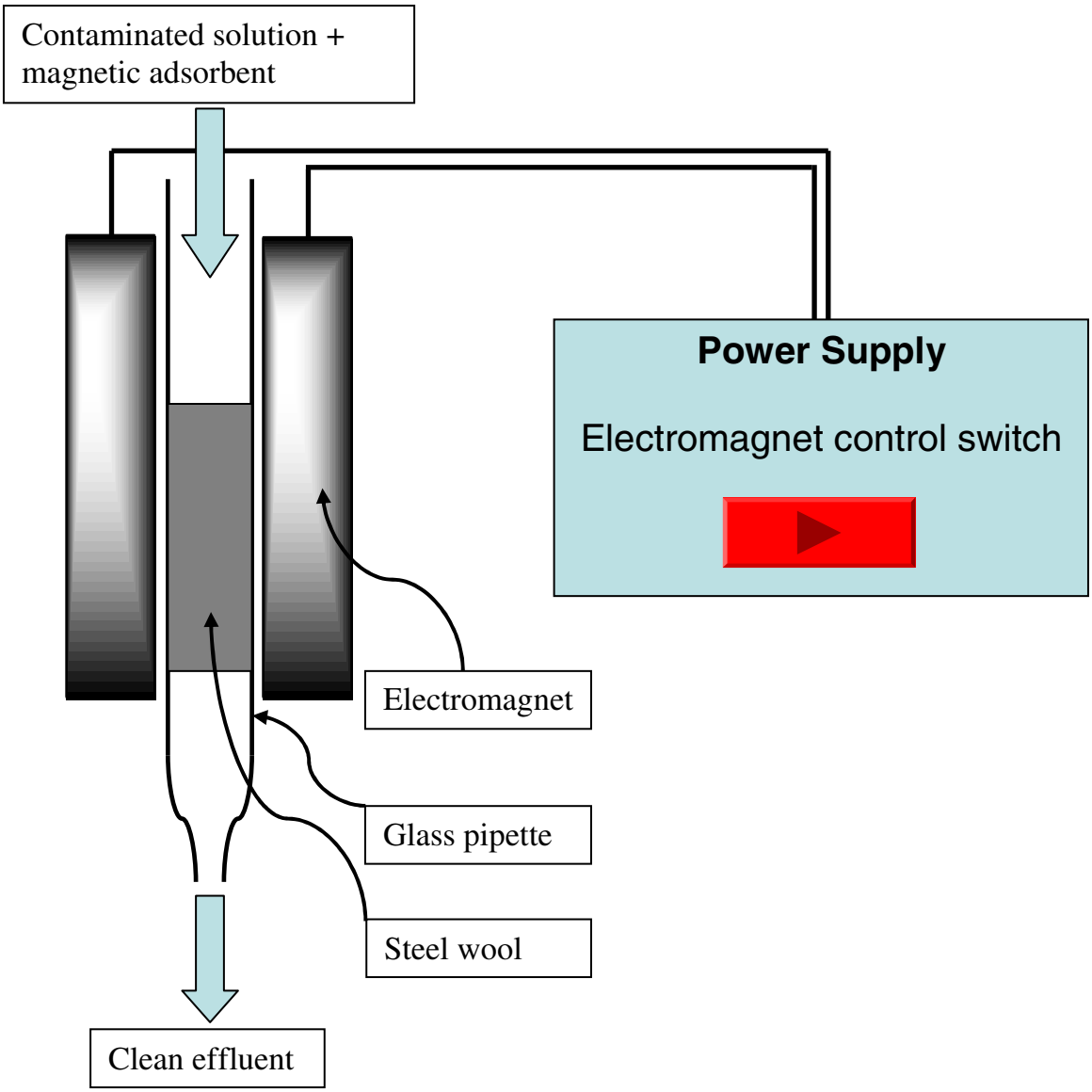

Figure 3-2: Sketch of the magnetic filtration device used in the water treatment procedure

Analytical measurements

UV/Vis spectra were recorded on an Agilent 8453 UV-visible spectrophotometer that uses two light sources, a deuterium and a tungsten lamp. Agilent chemstation software was used to analyze the generated data. The UV/visible spectrophotometer was used mainly with DNOC and Congo red dye extraction experiments.

Analysis of decane in treated solutions was performed using a Hewlett Packard G1800A gas chromatographic/mass spectroscopic (GC/MS) analysis instrument. The temperature program used was an initial hold of 2 min at 35 °C, a ramp of 5 °C/min to 170 °C, and a final hold of 5 min. The instrument was equipped with a HP5 column (crosslinked 5% PhME silicone) with dimensions of 30 m x 0.25mm. The injection port was set at 250 °C and the helium flow rate was 1 ml/min. The mass spectrometer was used in the selective ion monitoring mode with the parent ion of decane (m/e = 142 a.m.u).

RESULTS AND DISCUSSION

Adsorption of DNOC on sawdust and cellulose-based magnetic activated carbons

For this application, all experiments were performed at room temperature using 20 ml glass vials. The procedure consisted of maintaining a fixed amount of the adsorbent and varying the initial concentrations of the DNOC aqueous solutions. In each case, approximately 0.1 g of the adsorbent was added directly to the reaction vessel containing 10 ml of the DNOC solution. The series of DNOC concentrations in the aqueous solutions ranged from 20 to 40 ppm. The capped vials were mixed for 5 hours at around 70 rpm on a rotor mill in order to reach equilibrium. After equilibrium was attained, the adsorbent was magnetically retrieved using the previously illustrated magnetic filter. Equilibrium concentrations were determined using UV/Vis spectrophotometry, where the parent peak at maximum wavelength λ_{max} = 369 nm presented by the DNOC spectrum was used to quantify its concentration. The adsorbed

amount (mg) of DNOC was calculated from the difference between initial and equilibrium concentrations multiplied by the volume of solution used in liters.

A defined distribution of solute between solid and liquid phases exists at equilibrium [12]. At a given temperature, the relationship between the solute equilibrium concentration in a solution and the amount of solute adsorbed on the solid is normally expressed in an adsorption isotherm. A variety of different adsorption equations describing liquid phase adsorption for single-component systems have been proposed [13]. Basically, some of these models rely on theoretical foundations and some are of an empirical nature [12]. For the purpose of describing adsorption equilibria, the Langmuir isotherm equation is one of the simplest and most widely used. The derivation of the Langmuir equation is based on both statistical and thermodynamic considerations [14,15]. The basic assumption in the Langmuir model is localized adsorption, with only one molecule per adsorption site, no interaction between adsorbed molecules, and with equal adsorption energies for all active sites. Moreover, only one layer of adsorbed molecules can be formed on the surface [15]. The shape of the adsorption isotherms can be approximated by the Langmuir equation generally expressed as:

$$X = \frac{\theta^o K C_{eq}}{1 + K C_{eq}} \tag{1}$$

Where **X** is the amount of DNOC adsorbed per unit weight of adsorbent (mg g^{-1}), It can also be referred as the adsorption density at the equilibrium solute concentration (C_{eq}), $\mathbf{C_{eq}}$ is the equilibrium concentration of DNOC in aqueous solutions (mg l^{-1}), $\boldsymbol{\theta^o}$ (mg g^{-1}) is the maximum adsorption capacity corresponding to the complete adsorbate coverage of an adsorbent monolayer, and it's one of Langmuir constants, **K** (l mg^{-1}) is the Langmuir

constant related to the energy of adsorption by an Arrhenius-type equation expressed in the form:

$$K = K_o e^{\frac{-E}{RT}} \tag{2}$$

Where $\mathbf{K_o}$ is a constant containing the entropy, **E** is the adsorption energy, **R** is the universal gas constant, and **T** is the absolute temperature.

The rearrangement of Equation 1 gives the following linear form:

$$\frac{C_{eq}}{X} = \frac{C_{eq}}{\theta^o} + \frac{1}{\theta^o K} \tag{3}$$

A linear plot of C_{eq}/X versus C_{eq} using this equation implies that the Langmuir model fits the generated data. Figures 3-3 and 3-4 show the Langmuir isotherm plots for the adsorption of DNOC using various adsorbents. The monolayer adsorption capacities of the magnetic extractants in comparison to the non-magnetic commercial charcoal (CAC) along with the correlation coefficients are presented in Table 3-1. The coefficient of determination, R^2, values of the linear relationships are very close to unity, which demonstrates the applicability of the Langmuir model. The monolayer adsorption capacities of the different extractants are of the following order: CBAC < MAC-3 < MAC-7 < MAC-8 < CAC. As observed, cellulose and sawdust based magnetic adsorbents have comparable adsorption capacities as the Darco G-60 activated carbon. However, the latter's surface area is more than double that of the magnetic extractants. Thus the surfaces of the magnetic activated carbons have higher capacity for DNOC per unit area than the commercial activated carbon. Consequently, it is necessary to discuss the possible factors involved in this adsorption process. One of the basic facts related to

adsorption on activated carbon surfaces is the presence of oxygen surface complexes such as carbonyl, carboxyl, phenol, anhydride, lactone, quinone, hydroquinone, and ether. The dissociation of these oxygen-containing functional groups if they possess an acidic or basic character will result in the presence of negative and positive surface charges needed for adsorption [11]. Additionally, the participation of graphene layers in π-π dispersive interactions with aromatic molecules, will lead to their adsorption on the surface. The adsorption capacity of CBAC, an activated carbon made from pure cellulose, was found to be less than that of its' magnetic derivatives MAC-7 and MAC-8. Hence, it can be concluded that in addition to the previously mentioned factors, the presence of nanoparticulate iron oxides and ferrites throughout the carbon matrix of the MACs play an important role in enhancing the materials' adsorption capacity perhaps by also adsorbing the DNOC. In regards to the difference in performance between sawdust (MAC-3) and cellulose (MAC-7 and MAC-8) based magnetic adsorbents, the slight advantage held by the latter might be due to their higher organic character.

Table 3-1: Adsorption capacities, coefficients of determination, and surface areas of magnetic and non-magnetic activated charcoals used in the adsorption of DNOC

Adsorbent	**SSA m^2/g**	**R^2**	**θ^o (maximum adsorption mg g^{-1})**
Commercial activated carbon	651	0.98	4.83
MAC-7	288	0.98	4.10
MAC-8	279	0.99	4.11
MAC-3	273	0.99	3.84
CBAC	237	0.99	1.73

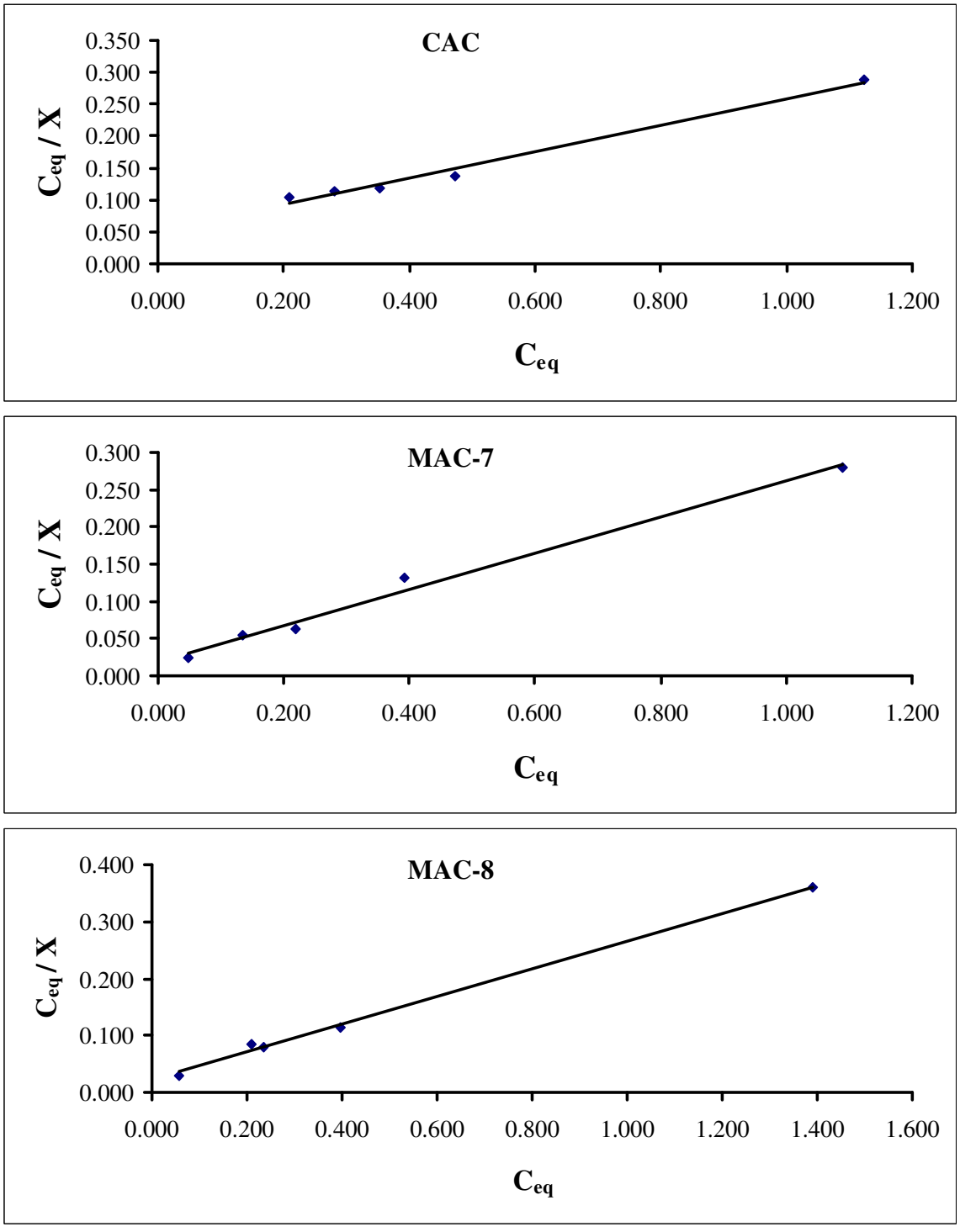

Figure 3-3: Langmuir isotherms for the adsorption of DNOC using commercial activated carbon, and cellulose-derived activated carbon/iron oxide composites, MAC-7 and MAC-8

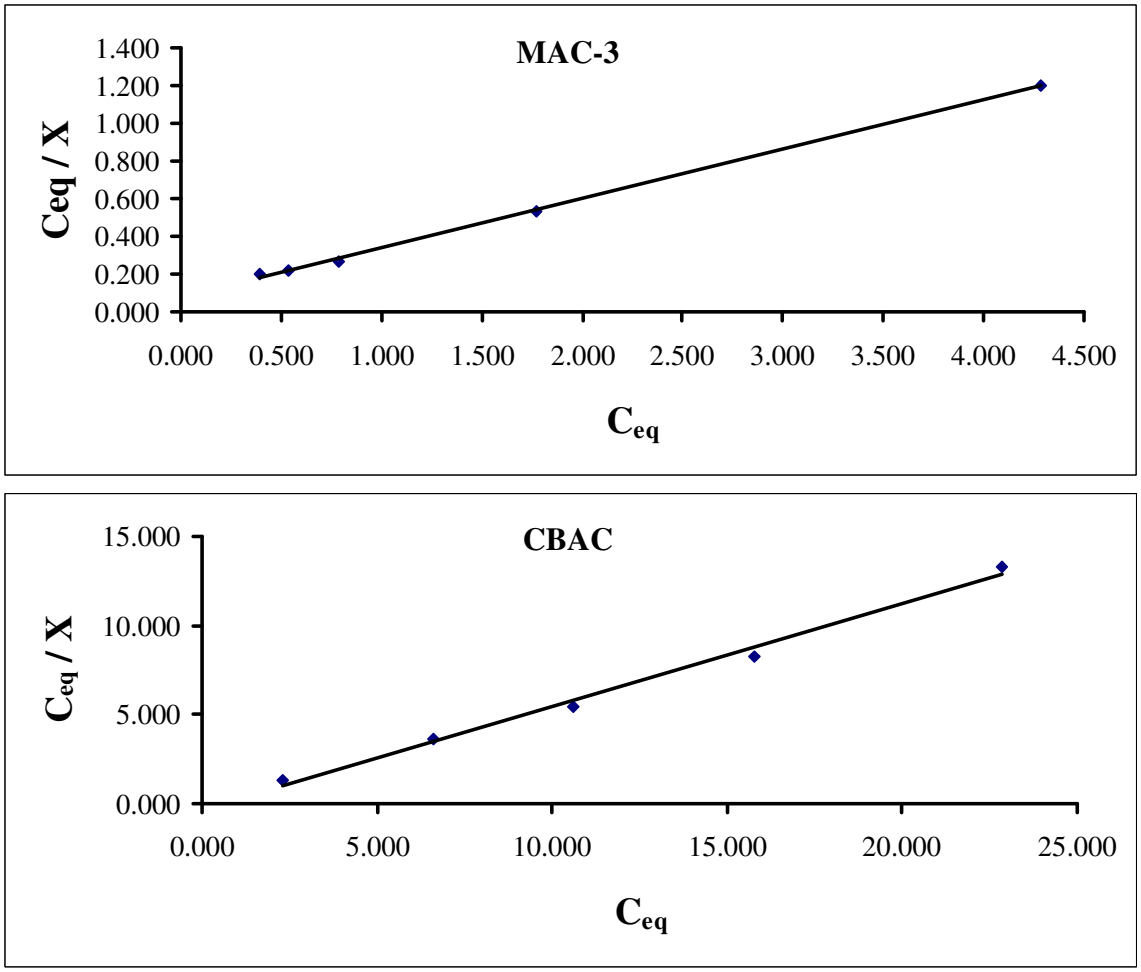

Figure 3-4: Langmuir isotherm for the adsorption of DNOC using sawdust-derived activated carbon/iron oxide composite (MAC-3), and cellulose-derived activated carbon (CBAC)

Adsorption kinetics of DNOC using MAC-7

Adsorption of 40 ppm DNOC solutions onto cellulose based magnetic activated carbon of highest surface area, MAC-7, was monitored for several hours. Plotting the measured concentrations as a function of time gives the graph shown in Figure 3-5.

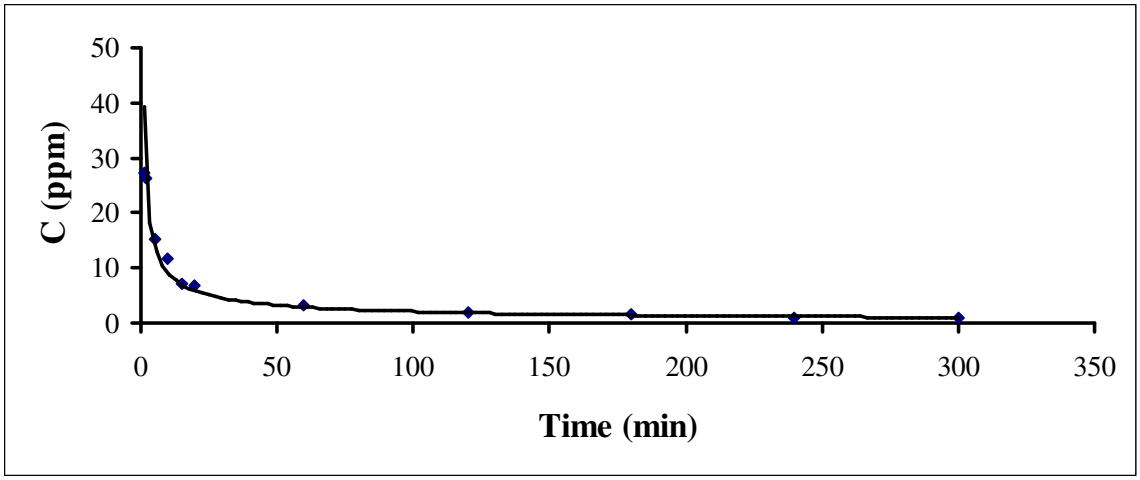

Figure 3-5: Adsorption behavior of DNOC from aqueous solutions of 40 ppm initial concentration onto MAC-7 as a function of time

In order to investigate the adsorption process of DNOC on the magnetic adsorbent, first order, and second order kinetic models represented in equations (a) and (b) respectively were applied [16].

$$LnC - LnC_i = -k_1 t \qquad \textbf{(a)}$$

$$\frac{1}{C} - \frac{1}{C_i} = k_2 t \qquad \textbf{(b)}$$

Where $\mathbf{C_i}$ is the initial concentration of adsorbate, **C** is the final concentration of the treated solution at time **t**. $\mathbf{k_1}$ and $\mathbf{k_2}$ are the rate constants for first order and second order models respectively.

The applicability of the kinetic models was tested by constructing linear plots of lnC versus t for first order model and 1/C versus t for second order model. Table 3-2 gives the rate constants determined from the slopes of the linear plots along with the coefficients of determination R^2. When these R^2 values are compared, it can be predicted that the first order model plotted in Figures 3-6 and 3-7 seem to be successfully

applicable in this case. The time needed to reach a definite fraction of equilibrium adsorption was previously reported to be independent of initial concentrations [7]. Similar observations indicating a first order process of Congo red adsorption on various activated carbons were also reported [6]. Due to the similarity in nature for the different adsorbents used in this project, the first order sorption kinetics can be extrapolated for the rest of the magnetic extractants.

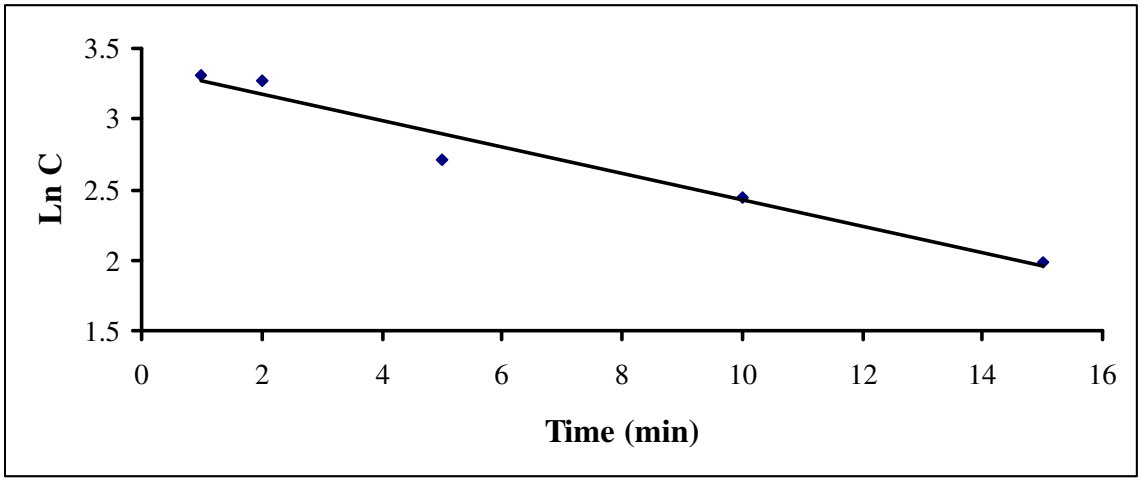

Figure 3-6: First order plot of lnC versus t (1 – 15 min) for DNOC adsorption using cellulose-derived magnetic activated carbon (MAC-7)

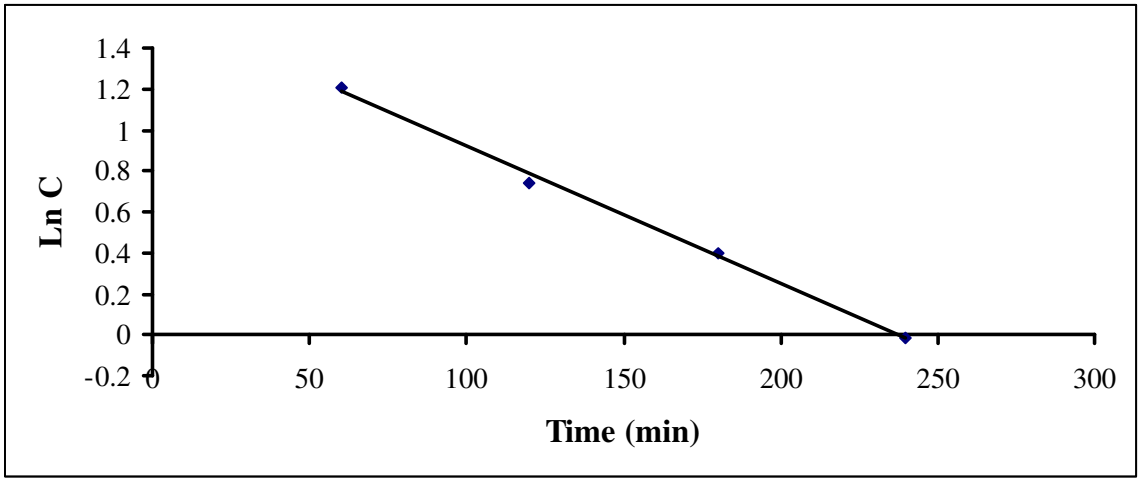

Figure 3-7: First order plot of lnC versus t (60 – 240 min) for DNOC adsorption using cellulose-derived magnetic activated carbon (MAC-7)

Table 3-2: Rate constants and coefficients of determination obtained from linear plots of the two kinetic models

Kinetic Model	Rate constants	R^2
First order (1 – 15 min)	$k_1 = 0.0939$	0.965
First order (60 – 240 min)	$k_2 = 0.0067$	0.997
Second order	$K_3 = 0.0038$	0.993

Removal of Congo Red dye from aqueous solution using MAC-9

After the Congo red dye is dissolved in an aqueous solution, the dissociation of the sulfonate groups generates the anionic dye ions.

$$R\text{-}SO_3Na \xrightarrow{H_2O} R\text{-}SO_3^- + Na^+$$

Congo red ions exhibit a tendency to aggregate in aqueous solutions [17]. Therefore due to this aggregation and the large size of the Congo red molecule, the adsorption is more likely to take place in the mesopores [18]. It was efficiently adsorbed by the magnetic activated carbon MAC-9. This successful adsorption can be attributed to a large number of mesopores within the adsorbent's structure in addition to the surface's partial occupation with ferrite particles. Upon water contact, ferrite particles develop a number of positively charged sites on the surface of the magnetic activated carbons. Consequently an increase in electrostatic attraction between the adsorbent's positively charged surface and the anionic dye is believed to enhance the adsorption capacity of the magnetic adsorbent.

Figure 3-8 show the Langmuir adsorption isotherm of Congo red dye by MAC-9. The adsorption capacity is equal to 4.92 mg/g which exceeds that of commercial carbons recently used for the same purpose (0.636 and 1.875 mg/g) [18].

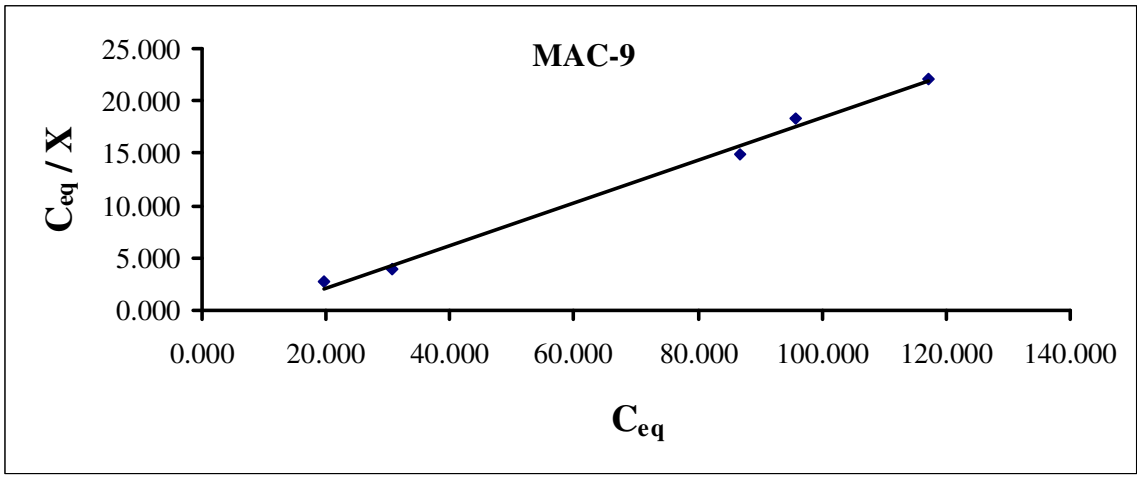

Figure 3-8: Langmuir isotherm for the adsorption of CR-dye using sawdust-derived activated carbon/nickel ferrite composite (MAC-9)

The effect of adsorbent dosage on the removal of Congo red was studied by plotting the mass of the adsorbent against the equilibrium concentration. An increase in the dye removal was observed to a certain limit. Increasing the adsorbent dosage will lead to higher adsorbent surface area which results in more availability of adsorption sites. Hence, the increase in adsorption can be directly attributed to the increase in adsorbent dosage. However, this increase in adsorbent dosage is accompanied by a decrease in unit adsorption. It is of importance to note that at lower concentrations (30 ppm), percent dye removal as high as 99.63% was reached using 0.2 g of the magnetic adsorbent in 7 ml CR solution.

Removal of decane from water using MACs synthesized from impregnated paper towels

The testing of the magnetic extractants (MAC-1 and MAC-2) made from iron and nickel gluconate impregnated paper towels for the extraction of decane from aqueous solutions with a concentration of 713 ppm was performed. This concentration falls below the solubility limit of decane in water, which provides a stringent separation challenge for the MAC since the adsorption of decane must be from solution and not from a non-aqueous phase that is much easier to separate from water. The low ratio of adsorbent to solution was 2.5 % and the contact time with aqueous solutions was kept short, a matter of only a few hours. After the magnetic filtration step, liquid-liquid extraction was performed on the aqueous solution using hexane and the extracts were analyzed for decane by GC/MS. Both extractants removed significant quantities of decane from the aqueous solutions. The results for these experiments are outlined in Table 3-3.

A stable emulsion was prepared according to the method of Shin and Kim and the ability to break it was tested using the nickel ferrite/activated carbon extractant (MAC-2) [19]. With such an emulsion, MAC-2 was briefly mixed then separated by magnetic filtration. Determining the effectiveness of treatment was attained by measuring the transmittance of the emulsion at 500 nm before and after treatment. A significant increase in transmission from 2 to 62% was observed. In terms of absorbance, a value of 1.66 was recorded before treatment while after it was found to be 0.21. Thus, magnetic extractants are capable of breaking emulsions and these initial results suggest that complete breaking of an oil in water emulsion could be accomplished by optimizing the magnetic extractants. Notably, it is likely that real world samples may not be as

challenging since the emulsion used in this investigation was extremely stable and very high in surfactant [20].

Table 3-3: Results from treatment of aqueous solutions of decane with paper towel-derived magnetic activated carbons (MAC-1 and MAC-2)

Adsorbent	Initial Concentration	Final Concentration	Percent Decane Removal
MAC-1	713 ppm	56.0 ppb	99.99 %
MAC-2	713 ppm	62.4 ppb	99.99 %

CONCLUSIONS

It was found that low-cost magnetic activated carbons are effective adsorbents for the removal of DNOC, Congo red dye, and decane from aqueous solutions via magnetic filtration. Additionally, successful separation of oil from aqueous emulsions was also possible using the same technique. The experimental adsorption equilibrium data for DNOC and Congo red on all the magnetic adsorbents studied show very good fit with the Langmuir isotherm. From a practical point of view, further optimization of the MACs is expected to insure their status as promising magnetic adsorbents for the magnetic separation of organic species from water.

REFERENCES

[1] Ribeiro, A.; Neves, M. H.; Almeida, M. F.; Alves, A.; Santos, L. *Journal of Chromatography, A* **2002**, *975*, 267-274.

[2] Salvador, F.; Merchan, M. D. *Carbon* **1996**, *34*, 1543-1551.

[3] Calace, N.; Nardi, E.; Petronio, B. M.; Pietroletti, M. *Environmental Pollution (Oxford, United Kingdom)* **2002**, *118*, 315-319.

[4] Easton, J. *Colour in dye house effluent*; Alden Press: Oxford, 1995.

[5] Khan, B.; Gupta, P.; Jala, S.; Goyal, D. *Indian Journal of Environmental Protection* **2003**, *23*, 415-418.

[6] Kannan, N.; Meenakshisundaram, M. *Water, Air, and Soil Pollution* **2002**, *138*, 289-305.

[7] Bhatnagar, A.; Jain, A. K.; Mukul, M. K. *Environmental Chemistry Letters* **2005**, *2*, 199-202.

[8] Sullivan, P. J.; Agardy, F. J.; Clark, J. J. J. *The environmental science of drinking water*; 1st ed.; Elsevier Butterworth-Heinemann: Burlington, MA, 2005.

[9] Apblett, A.; Al-Fadul, S. M.; Trad, T. M. *Ceramic Transactions* **2003**, *143*, 15-22.

[10] Rashwan, W. E.; Girgis, B. S. *Adsorption Science & Technology* **2004**, *22*, 181-194.

[11] Moreno-Castilla, C.; Rivera-Ultrilla, J. *MRS Bulletin* **2001**, *26*, 890-894.

[12] Cota-espericueta, A. D., New Mexico State University, 2003.

[13] Dastgheib, S. A., New Mexico State University, 2001.

[14] Clark, A. *The theory of adsorption and catalysis*; Academic Press: New York, 1970.

[15] Langmuir, I. *Journal of the American Chemical Society* **1918**, *40*, 1361-1402.

[16] Ayranci, E.; Hoda, N. *Chemosphere* **2005**, *60*, 1600-1607.

[17] Coates, E. *J. Soc. Dyers Colour.* **1969**, 355-365.

[18] Mall, I. D.; Srivastava, V. C.; Agarwal, N. K.; Mishra, I. M. *Chemosphere* **2005**, *61*, 492-501.

[19] Shin, S. H.; Kim, D. S. *Environmental Science and Technology* **2001**, *35*, 3040-3047.

[20] Allen W. Apblett, S. M. A., and Tarek Trad In *Integrated Petroleum Environmental Consortium* Tulsa, Oklahoma, 2001.

CHAPTER 4

SYNTHESIS AND CHARACTERIZATION OF CAPPED MAGNETITE AND NICKEL FERRITE NANOPARTICLES

INTRODUCTION

Magnetic nanoparticles have been the focus of many recent investigations and developments. Their interesting fundamental properties secured their value as attractive candidates for biomedical, environmental, and many other potential applications. Nanomaterials often possess remarkable magnetic, electrical, optical, and chemical properties that are different from their bulk counterparts [1]. The large percentage of surface atoms in nanoparticles exhibit a different bonding domain than the bulk atoms and this might be attributed to the difference in properties between nanoparticles and larger particles [2]. The structural, mechanical and chemical behaviors of these materials are not the only factors governing their technological usefulness. It is also the phenomena behind their finite size and the surface chemistry that influence the magnetic nature of individual nanoparticles [2]. Basic magnetic properties that are of importance to magnetic materials are those related to high-field irreversibility, extra anisotropy contributions, high saturation fields, and superparamagnetism. Normally, each area of application requires magnetic nanoparticles with suitable properties. Therefore, nanomaterials used

in data storage devices need to have the ability to switch its' magnetic state, while the specific criteria for magnetic nanoparticles used in environmental remediation and biomedical applications is superparamagnetism at room temperature. Furthermore, materials that are involved in medical diagnosis, magnetic fluid hyperthermia (MFH), and drug delivery should be stable in the physiological salinity of body liquid and in neutral pH of water [3,4].

In the last decade, extensive efforts were employed in the field of magnetic nanoparticles and their chemical synthesis, where a variety of magnetic nanomaterials was prepared from metals and ceramics [5]. Iron(III) oxides are among the most used metal oxides in various industrial and scientific applications [6]. Naturally occurring polymorphs of Fe_2O_3 such as alpha and gamma are found in nature as hematite and maghemite minerals. However, beta and epsilon polymorphs, and nanoparticles of iron(III) oxides have been synthesized using numerous chemical and physical methods [6]. Transformations of iron-bearing compounds by thermal induction in an oxidizing atmosphere are processes of high importance in the preparation of magnetic iron oxide nanoparticles. These processes can be classified into groups based on the initial iron-containing phase [6]. Thermal decomposition of iron(III) compounds including FeO(OH) and $FeCl_3$, thermal transformations of iron carbonyl and iron carboxylate complexes, and oxidation of magnetite and metal iron by thermal induction are thermal processes that have been adopted for the formation of ultrafine iron oxide nanoparticles [7-13]. Moreover, alternative routes for the synthesis of iron oxide nanoparticles such as electrochemical synthesis, sol-gel methods, oxygen-hydrogen flame pyrolysis, microemulsion techniques, and thermal decomposition of an aerosol upon a heated

substrate have yielded particles with various compositions and morphologies [14-18]. Nanoparticulate iron oxides have found an increasing popularity in many industrial applications due to their unique fundamental properties. They are utilized in magnetocaloric refrigeration, color imaging, optical devices, information storage, and magnetic recording media [19,20].

Another important group of magnetic materials are spinel ferrites, MFe_2O_4 (M = Ni, Zn, Co, Mg, Mn), with nickel ferrite $NiFe_2O_4$ being the most investigated for technological applications such as ferrofluids, microwave devices, and catalysts [21]. The composition and structure of the ferrite nanoparticles are significantly sensitive to the synthesis methodology which also influences their properties. Nano-sized nickel ferrites have been fabricated using techniques including co-precipitation, sonochemical preparation, sol-gel, and mechanical alloying. However, problems associated with particle morphology and agglomeration are still of major concern [22-25]. Due to the good control over particle morphology, hydrothermal methods have been preferred for the preparation of ferrite nanoparticles. Attractive properties exhibited by these magnetic ceramic nano-materials, allow their utilization as soft magnets and low loss materials at high frequencies [26]. At the nanoscale, anomaly was observed in the magnetic and structural properties of spinel ferrites, where the magnetic moment at low temperatures was reported to be appreciably lower than the value for bulk material for ultrafine nickel ferrite [27]. Additionally exceptional magnetic properties were observed for organic coated nickel ferrite nanoparticles [28]. Hence, particle size effects on magnetic behavior and activity of nano-size nickel ferrites as well as novel routes for their synthesis continue as very active fields of research in the field of material science.

Generally, the synthesis of transition metal oxide nanoparticles is accomplished via hydrolytic methods, where water is the solvent or reactant. Using nonhydrolytic techniques holds great potential for producing metal oxide nanoparticles with superior properties related to surface composition and defect structure [29]. Advantages resulting from nonhydroxylated surfaces may be of interest in cataylsis, ceramics, magnetic data storage, and environmental applications.

In the present chapter we describe a new nonhydrolytic single precursor route for the synthesis of capped magnetite and nickel ferrite nanoparticles. The surface composition and thermal stability of these materials was studied using infrared spectroscopy and thermogravimetric analysis respectively. Average particle size was determined using transmission electron microscopy and dynamic light scattering techniques. Structural characterization of all precursor and nanoparticle samples was carried out by the X-ray diffraction (XRD) technique. Due to an increased environmental importance, an investigation of the ability of these nanomaterials for the adsorption of 4,6-dinitro-o-cresol from water has been conducted and reported in Chapter 5.

EXPERIMENTAL

Chemicals

For all precursor synthesis reactions, reagents were of analytical grade and used as received. The chemicals used in this chapter were as follows; iron(III) chloride hexahydrate [$FeCl_3.6H_2O$, Aldrich]; iron(III) nitrate nonahydrate [$Fe(NO_3)_3.9H_2O$, Aldrich]; nickel(II) chloride hexahydrate [$NiCl_2.6H_2O$, Aldrich]; octanoic acid [$C_8H_{16}O_2$,

Eastman]; stearic acid [$C_{18}H_{36}O_2$, Aldrich]; cholic acid [$C_{24}H_{40}O_5$, Aldrich]; ammonium hydroxide [NH_4OH,]; 1,2,3,4-Tetrahydronaphthalene (tetralin) [$C_{10}H_{12}$, Fluka].

Synthesis of the iron carboxylate precursors

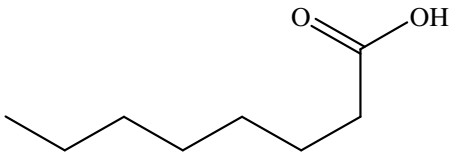

Octanoic acid

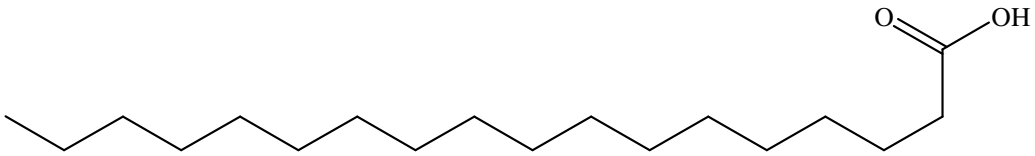

Stearic acid

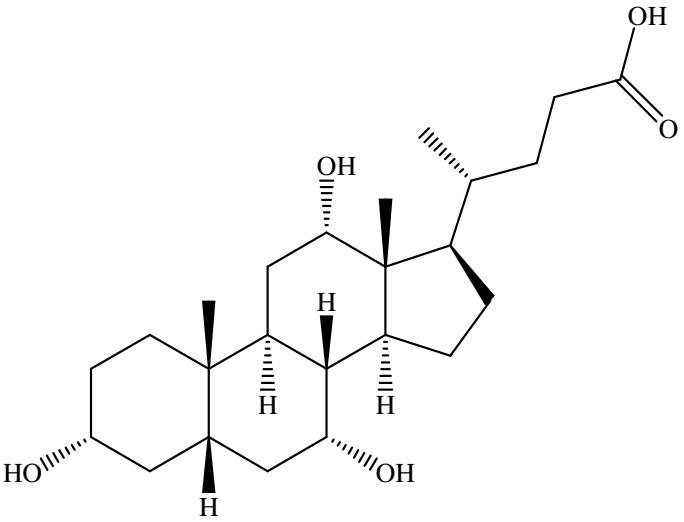

Cholic acid

Figure 4-1: The chemical structures of the carboxylic acid capping agents used in the synthesis of iron and nickel-iron carboxylate precursors

Figure 4-1 shows the chemical structure of the carboxylic acids used in the synthesis of the iron carboxylate precursors. The following sections in the experimental part of this chapter describe the synthesis of the precursors and nanoparticles derived from those precursors.

Iron(III) caprylate precursor preparation

A solution of 30.00 g of $Fe(NO_3)_3.9H_2O$ in 25 ml of commercial ethanol was added to another solution made by dissolving 10.70 g of caprylic acid in 50 ml of ethanol. This was followed by drop wise addition of 15 ml of concentrated ammonia under vigorous stirring over a period of 30 minutes. A light brown precipitate was instantly formed upon the addition of ammonia to the caprylate-iron nitrate mixture. The precipitate thus produced was centrifuged at 3900 rpm and washed several times with hot ethanol. The well-washed precipitate was finally dried under vacuum at room temperature for 24 hours. Caprylate groups ($C_7H_{15}COO^-$) in the precipitate were identified by the characteristic absorption bands at 1600 – 1400 cm^{-1} using infrared spectroscopy. The reaction yielded 16.00 g of product.

Iron(III) stearate precursor preparation

In a similar procedure as that described above, a 1:1 mole ratio of iron(III) nitrate nonahydrate to stearic acid starting material was prepared. 8.08 g of $Fe(NO_3)_3.9H_2O$ were dissolved in 70 ml ethanol, followed by the addition of a stearic acid solution made by dissolving 5.68 g of $C_{18}H_{36}O_2$ in 50 ml of ethanol. 7.00 ml of concentrated ammonia were added drop wise to the stirred mixture. The sludge-like dark brown precipitate that

formed was isolated by centrifugation and was washed with hot ethanol. The precipitate was left to dry under vacuum at room temperature for 24 hours. The yield was 7.05 g.

Ni-Fe(octanoate) precursor

10.80 g of $FeCl_3.6H_2O$ were dissolved in 20 ml of ethanol. Another solution was made by dissolving 19.00 g of $NiCl_2.6H_2O$ in 30 ml of ethanol and then gradually added to the Fe^{3+} solution. A sample of 14.40 g of caprylic acid in 40.00 ml ethanol was stirred to dissolution, and a colorless solution had formed. The caprylic acid solution was then added to the stirred Fe^{3+} / Ni^{2+} solution and a dark green solution was observed. Upon the addition of 10 ml of concentrated ammonia, a light brown precipitate was formed. With a large amount of hot ethanol, the precipitate was washed to remove all the residual unreacted starting materials. Finally, after filtration, the light brown powder was dried under vacuum for 24 hours. The reaction yielded 23.79 g.

Ni-Fe(stearate) precursor

The method used for preparing the Ni-Fe(octanoate) sample was adopted for this bimetallic stearate precursor. An Fe^{3+} solution made by dissolving 5.50 g of $FeCl_3.6H_2O$ in 10 ml of ethanol. 9.60 g of $NiCl_2.6H_2O$ were dissolved in 15 ml of commercial ethanol, and the Fe^{3+} solution was added to this Ni^{2+} solution and the mixture was stirred at room temperature. A sample of 5.6 g of stearic acid was dissolved in 80 ml of ethanol and the solution was added drop-wise to the stirred mixture of iron(III) and nickel(II) solutions. Upon that addition a brown precipitate was formed immediately. The precipitate was filtered and washed with enough hot ethanol to remove all unreacted

excess of starting reactants. Finally, the brown precipitate was dried under vacuum for 24 hours. The reaction yield was 11.24 g.

Octanoate and stearate capped magnetite nanoparticles' synthesis

Octanoate capped magnetite nanoparticles: 3.02 g of the iron(III) caprylate precursor were suspended in a 100 ml of tetralin. The suspension was degassed under vacuum for 1 hour and then purged with flowing helium for 30 minutes. Following this, the pyrex glass reactor containing the mixture was placed in a tube furnace and subjected to intense heating at 210 °C (boiling point of tetralin = 210 °C) for 12 hours. After the reaction was completed, the reactor was cooled to room temperature and a blackish brown stable suspension was observed. 300 ml of commercial acetone was added to the produced dispersion, and a dark brown precipitate was formed instantly. The precipitate was washed with acetone, isolated by centrifugation at 3900 rpm, and dried on a glass plate for 2 days at room temperature. Finally, the observed attraction of the fine powder to a permanent hand magnet indicated that the powder possessed bulk magnetic properties.

The reaction yielded 1.11 g.

Stearate capped magnetite nanoparticles: A sample of 2.00 g of the iron(III) stearate precursor was added to 80 ml of tetralin. The produced suspension was degassed under vacuum for 1 hour and then subjected to flowing helium for 20 minutes. The reaction tube was then placed in a tube furnace and the temperature was elevated to 210 °C and maintained for 12 hours. The black dispersion produced was cooled to room temperature and washed with 300 ml of acetone. After thorough washing, the precipitate was centrifuged at 3900 rpm, and the isolated powder was washed with acetone and finally

dried over a glass plate for 2 days under air and room temperature. The powder possessed bulk magnetic properties and weighed 0.42 g.

Synthesis of the capped nickel ferrite nanoparticles

Octanoate capped nickel ferrite nanoparticles: A sample of 3.00 g of Ni-Fe(octanoate) starting material was suspended in a 100 ml of tetralin. The suspension was degassed under vacuum for 1 hour and then purged with helium for 30 minutes. The reaction vessel was then placed in a tube furnace and the temperature was set at 210 °C for 12 hours. At room temperature the light brown suspension transformed to a dark brown stable dispersion (stable for more than a year) indicating the formation of nickel ferrite nanoparticles. Adding an excess volume of acetone (300 ml), the capped nickel ferrite nanoparticles were precipitated as brown powder, which was dried under air. The solid produced was magnetic in nature. The reaction yielded 1.43 g.

Stearate capped nickel ferrite nanoparticles: Similarly, this sample was prepared using 2.00 g of Ni-Fe(stearate) precursor suspended in 80 ml of tetralin. Conditions mentioned in the preparation of the previous nickel ferrite nanoparticles were used in this procedure. The yield of this reaction was 1.03 g.

Iron(III) cholate precursor and cholate capped nanoparticles' synthesis

Iron(III) cholate precursor: 1:2 mole ratio of iron(III) nitrate nonahydrate to cholic acid solution was prepared by dissolving the iron salt and the cholic acid in ethanol. Experimental details described in the previous precursor preparation were followed leading to the formation of a brown precipitate. IR peaks at 2924 and 2860 cm^{-1} due to

the C–H stretching frequencies of the cholic acid steroid skeleton along with peaks at 457 and 613 cm^{-1} indicative of an iron oxide hydroxide network, confirmed the formation of an iron-cholate structure [30].

Cholate capped nanoparticles: An interesting bile acid-magnetite nanocomposite was successfully synthesized by heating 0.825 g of the precursor in tetraline at 200 °C under a helium atmosphere. The nanoparticles were recovered by precipitating the reaction product with acetone and drying under air for 48 hours. The nature of the surface organics was analyzed using IR spectroscopy.

Methods of characterization

The magnetic nanoparticles and their precursors were characterized using several techniques. Powder X-ray diffraction (XRD) patterns were recorded on a Bruker AXS D8 Advance diffractometer using Cu Kα radiation with a current flux of 30 mA and an acceleration voltage of 40 kV. The diffractograms were recorded for a 2θ range of 17-70° with a step size of 0.02° and a counting time of 18 seconds per step. All the XRD patterns were collected at ambient temperature, and the phases were identified using the ICDD database. The peaks were profiled with a Pearson 7 model using Topas P version 1.01 software. The profiles of the standard and the sample were put into the Win-Crysize program version 3.05, which uses the Warren-Averbach evaluation method to determine crystallite size.

Infrared spectroscopic measurements were performed on a Nicolet Magna-IR 750 spectrometer. Approximately 10 mg of the precursor or the capped magnetic nanoparticles was added to a 100 mg FTIR-grade potassium bromide and mixed

thoroughly. The blend was then finely ground and spectra in the 4000 – 400 cm^{-1} region were collected by diffuse reflectance of the ground powder. Typically, 128 scans were recorded and averaged for each sample (4.0 cm^{-1} resolution) and the background was automatically subtracted.

Transmission electron micrographs (TEM) were obtained using a JEOL JEM-100CXII electron microscope operated at 80 kV. For this purpose a 0.1 % w/v stable dispersions of the nanoparticles in toluene were prepared. A drop of each of the powder dispersions was carefully placed on a copper grid surface and dried before micrographs were generated.

Dynamic light scattering (DLS) measurements were performed on the capped magnetite and nickel ferrite nanoparticles suspensions with a Malvern HPPS 3001 instrument. Particle size measurements were obtained at 25.0 °C with dispersant viscosity and refractive index values of 0.55 cP and 1.491 respectively.

Thermogravimetric analysis (TGA) was performed on the precursors and the nanoparticulate powders at a rate of 2.0°/min from room temperature to 1000 °C using a Seiko Instruments Exstar 6200.

RESULTS AND DISCUSSION

The XRD diffractogram of the nanoparticulate powder derived from iron(III) octanoate precursor after thermal treatment in tetralin is presented in Figure 4-2. The broad reflections exhibited by the starting material transform into well-distinct signals after heat treatment. Using the ICDD database, the formation of magnetite was confirmed

from the discernible signals obtained. The crystallite size of the ultrafine iron oxide particles was 7.2 Å as estimated from the Warren-Averbach method.

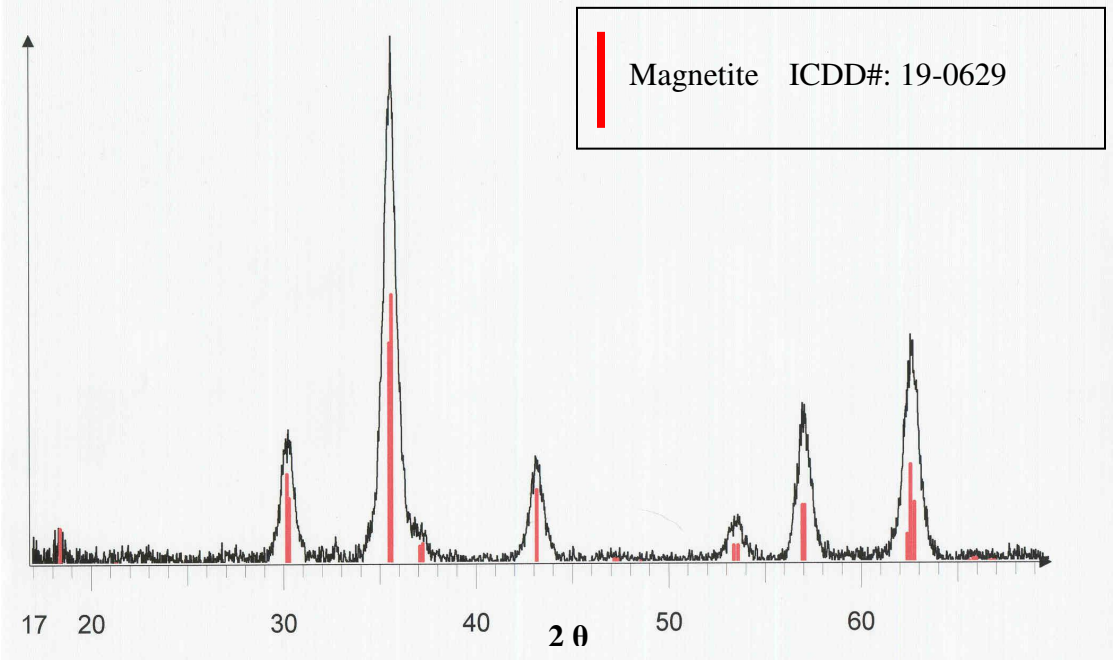

Figure 4-2: XRD pattern of octanoate capped magnetite nanoparticles

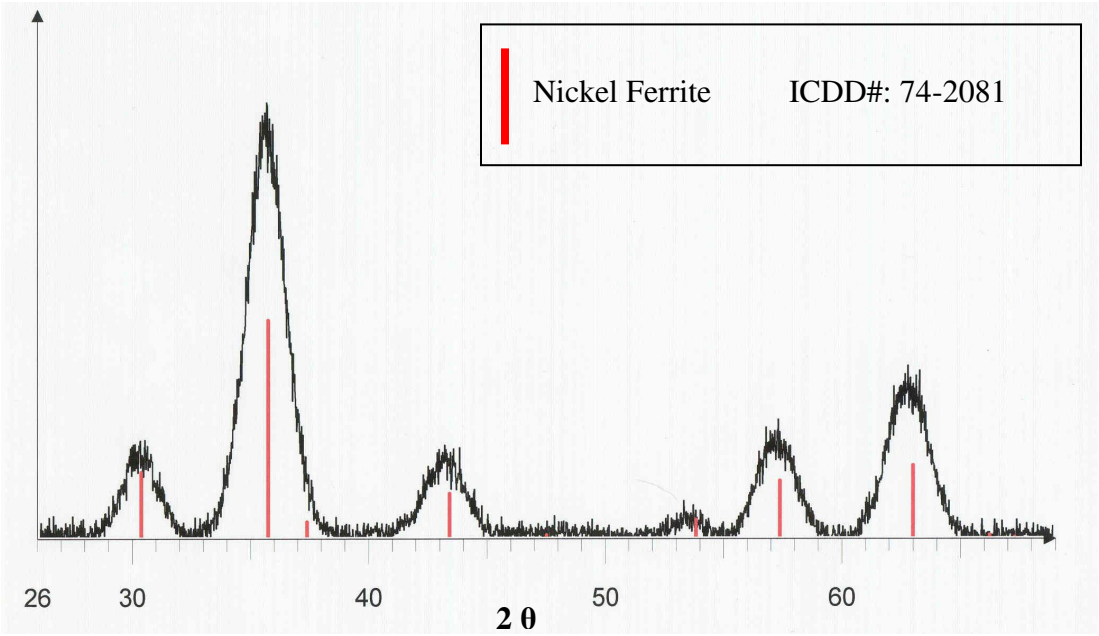

Figure 4-3: XRD pattern of octanoate capped nickel ferrite nanoparticles

The XRD diffractogram of the as-synthesized $NiFe_2O_4$(octanoate) nanoparticles is presented in Figure 4-3. The absence of sharp diffraction patterns characteristic of crystalline phases revealed the amorphous nature of the precursor. On the other hand many sharp and strong crystalline peaks were observed in the diffraction pattern of the resultant nanoparticles attributed to the formation of the face-centered cubic $NiFe_2O_4$ phase. A crystallite size of 2.2 Å was determined using the Warren-Averbach method.

Infrared spectroscopic measurements were used to confirm the presence of the capping agents on the surface of the magnetite and nickel ferrite nanoparticles. Figure 4-4 shows the IR spectra of the iron(III) caprylate precursor and the caprylate capped magnetite nanoparticles in the region 4000 – 500 cm^{-1}.

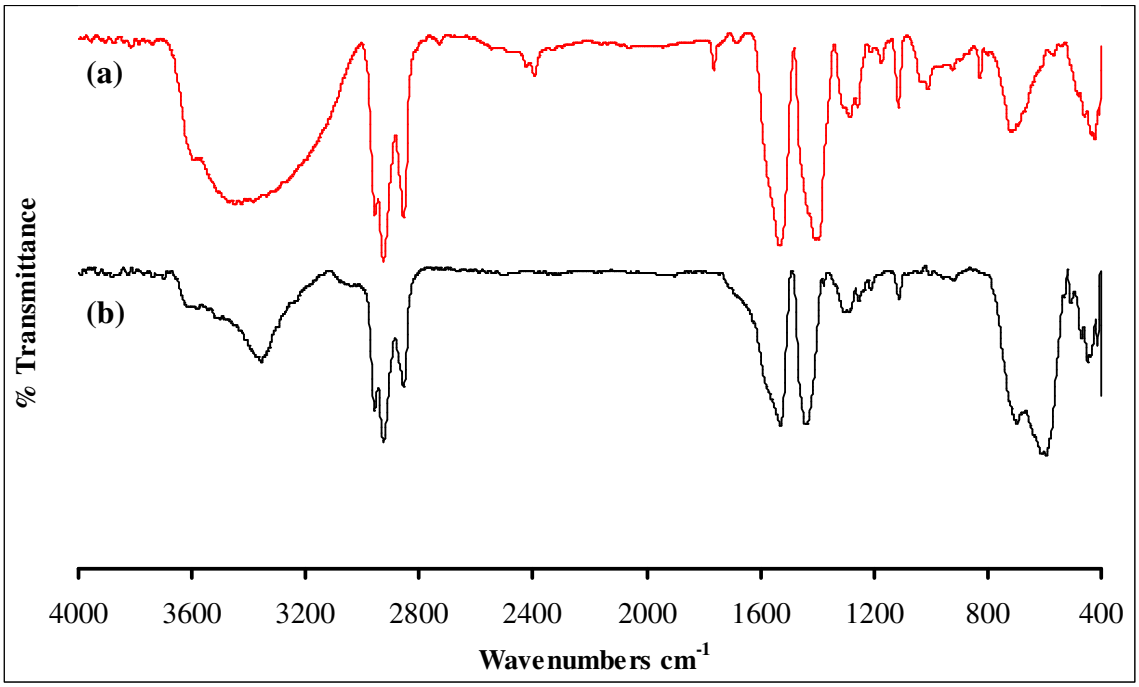

Figure 4-4: IR spectra of iron(III) caprylate precursor as prepared (a) and after heating in tetralin for 12 hours (b)

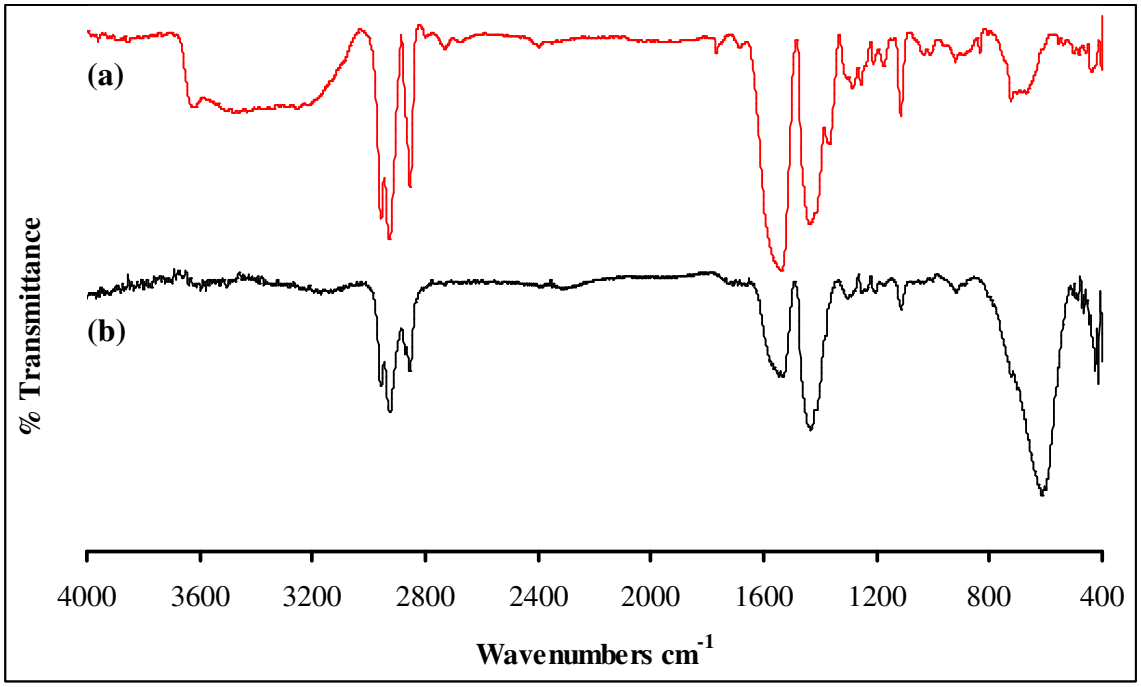

Figure 4-5: IR spectra of nickel-iron(octanoate) precursor as prepared (a) and after heating in tetralin for 12 hours (b)

The absorption bands at 2855 cm^{-1}, 2926 cm^{-1}, and 2956 cm^{-1} exhibited by the iron(III) caprylate precursor are attributed to the $–CH_3–$ and $–CH_2–$ aliphatic moieties, while the presence of the carboxylate ($–COO^-$) groups is confirmed by two absorptions at 1529 and 1439 cm^-. Observation of these IR bands confirms the anchoring of caprylate anions to the surface of the magnetite nanoparticles. The separation small separation of 90 cm^{-1} between the symmetric and asymmetric carboxylate stretches suggests a chelating or both chelating and bridging modes for coordination for the caprylate moieties to the surface [31]. Figure 4-6 demonstrates the chelating nature of carboxylate coordination (I), and combinations of chelating and bridging modes of carboxylate-metal coordination (II, III).

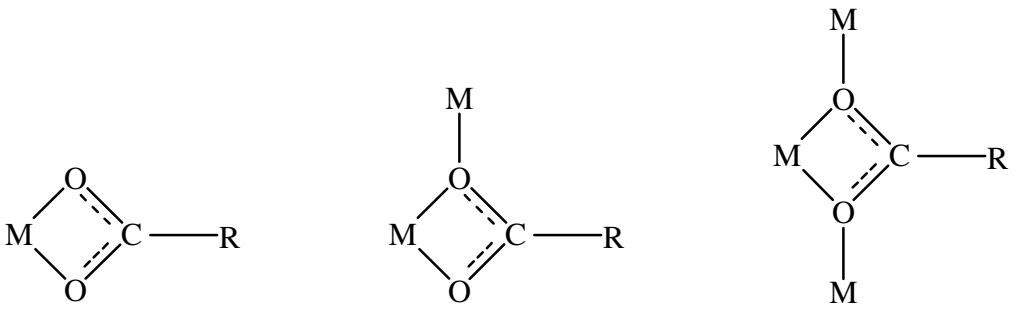

Figure 4-6: A carboxylate ion, RCO_2^-, coordinated to metal (M) as a chelating ligand (a), and in arrangements involving both chelation and bridging (b, c)

The iron oxide hydroxide nature of the iron(III) caprylate precursor is distinguished by the presence of IR bands at 697 and 594 cm^{-1} [32]. After the formation of capped magnetite nanoparticles due to thermal treatment in tetralin, the absorption bands characteristic for the aliphatic moieties were retained and are still clearly observed in the IR spectrum of the product (Figure 4-4 b). This reveals the preservation of the organic cap around the magnetic solid. Moreover, an enhancement of the peak at 594 cm^{-1} indicates the formation of a rigid iron oxide network within the product [33]. IR spectra of the nickel-iron(octanoate) precursor and its' corresponding capped nickel ferrite nanoparticles are presented in Figure 4-5. Absorption bands below 2956 cm^{-1} indicate that the aliphatic sheath remained around the nickel ferrite, while characteristic Fe–O stretching modes in $NiFe_2O_4$ phase were associated with absorptions found at ~612 cm^{-1} [34]. In a similar fashion, successfully synthesized octanoate and stearate capped nanoparticles showed similar infrared absorption data confirming the preservation of carboxylate groups around the magnetic core.

Figure 4-7 shows the thermogravimetric analysis (TGA) data of the iron(III) stearate precursor (a) and its derived nanoparticles (b). Generally, a loss of weight was observed

for the precursor starting at room temperature to about 387 °C. A minor loss of weight in the ranges between room temperature to 108 °C, and 108 °C to 200 °C were recorded. On the other hand, major weight losses occurred between the temperatures 200 °C to 280 °C, and 280 °C to 387 °C given. The 4 % weight loss in the first temperature range from room temperature to 108 °C is attributed to the evaporation of water molecules. The thermal decomposition of loosely bonded carboxylate entities, hydroxide ions, and organic groups occurs in the second weight loss range between 108 °C and 280 °C and results in a 28 wt% drop in the total weight of the sample. The third and major weight loss step between 280 °C and 387 °C corresponds to removal of the remaining fraction of organic and carboxylate species. A 46 wt% decrease was determined for this last step. Therefore, a loss by weight of 74 % illustrated in the TGA of the iron(III) stearate precursor (a), was mainly attributed to organic content decomposition and dehydration.

As shown in Figure 4-7 (b), two principal weight loss steps were observed for the nanoparticles. The first thermal range from room temperature to 107 °C is a 1 % loss by weight due to evaporation of water molecules. In the second step between 200 °C and 473 °C, a single weight loss was observed. The magnitude of this weight loss was 19 wt% which can mostly be ascribed to organic species degradation. However, an interesting curvature owing to an increase in weight was observed between 200 °C and 225 °C. Tthis slight weight gain is likely due to oxidation of magnetite (Fe_3O_4) to maghemite (γ-Fe_2O_3). To support this claim, the behavior of the stearate capped magnetite nanoparticles upon thermal treatment at different temperatures was investigated. Figure 4-8 shows the XRD diffraction patterns of the stearate capped magnetite nanoparticles as prepared, and upon heat treatment under air at elevated

temperatures. Indeed heating the sample to 225 °C resulted in a decrease in peak intensity and a slight shift indicating formation of maghemite. Heating the sample further to 470 °C led to the appearance of more intense, and narrower X-ray reflections that matched the ICDD pattern of hematite (α-Fe_2O_3). The thermal instability of maghemite allows for its quick transformation to hematite at higher temperatures. The structural phase transformation mechanism and the temperature are primarily dependent on the size of maghemite particles and experimental conditions [6]. It has been previously reported that the approximate temperature for maghemite conversion via a direct mechanism from well-developed crystals was 400 °C [35]. However when the particles are significantly smaller in size, the temperature needed for the phase change exceeds 400 °C, where ε-Fe_2O_3 is observed as an intermediate phase in the transformation of γ- Fe_2O_3 to α-Fe_2O_3 [36]. These reported observations were found to agree well with our experimental data.

It is of significant importance to address the factors leading to the magnetic phase formation as well as the proposed mechanism behind it. Synthesis conditions and the nature of the prepared precursors are the basic factors involved. During the non-hydrolytic thermal treatment of the precursors, anaerobic experimental conditions were required. In fact, only the hematite (α-Fe_2O_3) phase of iron oxide was produced in two supporting experiments [37]. The first was accomplished by heating iron(III) octanoate precursor in boiling tetralin without purging the reaction tube with helium. In the second experiment, the same precursor was heated at 170 °C overnight under an air atmosphere.

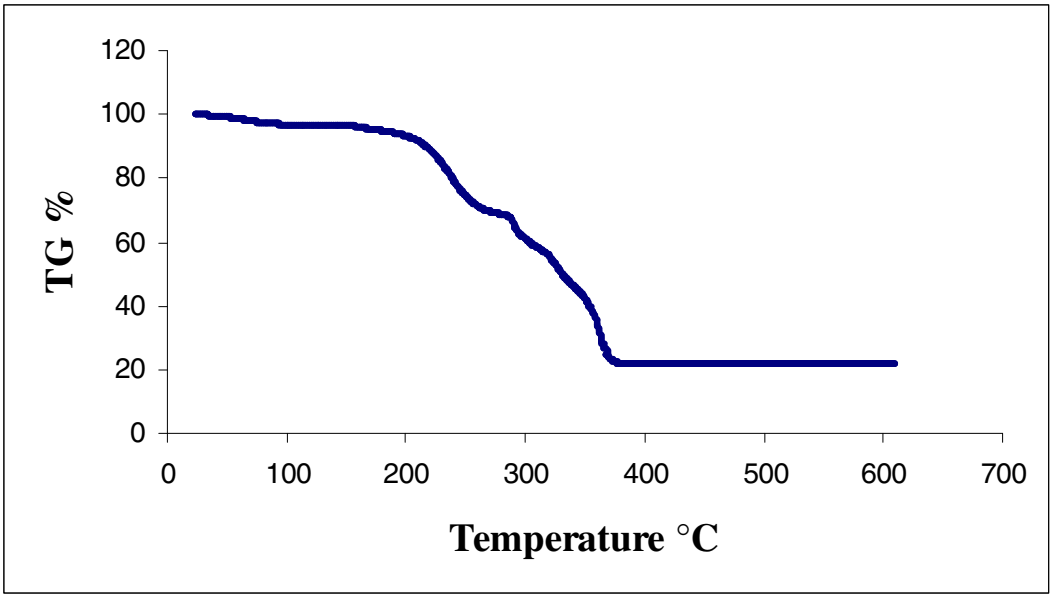

(a)

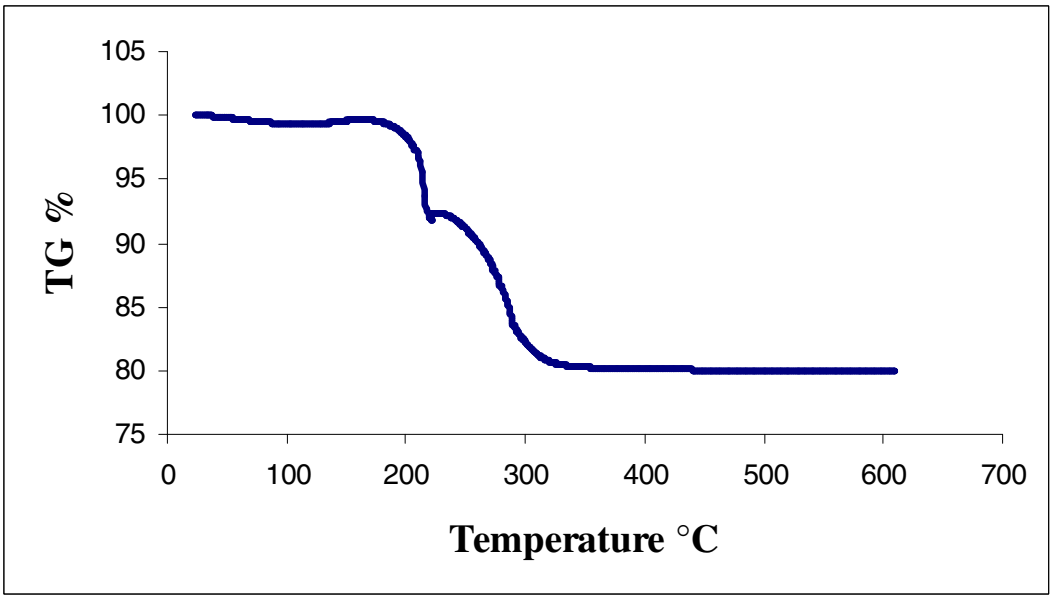

(b)

Figure 4-7: TGA data of iron(III) stearate precursor (a), and stearate coated magnetite nanoparticles (b)

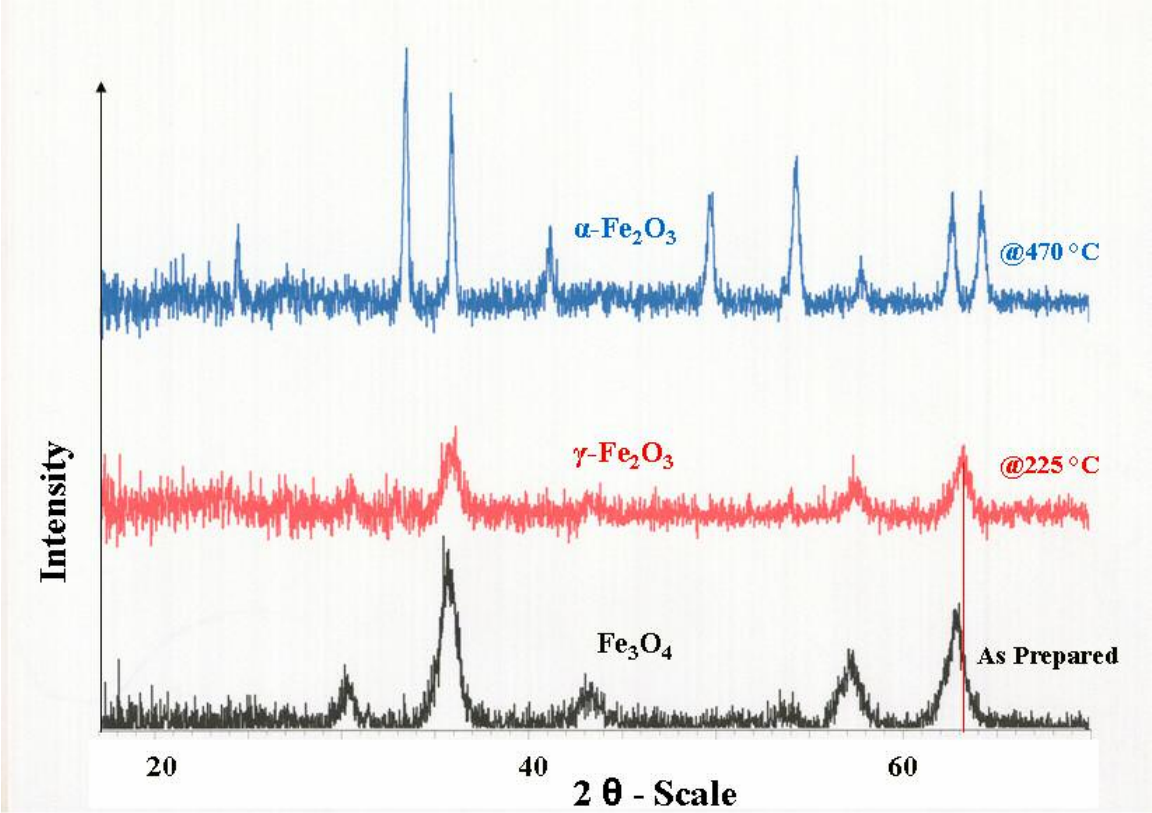

Figure 4-8: XRD pattern of stearate capped magnetite nanoparticles as prepared (a), heated to 225 °C under air, and to 475 °C under air as well (c)

On the other hand, the hydrolytic nature of the precursors and the reducing atmosphere provided by the organic decomposition products play an important role in fabricating the desired magnetic powder [29]. Therefore, inert reaction conditions associated with suitable metallorganic precursors are essential to realizing a magnetic phase.

Previous studies have shown that γ-Fe_2O_3 nanocomposites are preferentially formed through an initial reduction step of iron oxide-hydroxide polymeric material followed by oxidation [38]. Moreover, thermal investigations on the decomposition of ferric acetate and metal carboxylates under inert atmospheres have demonstrated that carboxylate groups play an important role as reducing agents in the partial reduction of trivalent iron to its divalent state [39,40]. Therefore, the major proposed route in the mechanism of

magnetite formation is the partial reduction of iron(III) precursors upon pyrolysis in tetralin in the presence of the carboxylate groups (octanoate, stearate, and cholate) to divalent iron. After the formation of crystalline magnetite through cation and vacancy reordering, subsequent oxidation might result in the coexistence of γ-Fe_2O_3 (maghemite) with magnetite capped nanoparticles [37]. An interesting observation showing no identifiable IR bands due to caprylate groups after thermal treatment of iron(III) caprylate in the absence of tetraline. Hence, tetralin can have an affect as a reducing agent, taking into consideration its well-recorded reducing properties [41].

All capped magnetite nanoparticles were slightly dispersable in chloroform, toluene, and tetrahydrofuran, while capped nickel ferrite nanoparticles were readily dispersible in the same solvents (solubility > 30 mg/ml). The latter particles yielded clear light brown dispersions in the organic solvents that were stable for months.

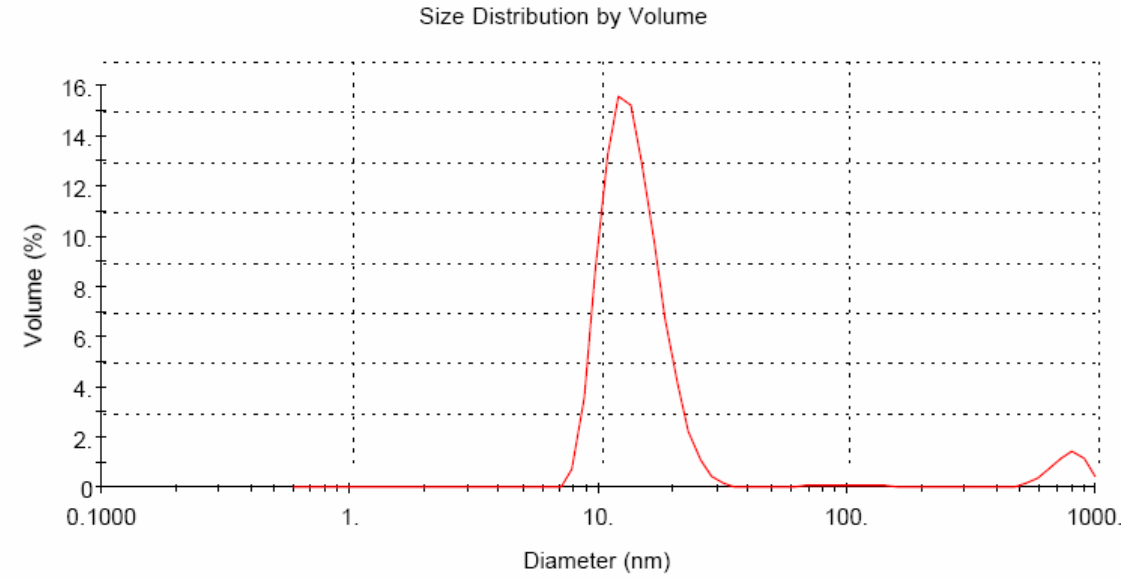

Figure 4-9: DLS data for the octanoate capped nickel ferrite nanoparticles showing their size distribution by volume

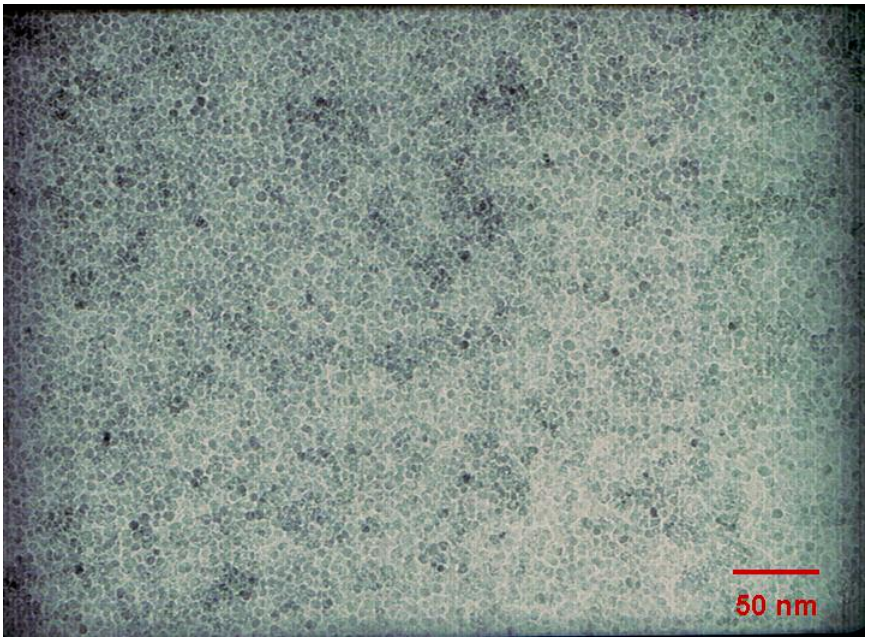

(a)

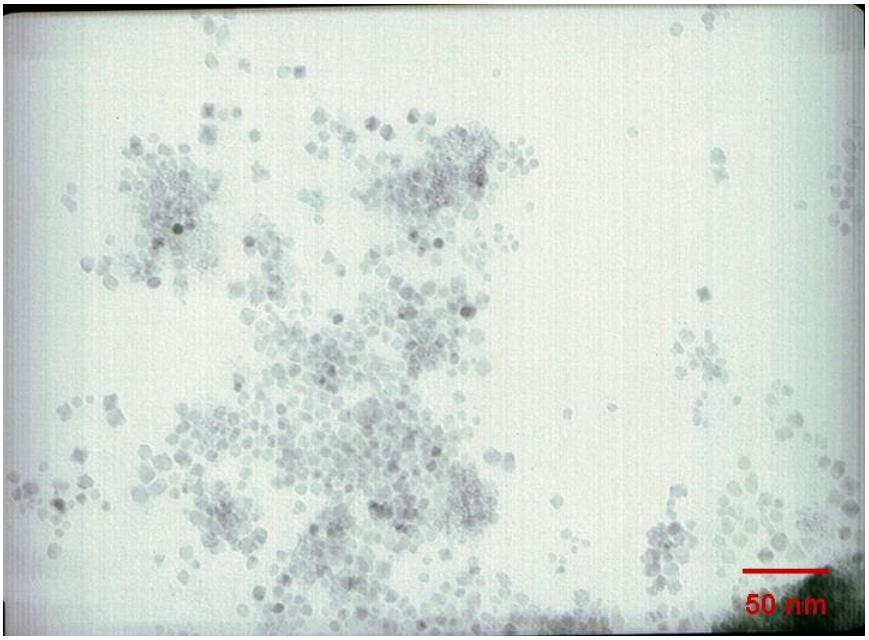

(b)

Figure 4-10: TEM images of octanoate capped nickel ferrite nanoparticles (a) and stearate capped nickel ferrite nanoparticles (b)

Octanoate capped nickel ferrite nanoparticles showed the best dispersability in toluene. Their particle size distribution using Dynamic Light Scattering (DLS) technique was calculated to be 14.1 nm (Figure 4-9). The sample dispersions used for this measurement were 0.1 % w/v dilutions of the capped $FeNi_2O_4$ in toluene, sonnicated for less than 3 minutes. It is interesting to note that without any vigorous sonnication and extreme dilution of the sample, the average size distribution determined using DLS was relatively close to values calculated from TEM micrographs. It is believed that due to limitations associated with the DLS technique such as the tendency of smaller particles to aggregate quickly in solutions resulting in a larger than expected average particle size, a smaller average particle size is expected using TEM. Therefore, for comparative purposes and better accuracy, transmission electron microscopy was used for average particle size determinations. TEM samples were prepared according to the following procedure:

0.1% w/v dilutions of the capped nickel ferrite powder materials in toluene were prepared. Diluted solutions were sonnicated for 3 minutes and a few drops were carefully placed on a copper grid for transmission electron microscopy measurements. After solvent evaporation resulting in a monolayer formation of the nanoparticles, TEM images were recorded.

Figure 4-10 shows the TEM micrographs of octanoate capped **(a)** and stearte capped **(b)** nickel ferrite nanoparticles. Spherical particles of somewhat uniform size distribution are observed for **(a)**. An average particle diameter of 5 nm and 11nm was calculated for **(a)** and **(b)** respectively. This difference in particle diameter can be attributed to the length of the organic capping agents used, a hypothesis that can be used as an advantage for better size control in future synthesis attempts.

CONCLUSIONS

Carboxylate capped magnetic nanoparticles were easily synthesized under anaerobic conditions using a novel non-hydrolytic approach. The prepared nanoparticles exhibited unique properties such as structural uniformity and small size. Their magnetic activity allows for future utilization in many environmental and biological applications.

Potential applications include rapid cleanup of oil spills, treatment of waste waters, separation of lipids from serum samples for medical analysis and as an alternative to liquid/liquid extraction in chemical and drug manufacturing.

REFERENCES

[1] Hyeon, T. *Chemical Communications (Cambridge, United Kingdom)* **2003**, 927-934.

[2] Drofenik, M.; Lisjak, D.; Makovec, D. *Materials Science Forum* **2005**, *494*, 129-136.

[3] Hood, J. D.; Bednarski, M.; Frausto, R.; Guccione, S.; Reisfeld, R. A.; Xiang, R.; Cheresh, D. A. *Science (Washington, DC, United States)* **2002**, *296*, 2404-2407.

[4] Yan, S.; Zhang, D.; Gu, N.; Zheng, J.; Ding, A.; Wang, Z.; Xing, B.; Ma, M.; Zhang, Y. *Journal of Nanoscience and Nanotechnology* **2005**, *5*, 1185-1192.

[5] Segal, D. *Chemical Syntheses of Advanced Ceramics Materials*; Cambridge University Press, 1986.

[6] Zboril, R.; Mashlan, M.; Petridis, D. *Chemistry of Materials* **2002**, *14*, 969-982.

[7] Yapp, C. J. *Geochimica et Cosmochimica Acta* **1990**, *54*, 229-236.

[8] Kanungo, S. B.; Mishra, S. K. *Journal of Thermal Analysis* **1996**, *46*, 1487-1500.

[9] Kanungo, S. B.; Mishra, S. K. *Journal of Thermal Analysis* **1997**, *48*, 385-401.

[10] Zhang, H.; Wang, R.; Zhang, G.; Yang, B. *Thin Solid Films* **2003**, *429*, 167-173.

[11] Uekawa, N.; Kaneko, K. *Journal of Materials Research* **1999**, *14*, 2002-2006.

[12] Feitknecht, W.; Mannweiler, U. *Helvetica Chimica Acta* **1967**, *50*, 570-581.

[13] Gleitzer, C.; Nowotny, J.; Rekas, M. *Applied Physics A: Solids and Surfaces* **1991**, *A53*, 310-316.

[14] Pascal, C.; Pascal, J. L.; Favier, F.; Moubtassim, M. L. E.; Payen, C. *Chemistry of Materials* **1999**, *11*, 141-147.

[15] Ennas, G.; Musinu, A.; Piccaluga, G.; Zedda, D.; Gatteschi, D.; Sangregorio, C.; Stanger, J. L.; Concas, G.; Spano, G. *Chemistry of Materials* **1998**, *10*, 495-502.

[16] Grimm, S.; Schultz, M.; Barth, S.; Mueller, R. *Journal of Materials Science* **1997**, *32*, 1083-1092.

[17] Ayyub, P.; Multani, M.; Barma, M.; Palkar, V. R.; Vijayaraghavan, R. *Journal of Physics C: Solid State Physics* **1988**, *21*, 2229-2245.

[18] Van Diepen, A. M.; Popma, T. J. A. *Solid State Communications* **1978**, *27*, 121-125.

[19] McMichael, R. D.; Shull, R. D.; Swartzendruber, L. J.; Bennett, L. H.; Watson, R. E. *Journal of Magnetism and Magnetic Materials* **1992**, *111*, 29-33.

[20] Nixon, L.; Koval, C. A.; Noble, R. D.; Slaff, G. S. *Chemistry of Materials* **1992**, *4*, 117-121.

[21] Zhou, J.; Ma, J.; Sun, C.; Xie, L.; Zhao, Z.; Tian, H.; Wang, Y.; Tao, J.; Zhu, X. *Journal of the American Ceramic Society* **2005**, *88*, 3535-3537.

[22] Yang, J. M.; Tsuo, W. J.; Yen, F. S. *Journal of Solid State Chemistry* **1999**, *145*, 50-57.

[23] Shafi, K. V. P. M.; Koltypin, Y.; Gedanken, A.; Prozorov, R.; Balogh, J.; Lendvai, J.; Felner, I. *Journal of Physical Chemistry B* **1997**, *101*, 6409-6414.

[24] Chen, D. H.; He, X. R. *Materials Research Bulletin* **2001**, *36*, 1369-1377.

[25] Shi, Y.; Ding, J.; Liu, X.; Wang, J. *Journal of Magnetism and Magnetic Materials* **1999**, *205*, 249-254.

[26] Son, S.; Taheri, M.; Carpenter, E.; Harris, V. G.; McHenry, M. E. *Journal of Applied Physics* **2002**, *91*, 7589-7591.

[27] George, M.; John, A. M.; Nair, S. S.; Joy, P. A.; Anantharaman, M. R. *Journal of Magnetism and Magnetic Materials* **2006**, *302*, 190-195.

[28] Kodama, R. H.; Berkowitz, A. E.; McNiff, E. J., Jr.; Foner, S. *Physical Review Letters* **1996**, *77*, 394-397.

[29] Rockenberger, J.; Scher, E. C.; Alivisatos, A. P. *Journal of the American Chemical Society* **1999**, *121*, 11595-11596.

[30] Xu, Q.; Yuan, X.; Chang, J. *Journal of Applied Polymer Science* **2005**, *95*, 487-493.

[31] Deacon, G. B.; Phillips, R. J. *Coordination Chemistry Reviews* **1980**, *33*, 227-250.

[32] Nasrazadani, S. *Corrosion Science* **1997**, *39*, 1845-1859.

[33] Martinez, B.; Roig, A.; Molins, E.; Gonzalez-Carreno, T.; Serna, C. J. *Journal of Applied Physics* **1998**, *83*, 3256-3262.

[34] Liu, X.-M.; Fu, S.-Y.; Huang, C.-J. *Journal of Magnetism and Magnetic Materials* **2004**, *281*, 234-239.

[35] Cornel, R. M. *The iron oxides. Structure, properties, Reactions and Uses*; Weinheim, 1996.

[36] Tronc, E.; Chaneac, C.; Jolivet, J. P. *Journal of Solid State Chemistry* **1998**, *139*, 93-104.

[37] Bourlinos, A. B.; Simopoulos, A.; Petridis, D. *Chemistry of Materials* **2002**, *14*, 899-903.

[38] del Monte, F.; Morales, M. P.; Levy, D.; Fernandez, A.; Ocana, M.; Roig, A.; Molins, E.; O'Grady, K.; Serna, C. J. *Langmuir* **1997**, *13*, 3627-3634.

[39] Jewur, S. S.; Kuriacose, J. C. *Thermochimica Acta* **1977**, *19*, 195-200.

[40] Mehrotra, R. C. *Metal Carboxylates*; Academic Press, 1983.

[41] Hoffman, C. J. *Inorg. Syn. (Jacob Kleinberg, editor. McGraw)* **1963**, *7*, 180-182.

CHAPTER 5

REMOVAL OF 4,6-DINITRO-O-CRESOL PESTICIDE FROM AQUEOUS SOLUTIONS USING OCTANOATE AND STEARATE CAPPED MAGNETIC NANOPARTICLES

INTRODUCTION

Nitroaromatic compounds have been heavily used as dyes, explosives, pesticides, plasticizers and solvents. Nitrated phenols such as 4,6-dinitro-*o*-cresol (abbreviated DNOC), 2,4-dinitrophenol (DNP), and 2-sec-butyl-4,6-dinintrophenol (Dinoseb) are listed among the first chemically synthesized pesticides [1]. In addition to being used as an acaricide, larvicide, and ovicide in controlling many dormant insects in orchards, DNOC was widely used as a selective agricultural herbicide in the cultivation of grain, hops, vines and fruits [2]. Large quantities of DNOC entering the environment are commonly detected in agricultural and industrial effluents. Therefore, their presence as adsorbed soil contaminants, components of industrial wastewater, and natural water pollutants is considered a major health threat for humans and animals [3,4]. High dependency on groundwater as a major source for drinking water raises many important questions concerning its quality and sources of contamination. Origins and routes of pesticide and herbicide transport into groundwater can be classified into two categories. The first include inadequate waste disposal from farm yard equipment, accidental spillage

near well-heads, and leakages from industrial manufacturing plants and agricultural chemical dealerships [5]. These sources are called “point sources”. Agriculture is the primary source of aquifer contamination and is classified as a “Non point” origin of contamination, where pesticides leach from top soil via matrix or preferential flow [6]. A consequence of the multitude of pesticidal contamination sources and transport routes is the continuing problem in preventing and treating groundwater contamination [7].

The herbicidal and insecticidal activities of DNOC are manifested by its uncoupling effect on mitochondrial oxidative phosphorylation [8]. It has been previously reported that this common biological effect is related to the reproductive toxicity of DNOC [8]. Other dinitrophenolic compounds including Dinoseb and DNP have also exhibited spermatotoxic effects and could result in male sterility as well as tumor formation in humans [9]. In response to these findings, the United States Environmental Protection Agency (USEPA) banned Dinoseb from use in 1986 [9]. In 1991, the World Health Organization classified DNOC as a (classIb) pollutant due to its high toxicity, which resulted in banning it from being utilized as a pesticide and herbicide in the United States [2]. However, DNOC and DNP are still used in Wolman wood preservatives, as dye intermediates, pH indicators, and inhibitors for the polymerization of styrene and vinyl compounds [2,8]. Also, large stocks of DNOC are available to this day in many parts of the world. It is still widely employed in third-world countries where its accumulation is of great danger to the aquatic environment [2].

Another substantial problem arises due to the low degradation rate for most of the degradable pesticides [7]. Since many nitroaromatic compounds have the ability to inhibit cell growth by uncoupling the respiratory chain from ATP production, microbial

degradation is rendered ineffective [10]. Therefore, there is a need for effective, economic adsorbents for the removal of nitroaromatic compounds (NAC's) from water. Removal of DNOC from water was performed in the past using a variety of adsorbents such as macroreticular resins, granular activated carbon (GAC), coal fly ash, and clay minerals [11-14]. The drawbacks of using these adsorbents are low efficiency and slowness of separation. In this chapter we report the utilization of octanoate and stearate capped magnetic nanoparticles as extractants for the removal of DNOC from water. The adsorbate concentration and the adsorption capacities of these materials for DNOC have been measured. Moreover, adsorption isotherms and experimental conditions were studied.

EXPERIMENTAL

Chemicals and methods

The preparation of the octanoate and stearate capped magnetic nanoparticles was accomplished according to the procedure described in Chapter 4. The nanoparticulate extractants used in this chapter were octanoate capped magnetite (OCM), octanoate capped nickel ferrite (OCNF), stearate capped magnetite (SCM) and stearate capped nickel ferrite (SCNF). The dinitrophenol 4,6-dinitro-o-cresol was reagent grade purchased from Aldrich and was used without any further purification. All glassware used in the adsorption reactions were washed with methylene chloride and then rinsed 7 – 8 times with distilled water. UV/visible spectra were recorded on an Agilent 8453 UV-visible spectrophotometer that uses two light sources, a deuterium and a tungsten lamp. Agilent chemstation software was used to analyze the generated data.

Adsorption experiments

The adsorption experiments were carried out in 20 ml capped glass vials. Standard solutions of DNOC in water were prepared for a series of concentrations ranging from 1 ppm to 40 ppm. These concentrations were determined using a spectrophotometer, where the wavelength corresponding to a maximum absorbance of DNOC was found to be 329 nm with an accuracy of 0.3 nm. For each extraction measurement, 0.5 g of the adsorbent was added to 20 ml of DNOC and the mixture was left to equilibrate. In order to generate adsorption data from treated solutions, the mixtures were shaken on an electric rotator at room temperature. After equilibrium was reached, the used adsorbents were magnetically separated from water using a magnetic separator. The laboratory scale magnetic separator developed for these experiments consists of a magnetometer connected to an electrically controlled magnet. A steel wool packed glass column was attached to the magnet and used as a fixed bed for the magnetic separation process. A clear illustration of this device with detailed dimensions is presented in Chapter 2. Finally, the concentrations of treated DNOC solutions were determined using the UV/Visible spectrophotometer.

Adsorption isotherms

Adsorption data were analyzed using the Freundlich model to describe the adsorption of DNOC from the aqueous solution. This isotherm represents the buildup of an initial layer of molecules on an adsorbent surface followed by a condensation effect resulting from strong solute-solute interaction. It is generally expressed as:

$$X = K_f C_{eq}^{1/n} \quad [15].$$

Where:

X is the amount of DNOC adsorbed per unit weight of adsorbent (mg g^{-1}). It can also be referred as the adsorption density at the equilibrium solute concentration (C_{eq}).

C_{eq} is the equilibrium concentration of DNOC in aqueous solutions (mg l^{-1}).

K_f and **1/n** are Freundlich constants dependent on a number of environmental factors. These values represent the adsorption capacity and intensity of adsorption respectively [16,17]. K_f also reflects the affinity of an adsorbent for the adsorbate.

The rearrangement of the above equation gave the following linear form:

$$\ln X = \ln K_f + \frac{1}{n} \ln C_{eq}$$

Obtaining a linear plot of ln X versus ln C_{eq} using this equation implies that the Freundlich model fits the generated data. After the linearization of experimental results, Freundlich constants 1/n and K_f can be determined from the slope and intercept [16].

RESULTS AND DISCUSSION

The competition between solute and solvent molecules for surface adsorption sites is of considerable influence to DNOC adsorption on magnetite and nickel ferrite nanoparticles. The difference in adsorption potential between a solute and a solvent governs the capacity of adsorption for this particular solute. Therefore, low adsorption potential energy is needed for an adsorbate in order to displace water from the surface of an adsorbent [18]. Adsorbent-solvent affinity is inversely proportional to the adsorption capacity for solutes. However, this affinity by itself is not sufficient to achieve favorable adsorption capacities. The solute-solvent affinity must be lower than the affinity of the

solute for the surface. Low solubility for DNOC in water (0.01 g/100 ml) allows for its adsorption to occur more readily on the surface of the capped magnetic extractants.

The capped nanomaterials used in this study were expected to show good adsorption capacities due to their small size and low affinity for water. Figures 5-1 and 5-2 show a simple plot between a series of DNOC concentrations versus the obtained final concentrations of the treated solutions using 0.05 g of the adsorbate in each case. It is observed from these plots that the capped nickel ferrite nanoparticles gave the highest improvement on the adsorption from each set. Consequently they were fitted to the linear form of the Freundlich equation and the results are shown in Figures 5-3 and 5-4. Adsorption data did not fit the Langmuir model possibly due to a variety of adsorption modes (adsorption on metal surface or by carboxylate groups) and to the presence of anionic and non-ionic forms of DNOC in solution. Summaries of the batch adsorption tests used to construct the linear relationships are tabulated (Tables 5-1 through 5-4). The highest percentages of adsorbed DNOC were reached when using OCNF, owing to its' smallest average particle size (5 nm) and lowest tendency for agglomeration in solution. On the other hand stearate capped extractants showed more particle agglomeration in DNOC solutions indicating the possibility of a decrease in available surface adsorption sites. This explains the difference in percentages of adsorption between OCM (Table 5-3) and SCNF (Table 5-2) indicating higher percentages for OCM even though it has a slightly larger particle size. To further clarify this observation, the Freundlich capacity and intensity of adsorption, K_f and 1/n respectively, were calculated using the linear equations and presented in Table 5-5. Although the maximum adsorption capacities of

OCM and SCNF are different, their intensities for DNOC adsorption are very close in agreement with our interpretation.

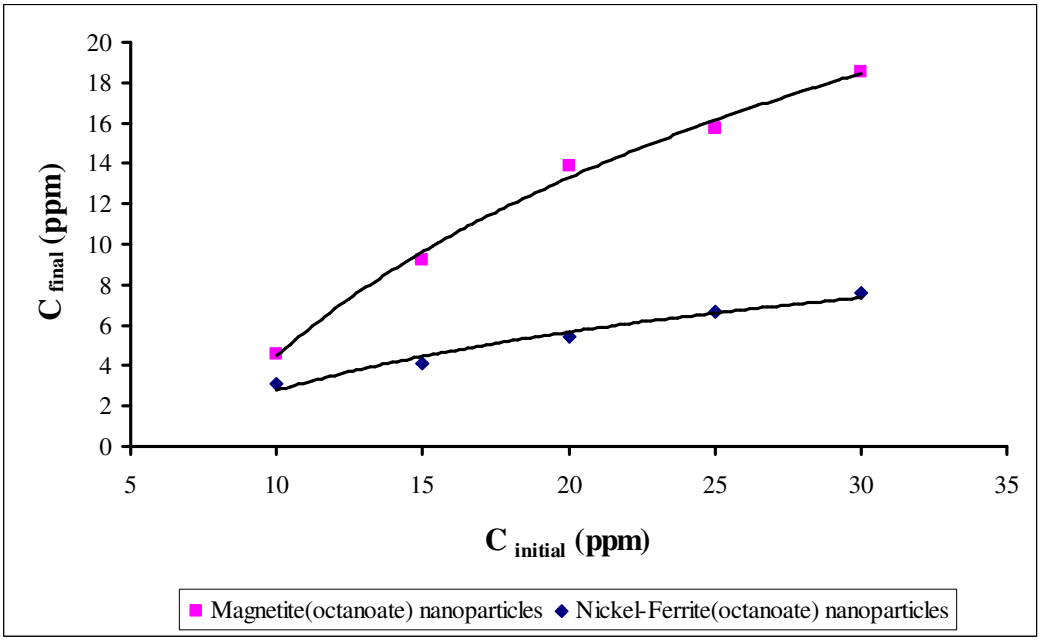

Figure 5-1: 4,6-dinitro-*o*-cresol adsorption data using octanoate capped magnetite and nickel ferrite nanoparticles

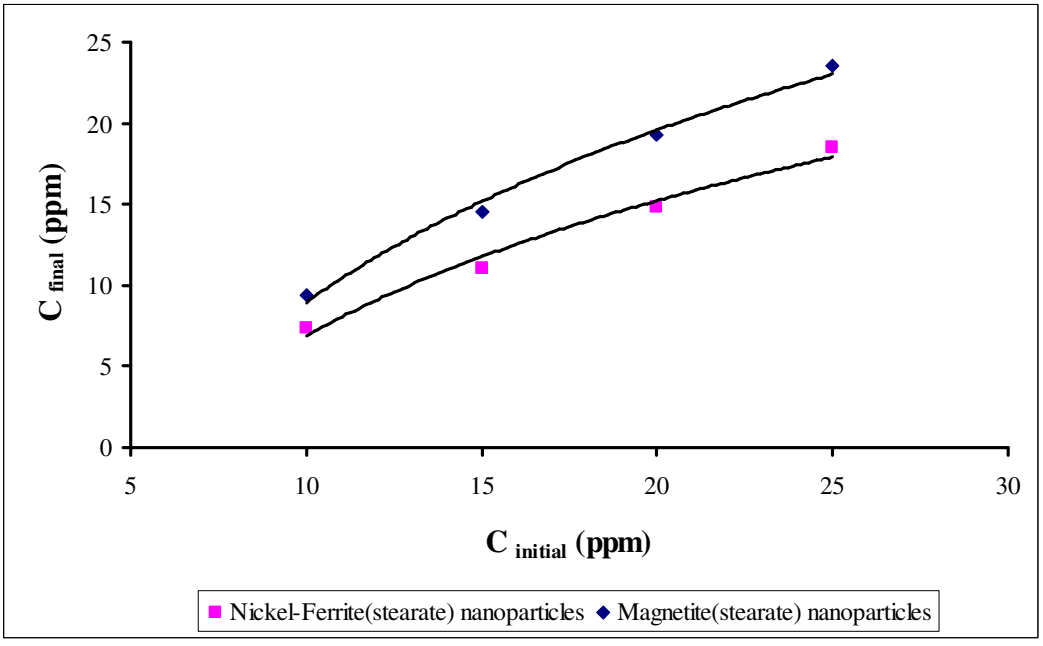

Figure 5-2: 4,6-dinitro-o-cresol adsorption data using stearate capped magnetite and nickel ferrite nanoparticles

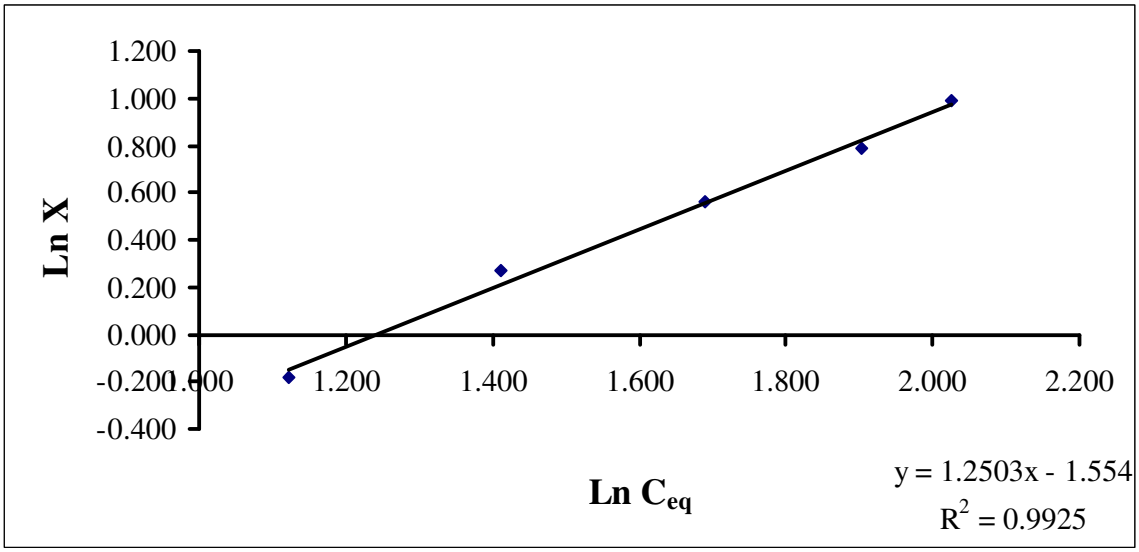

Figure 5-3: Linear adsorption model of DNOC on octanoate capped nickel ferrite nanoparticles using the Freundlich equation

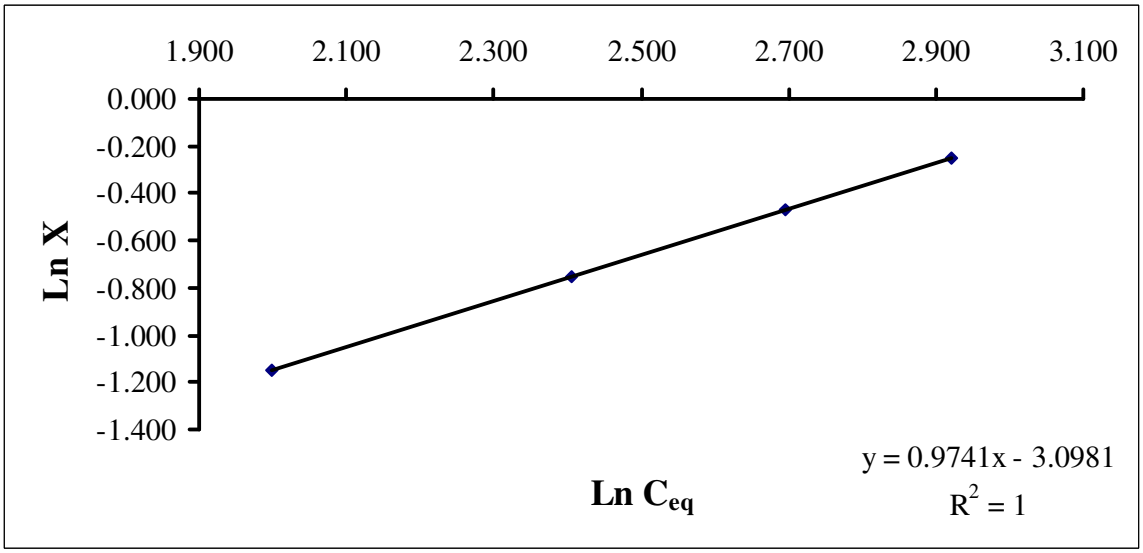

Figure 5-4: Linear adsorption model of DNOC on stearate capped nickel ferrite nanoparticles using the Freundlich equation

Table 5-1: Summary of the batch adsorption test results using octanoate capped nickel ferrite nanoparticles

Experiment number	C_i (initial concentration in mg/l)	C_{eq}	X	Ln C_{eq}	Ln X	% Adsorbed
1	10	3.075	0.831	1.123	-0.185	69.3
2	15	4.098	1.308	1.410	0.269	72.7
3	20	5.417	1.750	1.690	0.560	72.2
4	25	6.701	2.196	1.902	0.787	73.2
5	30	7.571	2.691	2.024	0.990	74.8

Table 5-2: Summary of the batch adsorption test results using stearate capped nickel ferrite nanoparticles

Experiment number	C_i (initial concentration in mg/l)	C_{eq}	X	Ln C_{eq}	Ln X	% Adsorbed
1	10	7.369	0.316	1.997	-1.153	26.3
2	15	11.082	0.470	2.405	-0.755	26.1
3	20	14.804	0.624	2.695	-0.472	26.0
4	25	18.539	0.775	2.920	-0.254	25.8

Table 5-3: Summary of the batch adsorption test results using octanoate capped magnetite nanoparticles

Experiment number	C_i (initial concentration in mg/l)	C_{eq}	X	Ln C_{eq}	Ln X	% Adsorbed
1	10	4.579	0.651	1.521	-0.430	54.2
2	15	9.259	0.689	2.226	-0.373	38.3
3	20	13.850	0.738	2.628	-0.304	30.8
4	25	15.765	1.108	2.758	0.103	36.9
5	30	18.54	1.375	2.920	0.319	38.2

Table 5-4: Summary of the batch adsorption test results using stearate capped magnetite nanoparticles

Experiment number	C_i (initial concentration in mg/l)	C_{eq}	X	Ln C_{eq}	Ln X	% Adsorbed
1	10	9.800	0.024	2.282	-3.730	2.00
2	15	14.520	0.058	2.676	-2.854	3.20
3	20	19.260	0.089	2.958	-2.421	3.70
4	25	23.560	0.173	3.160	-1.756	5.76

Table 5-5: Freundlich adsorption parameters of the capped magnetic nanoparticles

Extractant	1/n	K
Fe-Ni(octanoate)	1.250	0.211
Magnetite(octanoate)	0.975	0.072
Fe-Ni(stearate)	0.974	0.045
Magnetite(stearate)	2.16	1.7×10^{-4}

CONCLUSIONS

Initial laboratory studies showed promising removal of DNOC from water using capped magnetic nanoparticles. The amounts extracted were up to 75 % and no extractant particles were detected in the effluent. The exhausted adsorbent can be easily recovered using a magnetic separator, which makes the process of high environmental and industrial importance.

This project demonstrates the feasibility of using novel capped magnetic extractants for removal of DNOC from aqueous solutions. However, further investigations concerning different factors influencing the adsorption, optimizing experimental conditions, and enhancing extractant efficiency are needed to reach more favorable adsorption capacities.

REFERENCES

[1] Gisi, D.; Stucki, G.; Hanselmann, K. W. *Applied Microbiology and Biotechnology* **1997**, *48*, 441-448.

[2] Flox, C.; Garrido, J. A.; Rodriguez, R. M.; Centellas, F.; Cabot, P.-L.; Arias, C.; Brillas, E. *Electrochimica Acta* **2005**, *50*, 3685-3692.

[3] Goi, A.; Trapido, M. *Chemosphere* **2002**, *46*, 913-922.

[4] Schussler, W.; Nitschke, L. *Chemosphere* **2000**, *42*, 277-283.

[5] Barbash, J. *Pesticides in groundwater. Distribution, trends and governing factors*; Ann Arbor Press: Chelsea, MI, 1996.

[6] Blanchard, P. E.; Donald, W. W. *Journal of Environmental Quality* **1997**, *26*, 1612-1621.

[7] Albrechtsen, H.-J.; Mills, M. S.; Aamand, J.; Bjerg, P. L. *Pest Management Science* **2001**, *57*, 341-350.

[8] Takahashi, K. L.; Hojo, H.; Aoyama, H.; Teramoto, S. *Reproductive Toxicology* **2004**, *18*, 581-588.

[9] Crawford, M. *Science* **1986**, *234*, 422.

[10] Spain, J. C. *Annual review of microbiology* **1995**, *49*, 523-555.

[11] Kim, H.-J.; Lee, S.-S.; Sohn, J.-E.; Furuya, E.; Takeuchi, Y.; Noll, K. E.; Yamashita, S. *Korean Journal of Chemical Engineering* **1996**, *13*, 399-403.

[12] Kim, T. Y.; Kim, S. J.; Cho, S. Y. *Korean Journal of Chemical Engineering* **2001**, *18*, 755-760.

[13] Lu, M.-C.; Lin, C.-J.; Chyan, J.-M.; Liao, C.-H. *Fresenius Environmental Bulletin* **2005**, *14*, 526-530.

[14] Haderlein, S. B.; Weissmahr, K. W.; Schwarzenbach, R. P. *Environmental Science and Technology* **1996**, *30*, 612-622.

[15] Freundlich, H. *Colloid & capillary chemistry*; Dutton: New York, 1922.

[16] Muhammad, N.; Parr, J.; Smith, M. D.; Wheatley, A. D. *Urban Water Journal* **2005**, *2*, 33-37.

[17] Singh, D. K.; Srivastava, B. *Journal of Industrial Pollution Control* **2000**, *16*, 19-30.

[18] Cota-Espericueta, A. D., New Mexico State University, 2003.

CHAPTER 6

ARSENIC REMEDIATION USING MAGNETIC EXTRACTANTS

INTRODUCTION

Grave concerns have been raised in many parts of the globe regarding arsenic (As) contamination in water [1]. Arsenic's ingestion in drinking water can cause many health problems such as bladder, kidney, and skin cancers, muscular weakness, nerve tissue injuries, and blackfoot disease [2-4]. Millions of people worldwide have been reported to be at risk due to arsenic intake from natural waters [5]. In some areas in Bangladesh, concentrations as high as 1000 μg/l were found in shallow zones of ground water [6]. Considering arsenic's high toxicity and deleterious effect on human health, the World Health Organization (WHO) have shown a more stringent attitude towards the standard for arsenic in drinking water by recommending the 10 μg/l as maximum contaminant level (MCL) of arsenic in 1993 [7]. After reviewing the science and economics behind implementing the new standard set by the WHO, the United States Environmental Protection Agency (USEPA) decided to lower the MCL of arsenic from 50 to 10 μg/l starting January 2006 [8]. As a result of this new measure, effective and competitive technologies for arsenic remediation are needed in order to meet EPA's recent requirement.

It is essential to discuss the chemistry of arsenic, its sources and forms in aqueous media before reviewing the existing remediation methods for contaminated water. In nature, arsenic occurs in a variety of mineral forms of which a large proportion is present as arsenates and the remaining percentage includes arsenites, arsenides, sulfides, sulfosalts, oxides, silicates, and elemental arsenic [9]. In aqueous aerobic environments, inorganic arsenic is predominantly found in its thermodynamically stable pentavalent forms (H_3AsO_4, $H_2AsO_4^{-1}$, $HAsO_4^{-2}$, and AsO_4^{-3}), whereas, trivalent arsenite (H_3AsO_3, and $H_2AsO_3^{-}$) is more prevalent under reducing conditions such as anaerobic groundwaters [10,11]. Methyl and dimethyl arsenic acids are organic forms of arsenic which may also be found in natural waters as an outcome of application of organo-arsenical pesticides, and via biomethylation mechanisms of microorganisms [11]. Relatively low-toxicity arsenic species (arsenobetaine and arsenocholine) are present in lobster and shrimp from industrially polluted water [12].

Generally, sources of arsenic contamination in natural waters can be classified into two categories, natural and anthropogenic. Natural contamination of the subsurface water is mainly a result of dissolution or desorption of arsenic compounds from pyrite ores by geohydrological, geochemical, and geothermal activities [1,10]. Anthropogenic sources are varied and may be associated with the use of arsenic containing pesticides and herbicides, wood preservatives, feed additives, certain metal alloys, battery plates, dyes, and ceramics [12-15]. Additionally, seepages from hazardous industrial waste sites, smelting of metals, burning of arsenic containing coal for power generation, and mine tailings are possible origins of arsenic contamination [16-18].

Conventional techniques available for the removal of arsenic from contaminated water are: 1) coagulation/precipitation, 2) lime softening, 3) adsorption, 4) ion exchange, 5) membrane filtration, and electrodialysis [19]. These physico-chemical methods are primarily effective for As(V) remediation. Therefore, the effective removal of trivalent arsenic is usually accomplished by a pre-oxidation step [20]. Advanced biological methods such as phytoremediation and biological treatment with microorganisms can be used to treat arsenic contaminated water, however, they suffer from low efficiency, complexity of operation, and the need for pretreatment operations [19]. Limitations are also associated with the use of conventional treatment techniques. In certain cases, high operation and equipment cost, competitive interference of ions on removal performance, need for post treatment steps, use and handling of chemicals, and production of large quantities of high arsenic content sludge are limiting factors responsible for low efficiency [10].

To minimize drawbacks faced by existing treatment methods, adsorption along with separation by magnetic filtration approaches were chosen for further research. From an environmental point of view, nanomaterials are of considerable interest as adsorbents due to their small particle size, high surface areas, and low mass-transfer resistance [21]. Moreover, numerous problems such as plugging and fouling of packed columns and membranes, also the need of high pressure treatment streams associated with existing water treatment applications can be avoided by using nanoadsorbents in dispersed separation [22]. High Gradient Magnetic Separation (HGMS) technology was proven to separate nanoparticles with average particle diameters as low as 2 nm [21]. In this chapter, novel magnetic materials such as capped nickel ferrite nanoparticles and

magnetic activated carbons (MACs) previously prepared, described, and characterized in Chapters 2 and 4 were investigated for their ability to adsorb pentavalent arsenic from water. After the adsorption process, these materials were easily recovered using a lab scale magnetic filter.

EXPERIMENTAL

Materials

Arsenate standards were prepared using analytical grade sodium arsenate heptahydrate purchased from GFS chemicals and used without any further purification. The magnetic nanoparticles employed in these experiments were octanoate capped nickel ferrite and stearate capped nickel ferrite nanoparticles with average particle sizes of 5 and 11 nm respectively. Magnetic activated carbon, MAC-5, was also tested for the removal of arsenic and compared with Fisher Scientific's unmodified commercial activated carbon, Darco G-60.

Adsorption experiments and detection method

100 ml glass bottles used for the sorption reactions were cleaned with 10% nitric acid, and washed several times with de-ionized water. 100 ml aliquots of arsenate concentrations ranging from 800 µg/l to 2000 µg/l were treated with 0.1 g of the nanoparticle samples. The mixtures were shaken on a rotor at about 70 rpm for 5 hours. After equilibrium, the final concentrations were detected using the QUICK^{TM} (481396) Arsenic kit. In this detection method, tartaric acid and zinc dust are reacted with the treated solution for the reduction of arsenic compounds to arsine gas. The generated

arsine gas is then allowed to react with a mercuric bromide testing pad. The intensity of the color obtained is proportionately related to the concentration of arsenic in the sample and was determined using a standardized color chart. The reduction reactions are described as follows:

$$5\ H_2AsO_4^{-1} + 20\ Zn + 45\ H^+ \longrightarrow 5\ AsH_3(g) + 20\ Zn^{+2} + 20\ H_2O$$

RESULTS AND DISCUSSION

Generally, van der Waals force, electrostatic forces, exchange of ions, and the lyophobic nature of the adsorbate are the main factors involved in the adsorption process. In all the experiments presented in this chapter, the uptake of arsenate by the extractants is assumed to be an outcome of chemical coordination or physical attraction between the arsenate and the surface of the adsorbent. Therefore, the maximum number of surface adsorption sites must be finite. The dynamic equilibrium established between the adsorbate concentrations on the adsorbent surface and in solution at a constant temperature is expressed by the linearized Langmuir adsorption isotherm. The Langmuir equation is presented and discussed in Chapter 3. It has been found that the adsorbents developed and used for this specific application were superior to other adsorbents used for arsenic removal such as activated charcoal, hydrous ferric oxide, and zero valent iron [23]. At pH 6, all adsorbents in this study were able to reduce arsenate levels in solutions below new EPA standards (10 μg/l). Figure 6-1 shows the As(V) adsorption data fitted with the Langmuir model where good coefficients of determinations (R^2) were determined for the three adsorbents.

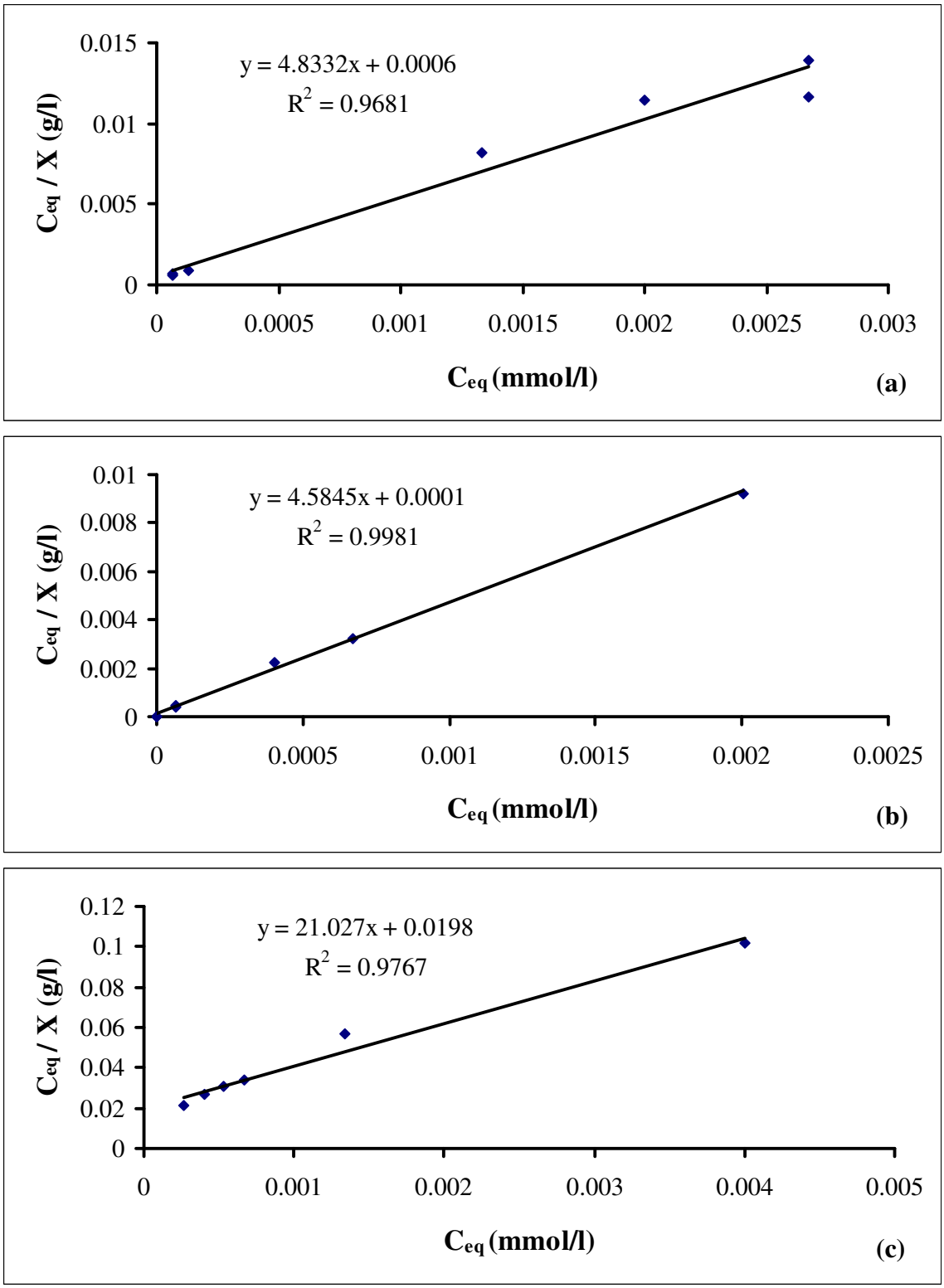

Figure 6-1: Langmuir isotherms for the adsorption of As(V) from aqueous solutions using octanoate and stearate capped nanoparticles (a and b), and MAC-5 (c)

Table 6-1: Adsorption capacities and coefficients of determination for the magnetic adsorbents used in the magnetic extraction of As(V)

Adsorbent	**R^2**	**θ^o (maximum adsorption mg g^{-1})**
Octanoate capped nanoparticles	0.96	15.0
Stearate capped nanoparticles	0.99	16.6
MAC-8	0.97	3.44

The maximum adsorption capacities and the R^2 values are presented in Table 6-1. As observed, the maximum adsorption capacities of the capped nanoparticles are comparable which proves that the presence of the two different organic moeities around the nickel ferrite particles does not significantly interfere with the adsorption of arsenate. Many researchers demonstrated the affinity of arsenate and arsenite to iron oxides [24]. Although different phases of iron oxide exhibit different structures, they do not influence the adsorption of arsenic [22]. This adsorption is mainly governed by surface properties of metal ferrites. In addition the adsorption behavior is affected by other factors such as solution pH and the oxidation state of arsenic [22].

Commercial activated charcoal was also used in arsenate adsorption experiments but showed no effectiveness for this application. However, magnetic activated carbon, MAC-8, exhibited good affinity towards arsenate adsorption. It is believed that presence of nickel ferrite nanoparticles within the activated carbon matrix is the major contributor

of active sites needed for arsenate adsorption. This cost effective, easy to prepare adsorbent holds numerous advantages over current complicated technologies for arsenic removal from water. Its efficiency and manageability makes it a promising material to be used in low-cost technologies for arsenic removal in rural communities.

CONCLUSIONS

Capped nickel ferrite nanoparticles and magnetic activated carbon MAC-8 were shown to be effective adsorbents for the magnetic extraction of arsenic from water. The possibility of removing more than 99% of As(V) from aqueous solutions using very small quantities of the nanoparticulate adsorbents is reported. By finding a pattern between adsorbent particle size and maximum adsorption capacity, these materials would be ideal for use in highly efficient magnetic separation systems.

REFERENCES

[1] Nguyen, T. V.; Vigneswaran, S.; Ngo, H. H.; Pokhrel, D.; Viraraghavan, T. *Engineering in Life Sciences* **2006**, *6*, 86-90.

[2] Chen, S.-L.; Dzeng, S. R.; Yang, M.-H.; Chiu, K.-H.; Shieh, G.-M.; Wai, C. M. *Environmental Science and Technology* **1994**, *28*, 877-881.

[3] Thirunavukkarasu, O. S.; Viraraghavan, T.; Subramanian, K. S. *Water Quality Research Journal of Canada* **2001**, *36*, 55-70.

[4] Thirunavukkarasu, O. S.; Viraraghavan, T.; Subramanian, K. S.; Tanjore, S. *Urban Water* **2002**, *4*, 415-421.

[5] Ratna Kumar, P.; Chaudhari, S.; Khilar, K. C.; Mahajan, S. P. *Chemosphere* **2004**, *55*, 1245-1252.

[6] Harvey, C. F.; Swartz, C. H.; Badruzzaman, A. B. M.; Keon-Blute, N.; Yu, W.; Ali, M. A.; Jay, J.; Beckie, R.; Niedan, V.; Brabander, D.; Oates, P. M.; Ashfaque, K. N.; Islam, S.; Hemond, H. F.; Ahmed, M. F. *Science (Washington, DC, United States)* **2002**, *298*, 1602-1606.

[7] World Health Organization. *Guidelines for drinking-water quality*; The Organization ; WHO Publications Centre USA: Geneva, Albany, NY, 1993.

[8] United States. Environmental Protection Agency. Office of Water.; United States Environmental Protection Agency, Office of Water: [Washington, D.C.], 2002.

[9] Wedepohl, K. H. *Handbook of geochemistry*; Springer: Berlin, 1969.

[10] Mondal, P.; Majumder, C. B.; Mohanty, B. *Journal of Hazardous Materials* **2006**, *137*, 464-479.

[11] Zouboulis, A.; Katsoyiannis, I. *Separation Science and Technology* **2002**, *37*, 2859-2873.

[12] Cullen, W. R.; Reimer, K. J. *Chemical Reviews (Washington, DC, United States)* **1989**, *89*, 713-764.

[13] Altundogan, H. S.; Altundogan, S.; Tumen, F.; Bildik, M. *Waste Management (Oxford)* **2000**, *20*, 761-767.

[14] Nickson, R. T.; McArthur, J. M.; Ravenscroft, P.; Burgess, W. G.; Ahmed, K. M. *Applied Geochemistry* **1999**, *15*, 403-413.

[15] Viraraghavan, T.; Subramanian, K. S.; Aruldoss, J. A. *Water Science and Technology* **1999**, *40*, 69-76.

[16] McNeill, L. S.; Edwards, M. *Journal - American Water Works Association* **1997**, *89*, 75-86.

[17] Leist, M.; Casey, R. J.; Caridi, D. *Journal of Hazardous Materials* **2000**, *76*, 125-138.

[18] Korte, N. E.; Fernando, Q. *Critical Reviews in Environmental Control* **1991**, *21*, 1-39.

[19] United States. Environmental Protection Agency. Office of Solid Waste and Emergency Response. *Arsenic treatment technologies for soil, waste, and water*; Solid Waste and Emergency Response: [Washington, D.C.], 2002.

[20] Nriagu, J. O. *Arsenic in the environment*; Wiley: New York, 1994.

[21] Moeser, G. D.; Roach, K. A.; Green, W. H.; Laibinis, P. E.; Hatton, T. A. *Industrial & Engineering Chemistry Research* **2002**, *41*, 4739-4749.

[22] Yean, S.; Cong, L.; Yavuz, C. T.; Mayo, J. T.; Yu, W. W.; Kan, A. T.; Colvin, V. L.; Tomson, M. B. *Journal of Materials Research* **2005**, *20*, 3255-3264.

[23] Kundu, S.; Pal, A.; Mandal, M.; Ghosh, S. K.; Panigrahi, S.; Pal, T. *Journal of Environmental Science and Health, Part A: Toxic/Hazardous Substances & Environmental Engineering* **2004**, *A39*, 185-202.

[24] Pierce, M. L.; Moore, C. B. *Water Research* **1982**, *16*, 1247-1253.

CHAPTER 7

CONCLUSIONS AND FUTURE DIRECTIONS

CONCLUSIONS

This research has shown the possibility of synthesizing effective magnetic adsorbents by simple chemical methods. The first group of these magnetic materials was low cost magnetic activated carbons exhibiting relatively high surface areas and no remanent magnetization. The ability of the magnetic charcoals to be easily manipulated by a low external magnetic field allowed for their use in liquid-phase environmental applications. Successful magnetic removal of Congo red dye, 4,6-dinitro-o-cresol, and decane with sufficient adsorption capacities was demonstrated. Moreover, separation of oil from aqueous emulsions was also possible using the magnetic separation technique. The experimental adsorption equilibrium data showed very good fit with the Langmuir isotherm.

Carboxylate capped magnetic nanoparticles easily synthesized under anaerobic conditions using a novel non-hydrolytic approach formed the second group of magnetic adsorbents. The prepared nanoparticles exhibited unique properties such as structural uniformity and small size. The magnetic removal of DNOC from aqueous solutions was

performed where the loaded adsorbent could be easily recovered using a magnetic separator.

Furthermore, capped nickel ferrite nanoparticles and magnetic activated carbon MAC-8 were excellent magnetic adsorbents for arsenic (V). More than 99% of As(V) from aqueous solutions was removed using very small quantities of the nanoparticulate adsorbents.

FUTURE DIRECTIONS

The advantages of the methodologies used in this study created a motivation to explore further possibilities for novel nano-adsorbent development and applications. A first step towards this task is to optimize the produced MACs and capped nanoparticles in order to achieve maximum performance possible. For example, using high organic content raw materials such as pistachio nut shells and coconut shells for the preparation of MACs could yield higher surface areas. Thorough analysis of the nature and percentage of available functionalities on the MACs' surface will give a good perspective on how to selectively control these functionalities to attain better selectivity. As for the capped nanoparticles, further development of the synthesis method for environmental compatibility and to achieve higher product yields is essential. Additional experiments involving competing ions in the adsorption of As(V) and other pollutants from aqueous solutions will help build a better understanding of the adsorbents activity.

Biocompatibility studies can extend the capped nanoparticles' possible areas of application to include drug delivery, magnetic fluid hyperthermia, separation of lipids

from serum samples for medical analysis, and as an alternative to liquid/liquid extraction in chemical and drug manufacturing.

VITA

Tarek Trad

Candidate for the Degree of

Doctor of Philosophy

Thesis: NOVEL MAGNETIC EXTRACTANTS FOR REMOVAL OF POLLUTANTS FROM WATER

Major Field: Chemistry

Biographical:

Personal Data: Born in Beirut, Lebanon, on October 4, 1977

Education:

Received his Bachelor of Science degree in Chemistry from Beirut Arab University, Beirut, Lebanon, in 1999.

Completed the requirements for the Doctor of Philosophy degree in Chemistry at Oklahoma State University in December, 2006.

Publications:

The author published several research papers and presented his work in numerous regional, national and international conferences.

Professional Membership:

American Chemical Society (ACS).

Phi Lambda Upsilon (PLU): National Honorary Chemical Society.

Name: Tarek Mohsen Trad Date of Degree: December, 2006

Institution: Oklahoma State University Location: Stillwater, Oklahoma

Title of Study: NOVEL MAGNETIC EXTRACTANTS FOR REMOVAL OF POLLUTANTS FROM WATER

Pages in Study: 120 Candidate for the Degree of Doctor of Philosophy

Major Field: Chemistry

SCOPE AND METHOD OF STUDY: This research aims at developing magnetic extractants that can be utilized in conjunction with magnetic filtration devices to efficiently and economically remove a number of pollutants from aqueous solutions and mixtures. Two types of magnetic materials were synthesized, characterized, and used in a variety of environmental applications. The first was based on activated carbon, where raw materials used for the development of high surface area activated carbon were modified to produce novel magnetically-active activated carbons (MAC's). The unique properties and adsorption capacity of these materials allowed their application in the extraction of hydrocarbons from water and in breaking oil in water emulsions. In the second phase of the project, nano-composites of organic-capped magnetite and nickel ferrite were successfully obtained by non-hydrolytic thermal treatment of organometallic precursors. The nanoparticles were characterized using a variety of techniques including transmission electron microscopy, infrared spectroscopy, X-ray diffraction, and thermogravimetric analysis. Finally, an investigation on the ability of the nanoparticulate extractants for the removal of 4,6-dinitro-o-cresol pesticide and arsenate from water was conducted.

FINDINGS AND CONCLUSIONS: Magnetic activated carbons prepared from industrial and household byproducts were effective for the removal of decane, 4,6-dinitro-o-cresol, arsenate, and a number of dyes from aqueous media. Additionally, MAC's were capable of breaking oil in water emulsions. Carboxylate capped magnetic nanoparticles were easily synthesized, and exhibited unique properties such as structural uniformity, small size, and high surface area. These nanoparticles showed remarkable results in the removal of 4,6-dinitro-o-cresol pesticide and arsenate from water. Moreover, magnetic activity exhibited by these extractants allowed for quick separation using magnetic filters.

Potential applications include rapid cleanup of oil spills, treatment of waste waters, separation of lipids from serum samples for medical analysis and as an alternative to liquid/liquid extraction in chemical and drug manufacturing.

ADVISOR'S APPROVAL: _____Dr. Allen W. Apblett_____